MSc. Thesis Report

from Solar to Hydrogen energy

Modelling, design and construction of a system for hydrogen production using photovoltaic panels

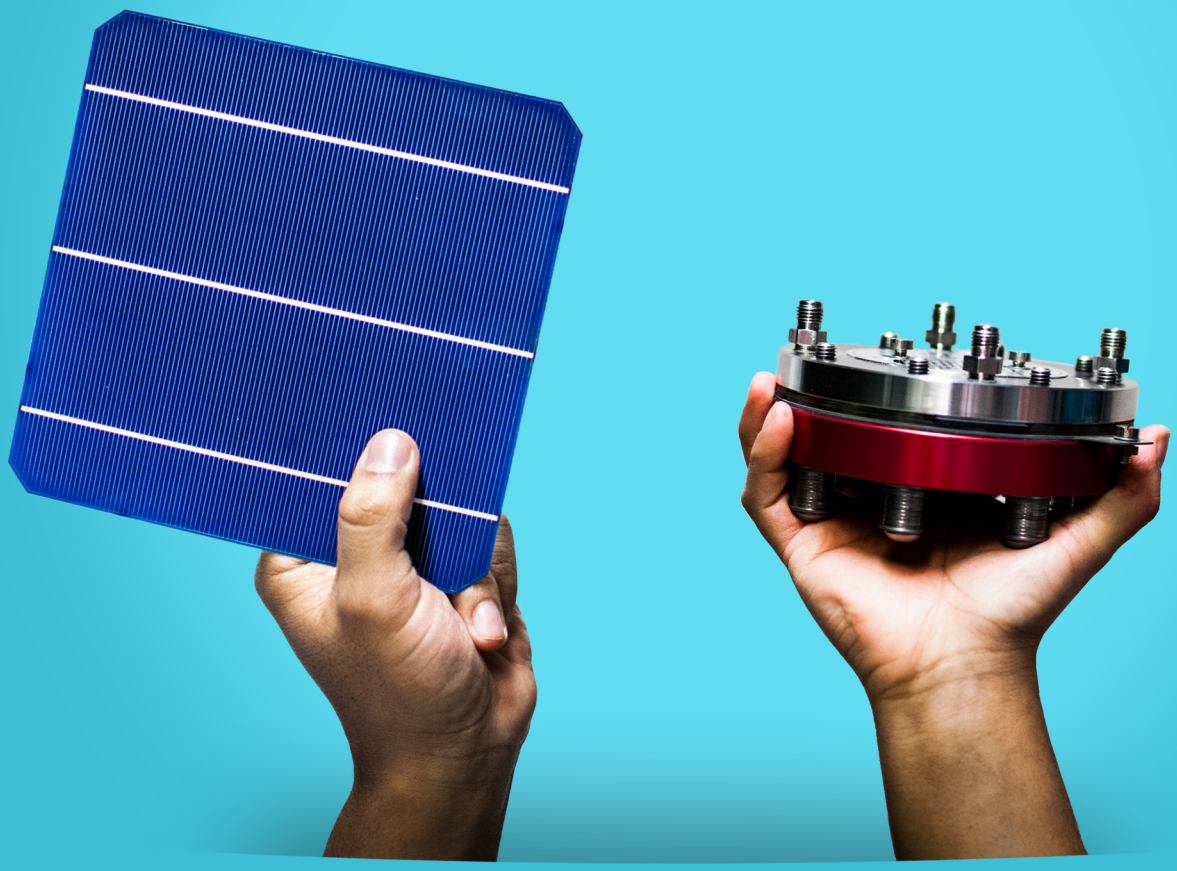

by Esteban Huaca

TU Delft

From Solar to Hydrogen Energy

Modelling, design and construction of a system for hydrogen production using PV solar panels

by

Esteban David Huaca Delgado

to obtain the degree of Master of Science in Sustainable Energy Technology
at the Delft University of Technology,
to be defended publicly on Monday March 12, 2018 at 14:30.

Student number:	4483731	
Project duration:	February, 2017 – March, 2018	
Thesis committee:	Prof. Dr. Arno Smets,	PVMD, supervisor
	Dr. R.A.C.M.M. van Swaaij,	PVMD
	Dr. Mohamad Ghaffarian Niasar,	ESE, external member

TU Delft

I have loved, and I have laughed,
I have hurt, and I have cried,
I have learned, and I have changed,
I have lost, and I have grown,
I have lived. And for all that, I am grateful.

Abstract

Efficiency improvements of solar cells, growth in photovoltaic cells manufacturing, and declining prices of solar modules are just a few of the factors that have allowed solar power to break records (320 GW) in global cumulative installed capacity in 2016. In the energy systems of the future, solar energy will be the predominant energy source. However, the growth in solar power brings new technical challenges to overcome. Power intermittency, grid flexibility, and surplus electricity are just a few of the challenges that must be addressed for the power systems of the future.

In the light of these challenges, this thesis provides new insights in the use of solar energy to produce hydrogen via a PEM electrolyzer. In order to achieve this goal, a hybrid power system model of hydrogen production using solar power was developed using existing modeling approaches. The system consists of a PV array, battery bank, PEM electrolyzer, hydrogen tank, and a power control unit.

The results are structured in two parts. First, simulations of three configurations between the panel and the electrolyzer: (i) direct coupling, (ii)including an MPPT, (iii) including a battery. Second, simulations of one hundred different sized combinations of PV arrays, a battery bank, and an electrolyzer stack. These simulations were analyzed for yearly irradiance levels from Delft.

For each of the three different arrangements in the first part, an analysis of energy yields of the PV array, hydrogen production, system efficiency, and the impact on the electrolyzer lifetime, is performed.

Additionally, *Wawa*, a lab-scale demonstrator system has been designed. *Wawa* was successfully built and tested. *Wawa* provides a practical hands-on understanding the hydrogen production using solar power.

Based on the simulation results for the multiple configurations, it is clear that the lifetime of the electrolyzer can be positively affected by including a battery as an energy buffer. An additional conclusion is that the shape of the irradiance curve plays an important role when sizing the system components.

Hopefully, this research will motivate students to address more in-depth research on how hybrid solar power systems can help to develop the power systems of the future.

Acknowledgements

Kindly I would like to thank a group of people that without their support, I could not have accomplished this project. First of all, I would like to thank Prof. Arno Smets for his supervision and critical feedback. I learned a lot and became an independent and more skilled researcher. Also, to Stefaan Heirman who helped me greatly on the building of the experimental setup with his vast technical knowledge. I am very thankfull for your time and help you dedicate into the desing of the printed circuit board.

To my parents Marcy and Henry, who always supported me to continue my academic education in the first place. I am sincerely thankful for all the support you continuously offered me over the time my masters lasted. I hope my work and dedication make you feel that all of your sacrifices as parents were worth it. To my dear brothers, André and Henry. Your encouragement from the distance when times got difficult are appreciated. I am blessed to have all of you with me. Many loving thanks to Megan, who always was there for me and supported me with loving care from a distance. You will always be in my heart.

Finally, many thanks to all of my friends that I met in Delft. You all made this chapter of my life unforgettable and full of awesome and happy memories. To Rik, Andrés, Irma, and Casper, for continued support and encouragement during my writing process of this thesis. Last but not least, golden thanks to my housemates -from the Sustainable Energy Technology (SET) student house "the Goldmine"- Alex, Andres, Kajan, and Rutger. I would like to express how lucky I feel with our friendship. This journey would not have been the same without you. Thank you for making my experience in the Netherlands more fun, and for always inspiring me to explore new possibilities. I hope the future has plans for us together in some way.

Contents

List of Figures

List of Tables

1

Introduction

This chapter presents a general framework to explain the importance of this research. First, the motivation behind the research is introduced by addressing the most important challenges and opportunities of the enormous growth in photovoltaic electricity. Followed by a section including the research objectives and questions of this thesis. Then, the research approach of this thesis is presented. Finally, the chapter closes with a brief outline of the entire thesis.

1.1. Motivation

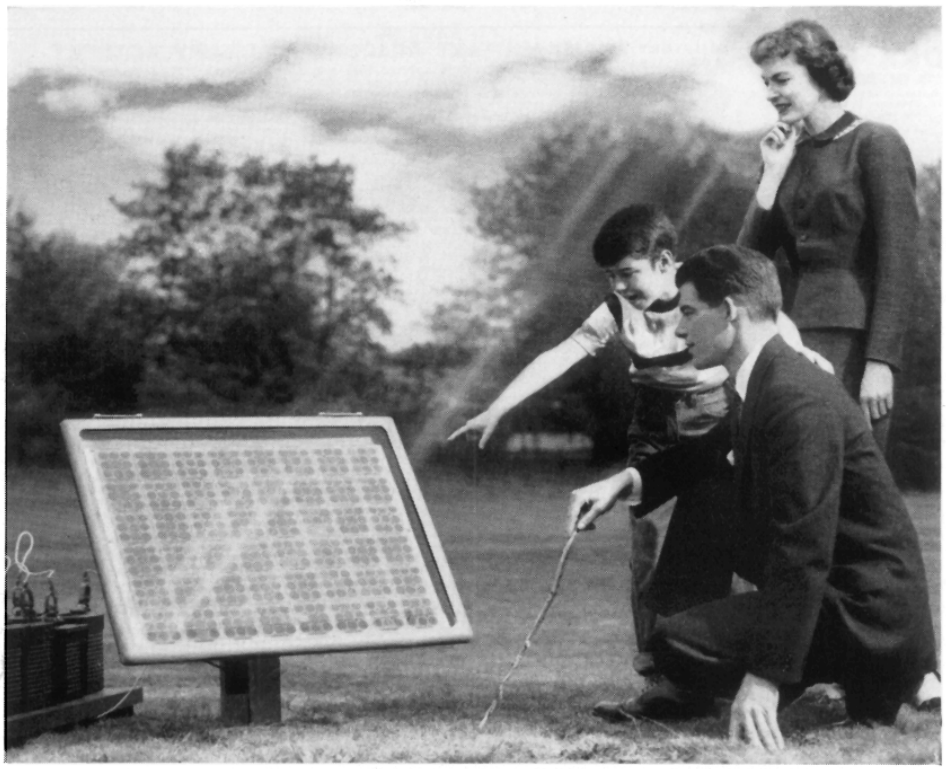

Something New Under the Sun. It's the Bell Solar Battery, made of thin discs of specially treated silicon, an ingredient of common sand. It converts the sun's rays directly into usable amounts of electricity. Simple and trouble-free. (The storage batteries beside the solar battery store up its electricity for night use.)

Figure 1.1: Photography used for the TIME magazine on May 1954 to announce the release of the first commercial solar panel.[2]

For the first time in the history of humanity, in 1954, the Bell Telephone Laboratories announced to the world the successful discovery of a device that was able to convert the sun's rays into useful electricity. This was the first commercial solar cell with about an efficiency of 6%. *"...This device has great possibilities for telephone services and all humanity..."*, quoted the TIME magazine in an article of that year [2].

Sixty-four years later, it turns out that not only the predictions were correct; they even underestimated the utility of solar panels. Photovoltaic (PV) technology has evolved at an amazing speed in the last decade. Both lower prices and higher conversion efficiencies have made solar electricity to become more attractive to the industry and consumers. Steadily, PV technology is becoming one of the most important energy technologies of our time.

The current record lab cell efficiency, for mono-crystalline silicon solar cell, is 26.7% [64]. The price of PV systems reached € 1,270 per kilowatt peak (kW_p) in the German market at the end of 2016 [27]. Furthermore, Trina Solar, the world's largest solar module manufacturer, produced PV modules with a total capacity of 5.74 GW in 2015 [61]. In summary, efficiency improvements, growth in manufacturing, and declining prices are three factors that have allowed the PV technology to break records in installed capacity.

Falling Prices of Photovoltaic Cells

During the last 30 years, the price of solar panels has shown a dramatic decline in price. The cost of solar panels has decreased by a factor of 250, going from $76 in 1977 to $0.30 per watt in 2015. Figure 1.2 shows the experience curve of PV technology, also known as the learning curve. This curve reflects the reductions in costs as a result of technological improvements and economies of scale. In the history of energy technology, there is no record of such a dramatic decrease in price other than for photovoltaic cells [50].

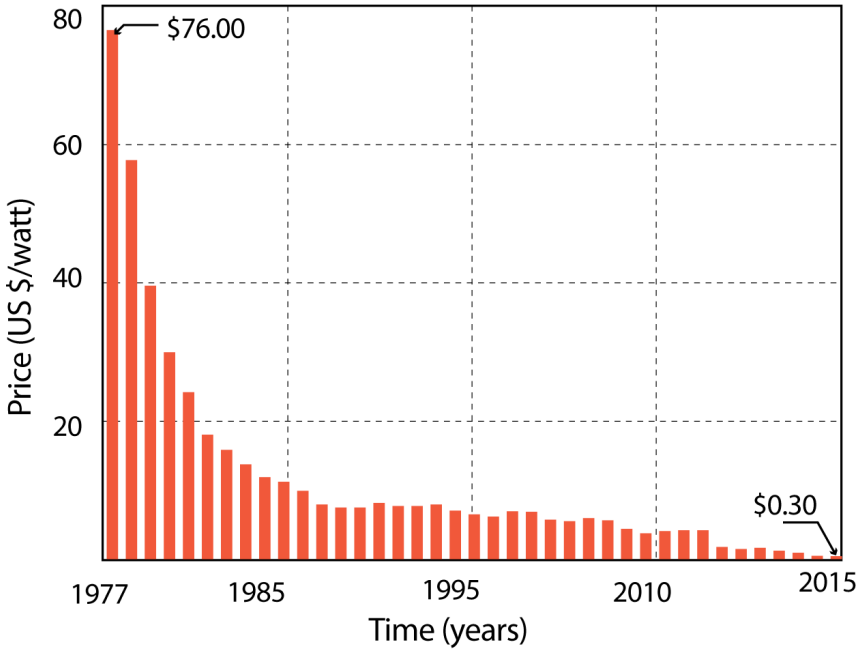

Figure 1.2: Price history of silicon PV cells. (Redrawing by the author) [35]

Learning rates in photovoltaic technology have experienced a very fast increase. PV modules learning rates have gone from 18% in 2010 to 22% in 2016. As a consequence, PV modules price dropped 80% since 2010 [11]. In the same period, the average cost of PV electricity from utility-scale fell from $0.36 to $0.11 per kilowatt-hour (kWh) [11]. Furthermore, the cheapest price ever to supply electricity, a $0.0179/kWh for a 300 MW photovoltaic plant in Saudi Arabia was received by Electricite de France SA in 2017 [12]. Combining the excellent solar resources, the supportive governments and high-efficiency PV technology, even lower cost can be achieved.

When looking at the PV systems cost, the cost of the balance of system (BOS) components is a relevant pa-

rameter. The PV module has the highest share in the cost price of a PV system at 55%, inverter at 11%, and 34% for the BOS [46]. Under a pessimistic scenario, and considering no module efficiency improvements, a BOS cost of €39 per kilowatt peak (kW_p) is expected by 2050. An optimistic prediction for the same year, prognosticates a BOS cost of €29 per kW_p.

Even for pessimistic scenarios, assuming no major technological improvements, it is expected that the photovoltaic industry will continue to experience important cost reductions. Depending on location and solar irradiance, a power cost of $ 0.04 per kilowatt-hour [46] by 2025 and a $0.02 per kilowatt-hour by 2050 is expected. Undoubtedly, solar energy is the cheapest forms of renewable energy. According to a report of Fraunhofer institute from 2015, even a conservative scenario will lead to significant PV growth in the future [46].

Rapid Growth of Solar Power

Declining prices of solar panels along with the necessity to reduce the world's CO_2 emissions create the perfect setting for turning the world's current energy system into one based on solar power generation. During 2016, solar energy was the fastest growing energy source worldwide [34]. For the first time, solar power exceeded the growth in power generation compared to all other power generation forms. Overall, renewable energy sources represent more than three-quarters of the newest electricity additions in 2016 [15]. Furthermore, according to the prediction of the International Energy Agency(IEA), the capacity will significantly grow further in the next five years [14].

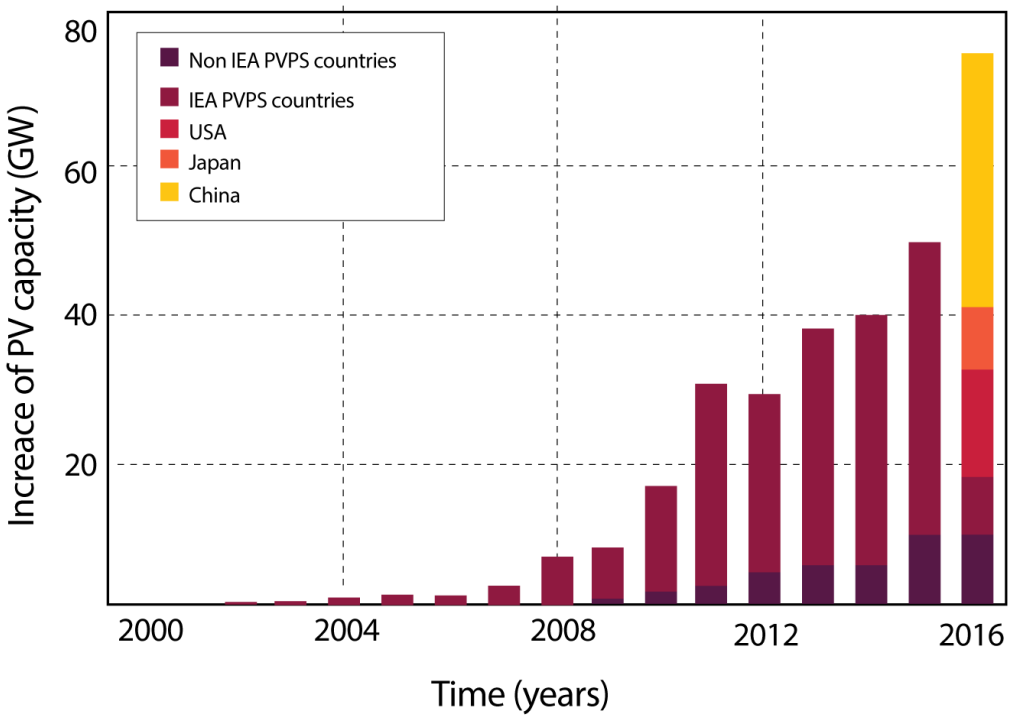

Figure 1.3: Evolution of annual PV installations. (Redrawing by the author) [17]

From 2015 to 2016, the PV installed capacity increased 33%, going from 227 GW to 320 GW of installed capacity. [38]. This was a record in the history of the PV industry. This growth turned the PV technology into the fastest growing energy source in 2016, beating coal and gas with 75 GW of net additions. Leading the new PV installations was China with almost 50% of the installed capacity in 2016. Japan (42.8 GW), Germany (41.2 GW) and the United States (40.3 GW) follow China closely in the total cumulative installed capacity [54]. New to the PV industry are the developing countries as PV is a solution to the strong demand for electricity in rural areas where an electrical grid is lacking. However, due to their lack of financial sources, growth is limited in those countries (see Fig. 1.3).

Worldwide, the PV installed capacity accounts for approximately 1.8% of the electrical power demand of the planet [17]. Overall, coal is still the biggest electricity generation fuel with 9000 TWh. However, from 2015 to 2016 the electricity generation from renewable sources saw an increase in 6.8%, from 5627 TWh to 6012 TWh, mainly due to solar power [51]. In other words, the world's PV installed capacity keeps growing year after year which shows that renewable energy sources will become the dominant energy suppliers of the future.

Climate Change

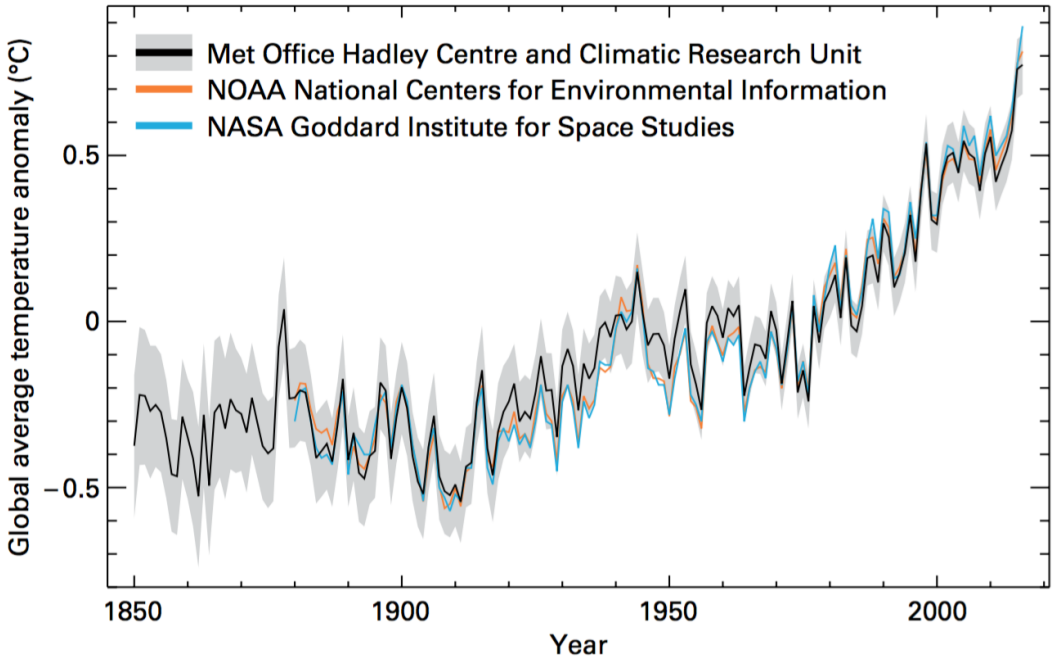

Figure 1.4: Global average temperature anomalies (1961–1990 reference period) for the three major data sets used in this Statement. The grey shading indicates the uncertainty in the HadCRU dataset. (Source: UK Met Office Hadley Centre)[5]

The planet is warming up. The production of energy by burning fossil fuels has been the primary source of carbon dioxide (CO_2) emissions for hundreds of years. Water vapor and CO_2 are the greenhouse gases mainly responsible for global warming. Global temperatures have continuously risen during the last century. During 2016, the global average temperature was 0.99 degree [5] Celsius warmer than in the mid-20th century (Fig. 1.4). This temperature increase made 2016 the hottest year on historical global record.

The increasing levels of carbon dioxide concentration in the atmosphere is one of the biggest challenges modern society is facing. According to the National Oceanic and Atmospheric Administration (NOAA), the carbon dioxide concentration will keep increasing year after year. From 2016 to 2017, the CO_2 levels increased from 404.42 ppm to 406.82 ppm [26]. The increment in 2.8 ppm in one year is relatively high. The latest similar increase was in 1998, with an increment of 2.7 ppm related with a strong El Niño year [4]. Atmospheric CO_2 concentrations are increasing 100 times faster than at the end of the last ice age (see Fig.1.5). Population growth, intensive agriculture, deforestation and increase in worldwide energy use are some of the causes for CO_2 rise concentrations.

Further, higher CO_2 levels means higher global temperature, melting glaciers, rising sea levels and more extreme weather events. One of the most destructive weather events on record was the Atlantic hurricane season in 2017. Hurricanes Harvey, Irma and Maria generated massive destruction in North America. Water and electricity services were not operational for days. Roads were completely destroyed and communication services were shut down. Recovery from such natural disasters will take years, and if temperatures keep rising, the frequency and intensity of similar events will be significantly higher. The effects of climate change are frightening and CO_2 emissions need to stop. Responding to climate change involves a committed society where politicians, educators, and researchers all are part of it.

The most important United Nations Climate Change Conference was hosted in Paris on 12 December 2015.

The output of the conference was the global agreement of 195 nations to combat climate change. The agreement comprises the country's intention to dedicate its efforts to mitigate climate change. The overall goal is to keep the increase of global average temperatures below 2°C. To achieve this goal, nations around the world need to take serious action regarding their pollution levels. Since most of the worldwide energy production is still based on fossil fuel sources, renewable energy generation is a key factor to reduce greenhouse gases.

Many countries support the initiative to an energy transition by implementing policies, and ambitious programs towards a CO_2 reduction. Producing energy from renewable sources is an efficient way to reduce CO_2 emissions. Denmark, for example, has set a target of 100% renewable energy production by 2050 [6]. The strategy to reach this goal is by redesigning the national energy policies motivating the industry to invest in long-term renewable energy technologies.

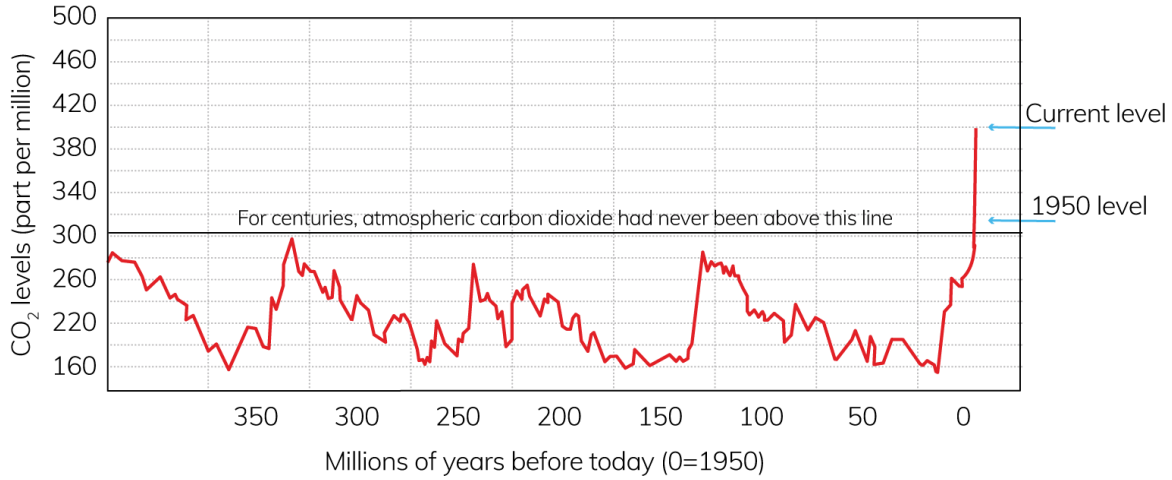

Figure 1.5: The relentless rise of carbon dioxide in the atmosphere (Source: NASA. Redrawing by the author) [13]

Japan has also set ambitious goals. The country's proposal includes a target of emission reduction by 25.4% by 2030 taking the year 2013 as a reference. The country's main effort to reduce emission is by investing more in renewable energy technologies. Taking advantage of the least expensive and vast water surfaces in Japan, Kyocera Corp. has begun the construction of the world's largest floating solar plant. The total power output will be 13.7 MW using 51000 Kyocera solar modules over a surface of 180000 m^2 [8]. This capacity represents a yearly amount of 8170 tons of CO_2 savings into the atmosphere. Furthermore, Japan is working towards a hydrogen society. One of its goals is to reduce the cost of hydrogen to one-fifth of current price by 2050 [7]. The idea behind this strategy is to increase the use of fuel cell vehicles (FCV) on the roads. It is expected to go from 40000 FCV in 2020 to 800000 FCV in 2030[7]. Japan's ambition is to become the world's leading fuel cell market in the near future.

The Green Refinery is another example of a great commitment to climate mitigation. The world's largest dynamic hydrogen electrolysis plant was inaugurated in Germany at the end of 2017 [9]. The heart of the plant is a water polymer electrolyte membrane (PEM) based electrolyzer with 5 MW of electric capacity corresponding to a 10 million euro investment. Also, it is expected the plant saves 2500 [10] tons of carbon output per year. The term "dynamic" means that the electrolysis process will take advantage of every surge in electricity production from wind or solar power plants. Currently, 2% of potential electric power is dumped in Germany because of the mismatch between supply and demand of electricity. The project brings the concept of "Green refinery" which is a clear example of a holistic approach to tackle climate change by reducing CO_2 emissions, increasing the use of renewable energy technologies, and enhancing the power grid stability.

The problem is clear. The Earth is warming up and it is crucial to stop it. Leaders around the world have agreed to mitigate climate change. A solution to this problem is to switch to solar energy and get rid of fossil fuel power generation. Producing electricity by solar photovoltaic panels allows declining both dependency on fossil fuels and CO_2 emissions. The abundance of solar energy over the earth is huge. Approximately, an average of 174.7 W/m^2 of solar irradiance [62] is falling on the earth surface, which represents a theoretical solar potential of 89,300 TW. The worldwide energy consumption can be covered 10000 times.

In conclusion, the growth of solar PV power is as a fact supported not only by its vast potential, the industry growth, and the decreasing price but also by the imperative necessity to reduce CO_2 emissions as an ethical and moral responsibility to all life on Earth.

1.2. Challenges of a New Era for Solar Power

The fast-moving solar power revolution occurring around the world has brought many positive impacts, both environmental and socioeconomic. However, the intermittent nature of solar energy has become a limiting factor. Related to that, there are two main challenges to tackle: negative prices and grid inflexibility

Challenge 1: Negative Market Prices

When power production exceeds the electricity demand, negative electricity prices can be triggered. With traditional fossil fuels, this can be controlled by simply changing the speed of the power generators. With solar power, this feature is not possible, since it depends on the irradiance conditions. When PV panels generate too much power, an adverse effect rises by oversaturating the grid. During those moments, solar electricity production exceeds the required production limits, creating an electricity surplus during low electricity demand moments. As a result of this, negative electricity prices are triggered in the electricity market, during those moments (see Fig. 1.6). An example of this happened in 2016, where German electric companies had to pay consumers to use electricity for few minutes in the day [63]. The same happened in California, US, during July 2017. The sun generated so much solar power that California power suppliers needed to pay consumers in another state to take the excess of electricity. This decision was made to avoid the overloading of the power grid [52].

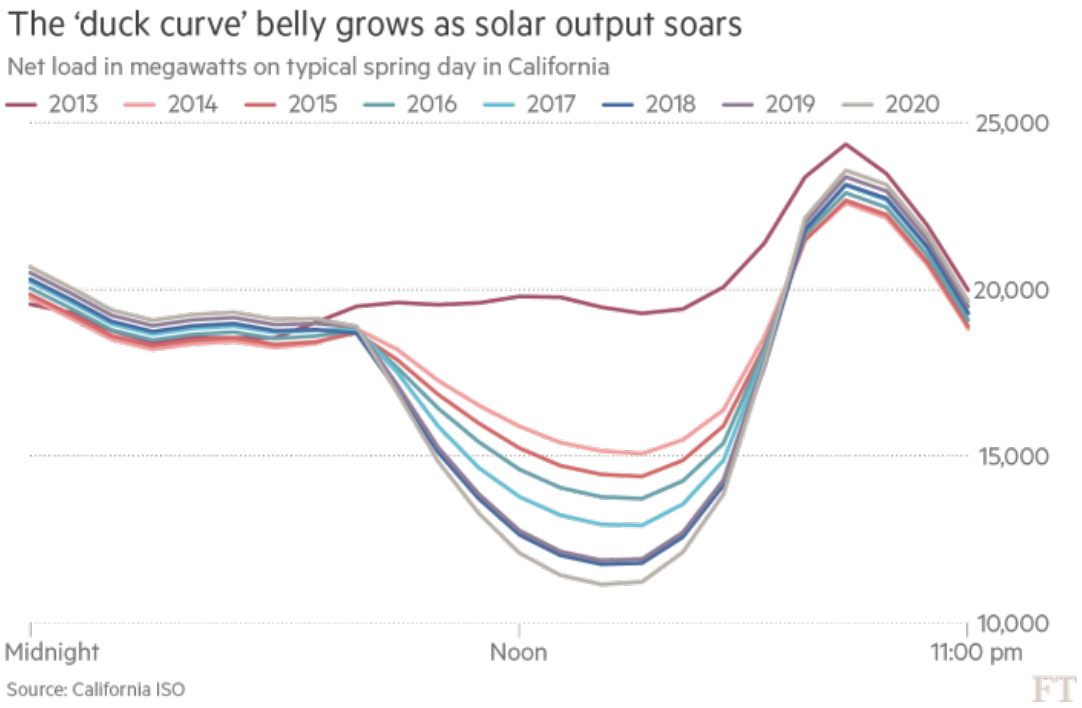

Figure 1.6: Power production in California, over the course of a day that shows the timing imbalance between peak demand and renewable energy production [39]

Challenge 2: Grid Inflexibility

The intermittent nature of solar energy makes it difficult to control its generated power completely. The fact that solar energy depends on external factors to generate power makes it difficult to control the power flowing into the grid. This means that during moments of low irradiance levels, the power-grid administrator cannot rely on the solar plant generators. On the other hand, during a sunny day in summer and low electricity

demand, the grid operator cannot easily stop the solar power generation. Hence, the inflexibility of the grid limits the penetrations of more solar power.

The difficulty associated with integrating variable sources of electricity stems from the fact that the power grid was designed around the concept of large, controllable electric generators. The power grid has minimal storage capacity and without a continuous balance between electricity supply and demand, the system will experience a blackout.

Intermittent renewables are challenging because they disrupt the conventional methods for planning the daily operation of the electric grid. Their power fluctuates over multiple time horizons, forcing the grid operator to adjust its day-ahead, hour-ahead, and real-time operating procedures. The prediction of how much additional electric generation will be produced during the next hour of the day, becomes a very complex problem. This creates an undesirable uncertainty in the power system that limits the capability to calculate exactly what the output of each panel will be. Fast fluctuations in output from solar energy do disrupt not only the hourly load of grid planning but also the second-to-second balance between total electric supply and demand. This causes that the grid operator has more reserve power ready to respond all the time to ensure the grid remains balanced. This intermittency compensation strategy represents a very high cost to the grid operation. Hence, a massive solar power implementation will not only disrupt the grid operation but also create a high operational cost associated with the uncertainty of solar power generation.

Summing up, there is a lack of strategies to manage the clean and intermittent energy being added to the grid. For the utility companies, an increase in installed PV panels means more electric power flowing into the grid. This increase introduces new challenges from technical, economic and regulatory perspectives. Negative electricity prices and grid inflexibility are challenges that need to be tackled in order to allow a massive solar PV power implementation.

1.3. New Opportunities in Photovoltaic Research

In the future it is expected to have more renewable electricity generation, the frequency of having negative prices may also increase. The surplus energy events in Germany and California highlight the necessity to find solutions to reduce the intermittency and inflexibility of power systems that lead to negative market prices due to renewable energy sources. Solutions for those challenges have already been proposed. The most promising ones are: (1) Integration of storage battery systems, (2) Alleviating power systems by producing fuel in an electrochemical process (electrolysis) and (3) Integration of hybrid power systems. Those three opportunities are further described in this section.

Opportunity 1: Battery Systems Integration

An already existing and mature solution to tackle the challenge of an inflexible power system is the use of large-scale battery systems. Batteries allow the storage of excess electricity to be used during times when there is a lack of sunshine. Using batteries allows the power operator to improve the grid flexibility by storing the excess of energy instead of turning off the power plant or triggering negative prices.

Since 2014, new large-scale storage projects started to develop all around the world, incentivized by the decreasing prices of batteries (see Fig. 1.7). A total installed battery capacity of 1650 MWh was predicted by the end of 2017, according to a report published by the Bloomberg New Energy Finance group [25]. Last year's battery price reduction along with the increase of large-scale projects make the battery technology a feasible solution to tackle the challenge of inflexible power systems. However this alternative is limited to short periods of time, and the effectiveness of this solution is a function of the electricity prices during charging and discharging periods [37].

Opportunity 2: Electrolysis Systems Integration

Electrolysis is another promising alternative to alleviate power grid and energy storage as it consumes the electricity delivered directly from the solar panels and uses it to produce hydrogen gas. Hydrogen is an energy carrier, and it can be used in many ways. For instance, hydrogen can be used directly to run a fuel cell and generate electricity. In addition, it can be combined with nitrogen to produce ammonia. Another promising

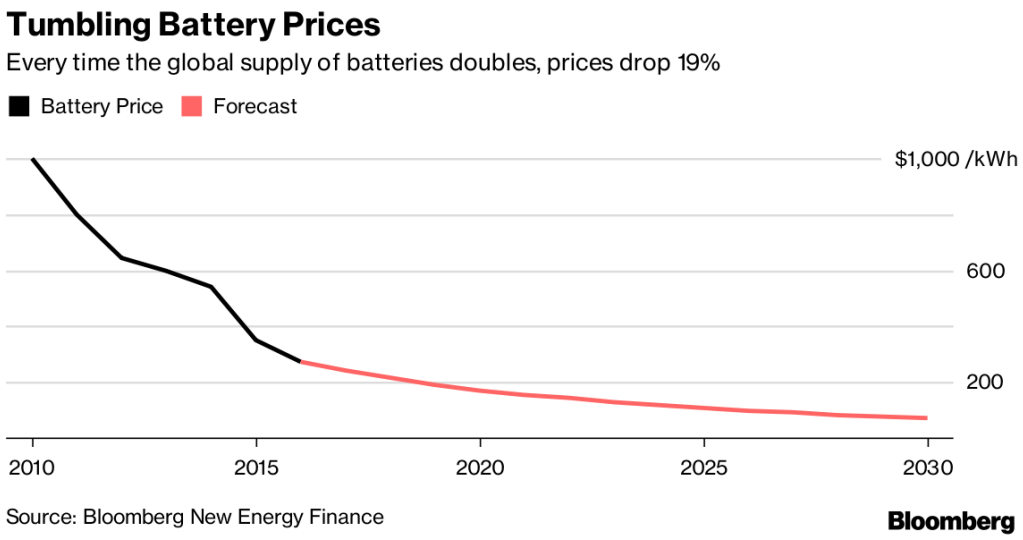

Figure 1.7: Battery price drop [25]

alternative is to let hydrogen react with carbon dioxide to produce synthetic natural gas. The concept of using electricity to generate hydrogen and let it react with carbon dioxide is known as Power-to-Gas (P2G).

Power-to-gas demonstrates that electrolysis is a promising alternative to solar electricity consumption and can alleviate pressure on the power grid and improve the balance within electrical systems. At the same time, it promotes the reduction of CO_2 by incentivizing the use of more renewable energy. Consequently, the concept of P2G is an alternative to effectively use the excess of renewable electricity instead of dumping it or creating negative electricity price.

Opportunity 3: Hybrid Power Systems Integration

Another alternative to tackle the fluctuating nature of renewable energy sources is the use of a hybrid power system. This kind of system involves a combination of more than one energy source. For instance, solar energy as the primary source and fuel cells as a controllable secondary source. This type of systems also includes components like, battery bank, electrolyzer units and extra power electronics. The main characteristic of those systems is the possibility to control the energy fluctuations of the primary source. By this, the system becomes more efficient and reliable. Challenges for hybrid power system include the development of power control management that is able to quickly respond to any load fluctuation.

1.4. Research Questions

The primary objective of this research is to gain fundamental insights into the promising process for hydrogen production using solar power. A second objective is to provide some general design rules of a solar-to-hydrogen system, along with the performance assessment of each component and the whole operation of the system. Literature review shows that there is a limiting knowledge about the sizing of each of the components in a solar-to-hydrogen system and also for the assessment of its performance. There is a need to understand how the solar-to-hydrogen system performs and what critical parameters need to be considered when designing such a system. Consequently, power suppliers, engineers, and students would benefit from a more profound knowledge of the specific operation and limitations of a solar-to-hydrogen system. Thus, the central research question of this study is:

How to gain fundamental understanding in the design, operation, and assessment of a system for hydrogen production via PEM electrolysis using solar panels?

To be able to answer the main research question (RQ), the following sub-questions have formulated:

- **RQ 1:** Which components need to be considered when designing a solar-to-hydrogen system?
- **RQ 2:** How does the irradiance levels affect the system performance when producing hydrogen with solar power?
- **RQ 3:** What is the impact of using a battery unit in a solar-to-hydrogen system?
- **RQ 4:** What are the critical parameters when producing hydrogen via PEM water electrolysis?
- **RQ 5:** What are the sizing guidelines for a solar-to-hydrogen system?

1.5. Research Approach

With regard to the research questions, two research approaches are developed: (1) a data analysis research approach, and (2) a quantitative experimental approach. The research approach focused on data analysis is based on computer simulation results. The performed simulations are taken from a computational model replicating a solar-to-hydrogen (S2H) system. The model contains the main components of a S2H system allowing to understand the relationship of variables such as irradiance, voltages, currents, battery state of charge, temperatures, gas production, and water consumption. The model was developed using Matlab/Simulink based on the physical theory behind each component.

The quantitative experimental research approach was done by designing and building a small-scale hydrogen production system. The design includes two multi crystalline silicon solar module (300 W_p each), a battery bank of two 24 V-70 Ah lead-acid battery, a charge controller with a maximum power point tracker (MPPT), a single cell PEM water electrolyzer (120 W rated power), and a house-made printed circuit board using an Arduino microcontroller. Additionally, the system includes some supplementary components to connect and sense the system signals. The experimental setup may also be used in further laboratory applications to help and motivate students to learn about the system energy flow, the system efficiency, and implementing interesting system configurations for different working conditions.

The present thesis was developed adopting the two above described approaches to explore more about the hydrogen production using solar electricity. The computer modeling allows a fast and easy simulation for different system configurations. And, the experimental research allows a hands-on investigation of the system operation.

1.6. Thesis Outline

Chapter 2 provides a theoretical background of fundamental concepts about solar energy and water electrolysis. Also, an overview of previous studies and their key results along with the challenges involved to produce hydrogen via electrolysis using solar electricity (to answer RQ 1).

Chapter 3 describes the components used to build the experimental setup and the general guidelines for the system operation. (to answer RQ 4).

Chapter 4 presents the developed model for each component of the system using Matlab/Simulink, and the description of the performed simulations in this thesis. The chapter closes describing six-non dimensional factors to assess the system performance (to answer RQ 1, RQ 5).

Chapter 5 presents the results of the computer simulations. Three main system configurations were analyzed: (1) system operation for direct coupling, (2) system operation including an MPPT, (3) system operation including a battery bank. Additionally, simulations of several combinations of several size components to evaluate the system performance by using six non-dimensional sizing factors (to answer RQ 2, RQ 3, RQ 4).

Finally, Chapter 6 closes with the concluding results generated by this study, thus answering the central research question.

2

Literature Review

This chapter starts introducing the basics concepts of solar cells and its operational principles. Next, the fundamental electrochemistry and thermodynamic concepts of water electrolysis are introduced. Then, the hydrogen production using solar electricity is presented. Additionally the concept of power-to-gas along with its main characteristics and advantages is introduced. Furthermore, a compilation of selected studies discussing: (1) performance, (2) operation, and (3) designing aspects of solar-to-hydrogen systems are presented. Finally, the importance of this thesis research is presented.

2.1. Photovoltaic Basics

2.1.1. Solar Radiation

Occupying more than 99.68% [57] of the total mass in the solar system, the Sun, is the biggest and closet star to us. Nuclear fusion reactions, taking place in the core of the Sun, are responsible of all its energy. The Sun emits some of its energy to the entire universe as electromagnetic radiation. Ideally, the Sun can be considered as a black body with a temperature of 5800 K.

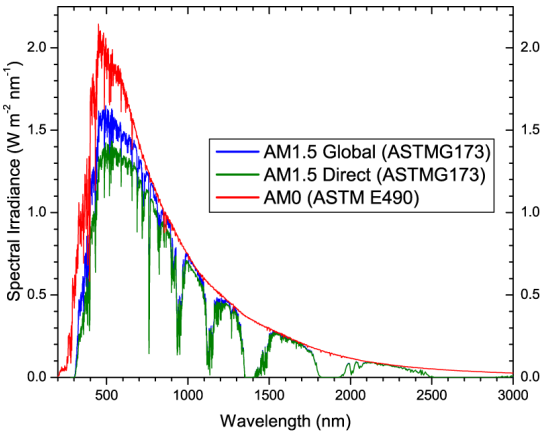

Figure 2.1: Standard Solar Spectra for space and terrestrial use.[3]

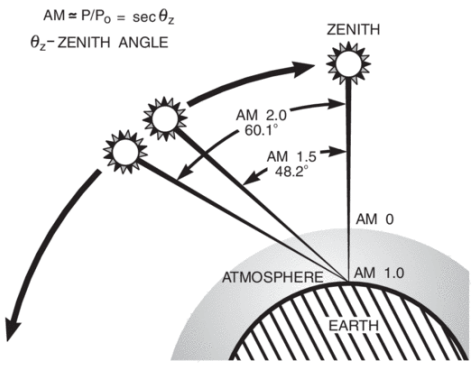

Figure 2.2: Spectral conditions in units of Air Mass changing with the zenith angle. [56]

The amount of solar radiation reaching the Earth at the outside of the atmosphere is approximately 1362 W/m^2 [60]. When the solar radiation penetrates the Earth's atmosphere, it gets attenuated. The air and dust in the atmosphere are responsible of the solar irradiance reduction. Also, the relative position between the

Earth and the Sun, highly influence the intensity of solar irradiance. This reduction in solar irradiance can be quantified by using the concept of the Air Mass (AM). For space applications, the air mass coefficient is referred as AM0. The reduced spectral illumination after traveling through the atmosphere, in a plane perpendicular to the Sun's direction is defined as AM1.0. This spectral conditions change by the angle θ with the zenith as illustrated in figure 2.2.

The actual amount of solar radiation over a specific location in the Earth's surface is extremely variable. Thus, some reference conditions has been establish for evaluation and comparison purposes, of solar cells. These conditions include spectrum, intensity and temperature with values of: AM1.5 spectrum, 1000 W/m^2 and a cell temperature of 25°C.

The variations of the solar spectrum are important for the design and optimization of solar cells. For a different wavelength region in the solar spectrum, a different solar cell technology might be more suitable, based on the bandgap energy of the photovoltaic active material. Also an understanding of the solar irradiance availability is important for an optimal design of a photovoltaic system.

2.1.2. The Solar Cell

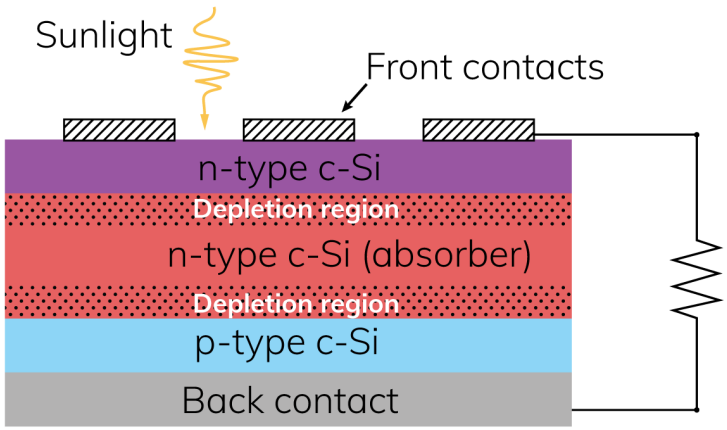

Figure 2.3: Simplified representation of a solar cell. (Redrawing by the author) [57]

The energy from the sun can be directly converted into electricity by using a solar cell. A solar cell is an electronic device made from a semiconductor material. Crystalline silicon is one of the most used materials for solar cells. Almost all solar cell consists of essential layers to make it operate as a solar cell. The layers of a solar cell contains junctions of different materials or doping. Doping is a technique used to change the concentration of either the electrons or holes in semiconductors. For instance, increasing the electron density creates an n-type material. On the contrary, the absence of electrons in a material creates holes. A material with holes as majority charge carriers is called p-type [57].

A simplified structure of a conventional solar cell consist of few essential layers to make it operate as a solar cell. First,as a central layer, a crystal silicon absorbent. Between this layer, a p-n junction is located in each side, to separate the light-excited carriers. To collect the electrons, a metal contact on the front and back side is located. Figure 2.3 represents a simplified silicon based solar cell.

2.1.3. Working Principle of Solar Cells

Useful electricity can be directly generated by a solar cell, when it is exposed to electromagnetic radiation. The principle behind that phenomenon is called the *photovoltaic effect* [57]. This is, the generation of an electric potential difference at the junction of two different semiconductor materials, when this is exposed to light.

The photovoltaic effect can be explained in three simple processes: (1) generation of charge carriers, (2) separation of the photo-generated charge carriers, and (3) collection of the photo-generated charge carriers.

First, charge carriers are generated when a photon is absorbed in a p-n junction. Those charge carriers are electron-hole-pairs. The charge carrier generation is possible when the photon energy (E_{ph}) is higher than the bandgap energy (E_g) of the material [57].

Second, the excited electron-hole pair will try to find its equilibrium state by recombining. This means that the energy in the material will be lost. To avoid this, a semipermeable membrane, inside solar cell, collects the electrons into the n-type, and holes in the p-type.

Finally, the electrons are collected at the metallic electrodes of the solar cell. As a result, an electrical current is deliver by the solar cell, when this is connected to a load [57]. Figures 2.4 and 2.5 show the basic steps of the solar cell operation.

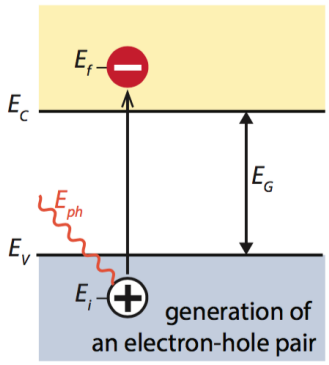

Figure 2.4: Illustration of the electron hole generation by a photon in a semiconductor with a bandgap energy E_G. [57]

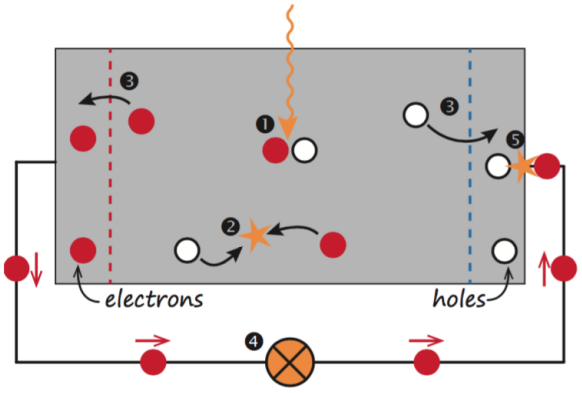

Figure 2.5: Illustration of the basic steps in a solar cell. [1] Absorption of a photon generates an electron-hole pair. [2] Electron-hole recombination. [3] Electron-hole separation by a semipermeable membrane. [4] Generated electric current. [5] Electron-hole recombination. [57]

2.1.4. External Parameters of Solar cells

Solar cells are characterized by four main parameters: (1) the short-circuit current density, (2) the open circuit voltage, (3) the maximum power, and (4) the fill factor. Further, these parameters are tested at standard test conditions and can be represented in a current voltage (I-V) characteristic curve.

Short Circuit Current (J_{sc})

The current density delivered by a solar cell at 0 V bias is defined as the short circuit current density J_{sc}. This current is generated when the electrodes of the solar cell are short circuited. This value highly dependent on the photon flux over the solar cell, the area and the material properties of solar cell [57].

Open Circuit Voltage (V_{oc})

The voltage under open circuit conditions of a solar cell is referred as the open circuit voltage [57]. This value is the voltage at which no current flows through the external circuit. The V_{oc} depends on the material properties and photocurrent density. The V_{oc} value can be calculated using Eq. (2.1)

$$V_{oc} = \frac{k_B T}{q} \ln\left(\frac{J_{ph}}{J_o} + 1\right) \approx \frac{k_B T}{q} \ln\left(\frac{J_{ph}}{J_o}\right) \tag{2.1}$$

where, $k_B = 1.38 \times 10^{-23} J/K$, is the Boltzmann's constant, $q = 1.602 \times 10^{-19} C$, is the elementary charge, T is the cell's temperature in kelvin (K), J_{ph} is the photo-generated current density and J_o is the saturation current. The approximation, in Eq. (2.1), is justified because $J_{ph} >> J_o$ [57].

Maximum Power (P_{max})

The maximum produced power P_{max} from a solar cell is the operational point of the solar cell at which $V \times I$ maximizes. This point is where the solar cell can deliver its maximum electrical power at a certain level of irradiance.

Fill Factor (FF)

The fill factor is defined as the ratio between the maximum power generated by the solar cell and the product of the open-circuit voltage and short-circuit current [57], as shown in Eq. (2.2). Where, $P_{max} = J_{mpp}V_{mpp}$ stands for the power at the maximum power point (MPP). The fill factor provides a relative quality index of the solar cell. For instance, the best crystalline silicon solar cell, has a FF=0.846, achieved by Yoshikawa [64]. For different technology, like GaAs solar cell, a FF=0.89 has been achieved [57].

$$FF = \frac{P_{\max}}{J_{sc}V_{oc}} \tag{2.2}$$

2.1.5. Solar cells performance

The performance of a solar cell is evaluated by its efficiency. This parameter is equal to the ratio between the energy output delivered by the solar cell, and the input energy from the sun (I_{in}), as shown in Eq.(2.3). The efficiency is the most commonly used parameter to compare the performance of one solar cell to another. The efficiency of a solar cell can significantly change for different temperature and irradiance conditions. Thus the efficiency is measured under the standard test conditions. The highest efficiency record for a crystalline silicon solar cell is 26.6% [64].

$$\eta = \frac{P_{\max}}{I_{in}} = \frac{J_{sc}V_{oc}FF}{I_{in}} \tag{2.3}$$

2.2. Fundamentals of Electrolysis

2.2.1. Redox Reaction

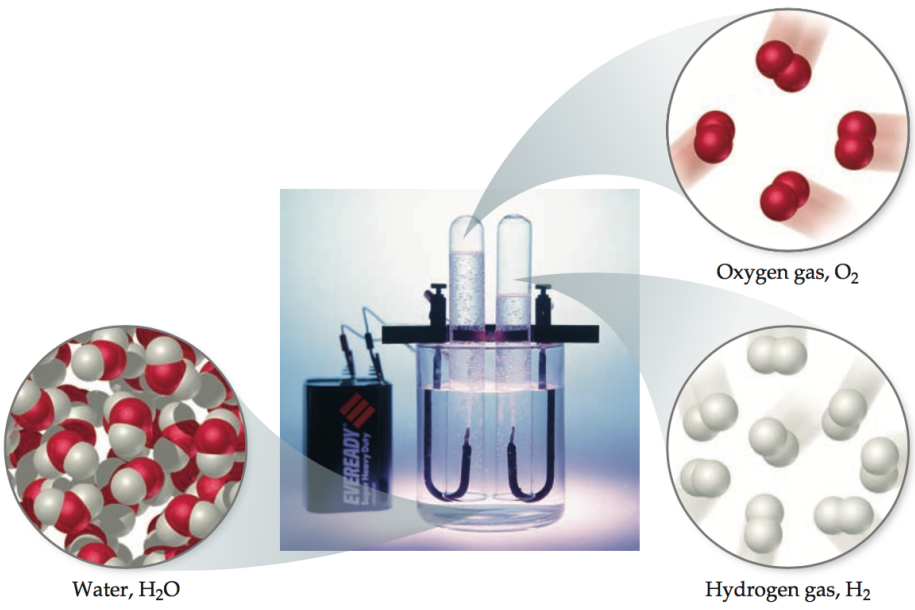

Figure 2.6: Electrolysis of water. Water decomposes into its component elements, hydrogen and oxygen, when an electrical current is passed through it. The volume of hydrogen, collected in the right test tube, is twice the volume of oxygen.[20]

Electrolysis is the electrochemical process to split water into hydrogen and oxygen. This process involves a reduction-oxidation reaction. In general, an electrolyzer is composed of an anode (positive electrode), a cathode (negative electrode) and an electrolyte. For starting the electrolysis, a voltage must be applied between the two electrodes. Under applied voltage, the positively charged ions migrate to the negative electrode, where these gain electrons and are reduced. Conversely, negatively charged ions move to the positive electrode losing electrons and oxidizing. As a result, hydrogen is generated in the cathode and oxygen in the anode. The governing reaction of electrolysis is expressed by Eq. (2.4). Figure 2.6 illustrates a simple setup of the water electrolysis .

$$H_2O_{(l)} \rightarrow H_{2(g)} + {}^1/_2 O_{2(g)} \tag{2.4}$$

Based on the type of electrolyte, there are three main type of electrolyzers: (1) alkaline, (2) proton exchange membrane (PEM) , and (3) solid oxide. Depending on the nature of the electrolyzer (acid or basic), the anode and cathode experience different reactions. Table 2.1 summarizes the electrochemical reactions occurring in the three types of electrolysis. Figure 2.7 shows a schematic representation of the three electrolyzer configurations and the direction of the reactions. A short comparison between alkaline and PEM is shown in table 2.2.

Table 2.1: Anode and Cathode reactions for three type of electrolyzers

	Alkaline	**PEM**	**Solid Oxide**
Anode	$4OH^- \rightarrow 2H_2O + 4e^- + O_2$	$2H_2O \rightarrow 4H^+ + 4e^- + O_2$	$2O^{2-} \rightarrow 4e^- + O_2$
Cathode	$4H_2O + 4e^- \rightarrow 4OH^- + 2H_2$	$4H^+ + 4e^- \rightarrow 2H_2$	$2H_2O + 4e^- \rightarrow 2O^{2-} + 2H_2$

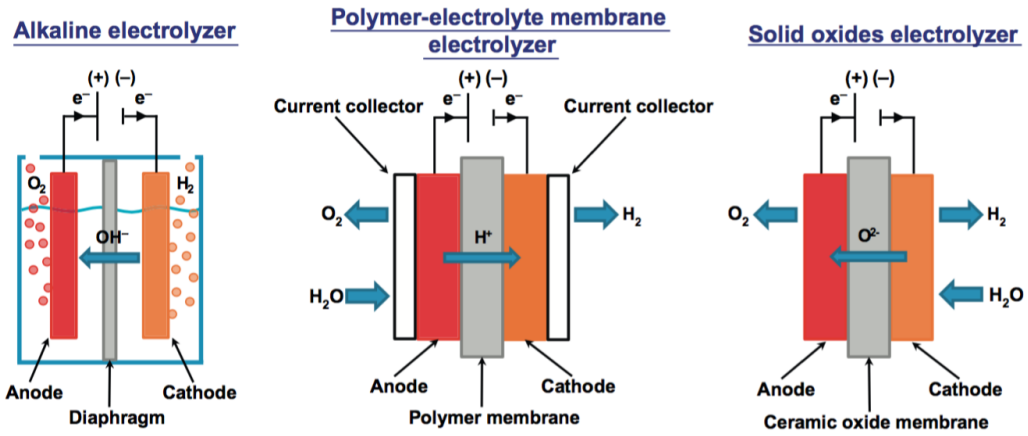

Figure 2.7: Schematic representation of different water electrolysis for water splitting. [24]

Understanding the nature of reactions and the technology of the electrolyzer is important to select the most suitable method. Temperature and pressure are two important parameters to keep in mind when choosing the electrolyzer. Also, size lifetime and price are important parameters when selecting the electrolyzer technology.

2.2.2. Electrochemistry and Thermodynamics

From the electrochemical perspective, the energy required for water splitting can be obtained from the standard potentials, for the two half reactions. The standard potential measures the ability of an element to start

Table 2.2: Comparison of water electrolysis methods [22]

Parameter	**Alkaline electrolyzer**	**PEM electrolyzer**
Cell temperature (°C)	60 - 80	50 - 80
Cell pressure (105 Pa) (bar)	<30	<30
Current density (mA cm^{-2})	0.2 - 0.4	0.6 - 2.0
Cell voltage V	1.8–2.4	1.8–2.2
Power density (mW cm^{-2})	< 1	< 4.4
Efficiency (HHV) (%)	62 - 82	67 - 82
Specific energy consumption stack (kW h) (Nm^3)	4.2 - 5.9	4.2 - 5.6
Partial load range (%)	20 - 40	5 - 10
H2 production rate (Nm^3 h^{-1})	< 760	< 10
Lifetime stack (h)	< 90 000	< 20 000
Degradation rate (mV h^{-1})	< 3	< 14

reducing at 1 atm and 298 K. For a PEM electrolyzer, the reactions and standard potentials for the anode and cathode are given by expressions (2.5) and (2.6).

$$Anode: \quad 2H_2O \rightarrow 4H^+ + 4e^- + O_2 \quad E^o = -1.23V \tag{2.5}$$

$$Cathode: \quad 4H^+ + 4e^- \rightarrow 2H_2 \quad E^o = 0V \tag{2.6}$$

Then, the standard cell potential (E^o) for the complete reaction of water electrolysis is given by the equation (2.7)

$$E^o = {E^o}_{cathode} - {E^o}_{anode} = 1.23V \tag{2.7}$$

At standard conditions, water splits into hydrogen and oxygen when a voltage of at least 1.23 V is applied to the electrodes. This potential is the reversible voltage required to split water electrolytically [22]. This means that all the energy supplied to the reaction will be maximized to only split water with zero heat losses. The second law of thermodynamics tell us that this will never occur. The reversible voltage is related to the Gibbs free energy (ΔG^o) by the equation (2.8).

$$E^o = \frac{\Delta G^o}{nF} \tag{2.8}$$

where, n= 2, is the number of electrons involve in the reaction, and F=96485 C/mol, is the Faraday's constant. Substituting values in equation (2.8) results in a Gibbs free energy value of ΔG^o= 237.22 kJ/mol [48].

From the thermodynamic perspective, the energy needed to split water can be determined by the change in enthalpy (ΔH^o). This energy involves the internal energy of the system (ΔG^o), and the amount of energy transferred as heat ($T\Delta S^o$). The thermodynamic relationship is expressed by Eq. (2.9).

$$\Delta H^o = \underbrace{\Delta G^o}_{electricity} + \underbrace{T\Delta S^o}_{heat} \tag{2.9}$$

By application of equation (2.9), the Gibbs free energy ΔG^o= 237.22 kJ/mol, and the ideal entropy (ΔS^o = $0.163 kJ\ mol^{-1}\ K^{-1}$) of gaseous water at standard conditions (298 K and 1 atm) [48], the standard entalphy change of formation of liquid water results in a value of $\Delta H^o = 285.8\ kJ/mol$.

The electrical potential related to enthalpy energy change is commonly called thermoneutral voltage (${V^o}_{tn}$) [24]. Using ΔH^o in equation (2.8), the thermoneutral voltage to split water, at standard conditions, is V_{tn} =

1.48 V. This value represents the global energy required for the reaction to occur. An electrolyzer with operating voltage equals to 1.48 V would be 100% efficient. In reality, a further potential needs to be applied to accelerate the reaction to a practical rate.

Summarizing, the thermoneutral ($V^o{}_{tn}$) and reversible (E^o) voltages establish the conditions for the electrolysis process. When the applied voltage is lower than the reversible voltage ($V_{cell} < E^o$), the reaction does not occur. If the applied voltage is between $V^o{}_{tn}$ and V_{rev}, extra heat is required to operate the reaction. And when the applied voltage is bigger than the thermoneutral voltage ($V_{cell} > V_{tn}$) the reaction occurs and produces heat [24].

Figures [2.8 and 2.9] illustrate the temperature dependence of the energy and voltages involved during water electrolysis. The increase in thermal energy during water electrolysis is compensated by the decrease in electrical energy in the process.

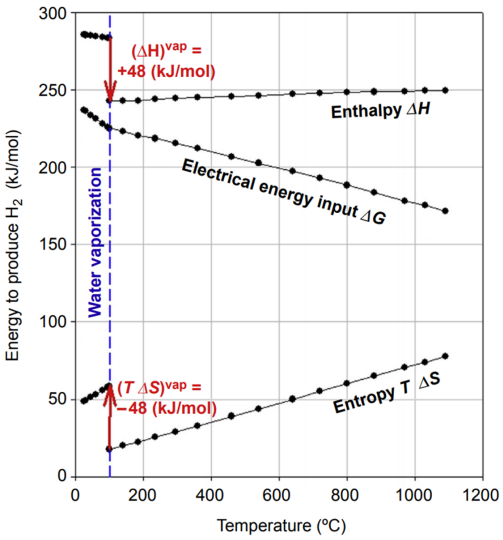

Figure 2.8: Temperature dependence of main thermodynamic parameters for water electrolysis at 1atm. [48]

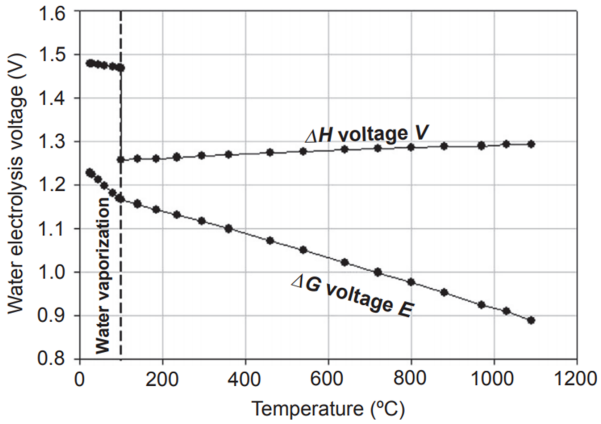

Figure 2.9: Thermodynamic and enthalpy water splitting voltages as a function of operating temperature at 1atm. [48]

Nerst Equation

All the thermodynamic values in equation (2.9) are temperature and pressure dependent. For conditions different than 1 bar and 298 K, the voltage to start the reaction significantly changes. The effect of pressure and temperature in the reversible potential can be evaluated by using the Nerst equation [24], expressed by Eq. (2.10)

$$V_{tn} = E^o + \frac{RT}{2F} \ln\left(\frac{[p_{H_2}][p_{O_2}]^{1/2}}{[p_{H_2O}]}\right) \tag{2.10}$$

where, T is the temperature in kelvin (K), R=8.314 J$\cdot$ mol$^{-1} \cdot K^{-1}$, is the universal gas constant, and p_x are the partial pressure of each of the species.

2.2.3. Kinetics Aspects

Practically speaking, to produce hydrogen from water a voltage significantly higher than the reversible potential is needed. As current density increases the cell losses due to membrane, electrode, and interfacial resistances become more important and are known as overpotentials (ΔV) [55]. This, results in a overall cell potential (V_{cell}) equal to the standard potential (E^o), plus the overvoltage (ΔV). The overvoltage has three main components: (1) activation, (2) concentration, and (3) ohmic, as presented in Eq. (2.11)

$$V_{cell} = V^o{}_{tn} + \Delta V_{act} + \Delta V_{con} + \Delta V_{ohm} \tag{2.11}$$

Ohmic Overpotential
The ohmic overpotential (ΔV_{ohm}) is mainly caused by electrical resistance in the conductors, the electrodes and across the proton exchange membrane. The membrane cause a resistance to the hydrogen ions passing through it. This resistance is related to the humidification, thickness and temperature of the membrane [47]. The energy loss regarding to ohmic voltage is transformed into heat during the electrolysis process, which most of it is carried out by the reactant water. The relation between voltage and current is relatively linear, defined by Ohm's law as $V_{ohm} = i_e \cdot R_{ohm}$, where, i_e, is the electrolyzer current; and R_{ohm} is the equivalent resistant in the electrolyzer.

Activation Overpotential
The activation overpotential is a measure of the activity in the electrodes [47]. The activation overpotential (ΔV_{act}) is caused by the reaction interface between anode/membrane and cathode/membrane. Both anode (η_a) and cathode (η_c) overpotentials, represent irreversible losses and become dominant at lower current densities in a PEM electrolyzer [55]. The activation overpotential in a PEM electrolyzer is much smaller in the anode than in the cathode [47]. Equations (2.12) and (2.13) are empirical expressions developed to determine the activation overpotential in function of the current density for both anode and cathode [55].

$$\eta_a = \frac{RT}{\alpha_a zF} \ln\left(\frac{i}{i_{a,o}}\right) \tag{2.12}$$

$$\eta_c = \frac{RT}{\alpha_c zF} \ln\left(\frac{i}{i_{c,o}}\right) \tag{2.13}$$

where, α_x, are the electron transfer coefficients of each electrode, $i_{x,o}$, are the exchange current densities in (A cm^{-2}) for each electrode and i, is the current density of the stack in(A cm^{-2}). The electron transfer coefficient is a measure of the symmetry of the activation energy barrier and can range from 0 to 1 [19].

Concentration Overpotential
The concentration overpotential (ΔV_{con}) is caused due to the mass transport limitations. This transport limitation involves the depletion of charge-carriers at the electrode surface. At lower current this potential can be neglected, however at significantly higher currents when the reactions are at higher rate, the concentration overvoltage becomes relevant. The concentration overpotential can be neglected during normal operation conditions, because the gas transport limitations in PEM electrodes are insignificant [47]

Understanding the kinetics involved in water electrolysis is important to reduce losses, and make the process more efficient. Furthermore, reducing the overvoltages can lead to significant energy savings in the hydrogen production. The three main overpotentials involved during water electrolysis are graphically represented by the I-V characteristic curve of the electrolyzer as shown in Fig. 2.10.

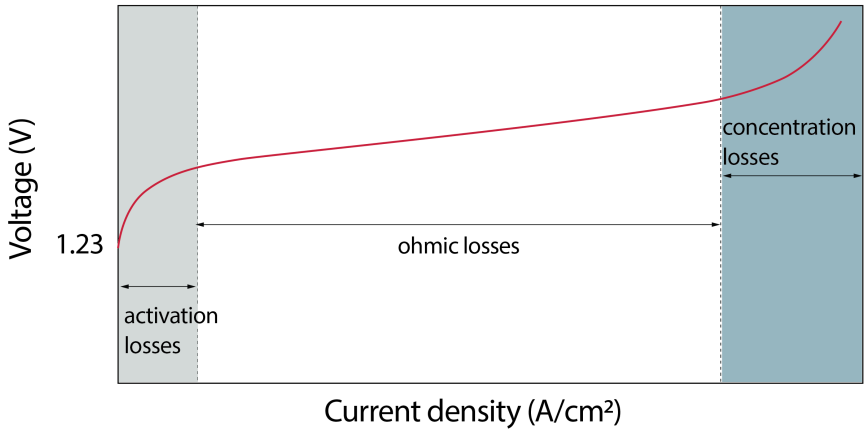

Figure 2.10: Polarization curve depicting three main losses attributed to PEM electrolysis cell operation. (Redrawing by the author)[47]

Polarization Curve
The operation of an electrolyzer is characterized by the current density and voltage (I-V) curve or also known

as polarization curve. This curve includes information of the potentials and currents involved during the electrolysis process at specific temperature and pressures. For a PEM electrolyzer the characterization is made at 1 atm and 298 K. Three main regions, representing the energy losses, are identified in a polarization curve: (1) activation losses, (2) ohmic losses and (3) mass transport or concentration losses. Figure 2.10 depicts the losses attributed to a PEM electrolyzer.

2.2.4. Efficiency

The efficiency of a water electrolyzer is equal to the ratio between the energy content in the produced hydrogen and the electrical energy supplied to the process. The energy content in a specific amount of hydrogen can be calculated by using the molar higher heating value (HHV=283.6 kJ/mol) [53]. This value is the amount of energy produced per number of molecules, by the complete combustion of hydrogen. The energy efficiency of the electrolyzer (η_{el}) can be calculated by Eq. (2.14).

$$\eta_{el} = \frac{\dot{n}_{H_2} \cdot HHV}{P_{in}} \tag{2.14}$$

where, $\dot{n}_{H_2}$ is the molar rate of hydrogen produced in (mol/s), $P_{in} = i_e \cdot V_{cell}$ is the total power supplied to the electrolyzer in kilowatts (kW). An alternative version for the electrolyzer efficiency as its voltage function (V_{cell}), is given by Eq. (2.15).

$$\eta_{el} = \frac{1.48}{V_{cell}} \tag{2.15}$$

Hydrogen mass flow rate

The amount of hydrogen produced, by water electrolysis, is directly proportional to the electrical current passing through the electrolyzer. According to the second Faraday's law, the hydrogen mass flow rate ($\dot{m}_{H_2}$) can be determined by Eq. (2.16).

$$\dot{m}_{H_2} = \frac{M_{H_2} \cdot i_e \cdot n_c}{n \cdot F} \eta_F \tag{2.16}$$

where, i_e is the electrical current ampers (A), M_{H_2}=2 g/mol is the molar mass of hydrogen, n_c is the number of cells in the electrolyzer, $n = 2$ is the number of electrons in the reaction, F is the Faraday's constant, and η_F is the Faraday's efficiency.

Faraday's Efficiency

The Faraday's efficiency (η_F) is a parameter to assess the utilization of electrons during the water electrolysis [49]. It is calculated as the ratio between the experimental and the theoretical volume of produced hydrogen. When all the supplied electrons, during the reaction, are producing only hydrogen and oxygen, $\eta_F = 1$. This occurs when the electrodes are very well resistant to corrosion and behave completely stable during the reactions. Electrodes resistant to corrosion are important in order to produce very pure hydrogen during electrolysis. The Faraday's efficiency can be calculated according to the empirical expression given by Eq. (2.17), where, i_e is the electrolyzer current in (A).

$$\eta_F = 0.965 \exp\left(\frac{0.09}{i_e} - \frac{75.5}{i_e^2}\right) \tag{2.17}$$

2.3. Hydrogen Production from Solar Power

Up to now, this chapter has described the principles of solar energy and presented a brief introduction of water electrolysis and the potential of hydrogen as an energy carrier. In this section, a review of how both technologies can be coupled is presented. First, a solar-to-hydrogen (S2H) system and its components are

presented. Next, the concept of power-to-gas (P2G), and some of the implemented projects are introduced. Furthermore, a short review of previous studies focusing on: (1) system performance, (2) operation and system configuration, and (3) design and sizing aspects of the S2H system, are described.

2.3.1. Solar-to-Hydrogen: System Description

Photovoltaic systems can be coupled with water electrolyzers to produce hydrogen. Hydrogen from solar energy becomes a promising alternative to satisfy the power demand of the future. The system configuration to produce hydrogen from solar energy is relatively simple. It comprises: PV panels, direct current (DC/DC) power converter, electrolyzer stack, water and hydrogen storage. The direct current electricity produced from the solar panels can directly feed into to the electrolyzer and produce hydrogen. However, the voltage applied to the electrolyzer is limited by the output power of the solar panels, and the operation voltage of the electrolysis is limited by the operating characteristic of the electrolyzer. Thus a DC/DC power converter is needed to adjust the voltage levels. Including a battery into the system configuration allows having an extra energy storage source to the system operation. Water quality requirements differ between electrolyzers. For instance, a PEM electrolyzer includes a deionizer unit before the water is fed into the electrolyzer. For an alkaline electrolyzer, water is mixed with potassium hydroxide (KOH) to increase the pH of water. Once the hydrogen is produced, a storage unit is necessary to store the hydrogen. Also, depending on the size and volume production, a distribution system for the hydrogen is needed. Distribution and storage systems become limiting factors when the hydrogen generation is centralized. Additionally, extra components like water separators, gas purification, gas dryer, pipeline, pumps and compressors are needed for an optimal operation [31]. A simple representation of the solar-to-hydrogen system configuration is shown in Fig. 2.11.

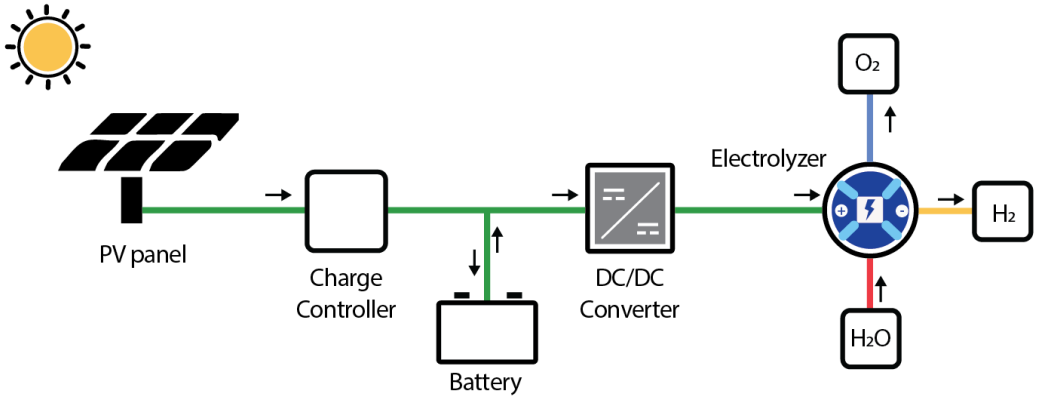

Figure 2.11: Schematic representation of a photovoltaic-electrolyzer hydrogen generation system. (Redrawing by the author) [31]

Producing hydrogen using PV electricity is a way of storing solar energy and tackle the limitations of its intermittent nature. However, the intermittency of solar energy brings challenges to the operation of the electrolyzer and determines whether the production of hydrogen is economically viable. Power control management, assessment of the system performance, and designing system guidelines are some of the most important concepts needed to investigate, in a solar-to-hydrogen system, to increase the fast integration of renewable energies using hydrogen.

2.3.2. The Power-to-Gas Technology (P2G)

Power-to-gas is a process that uses electricity to produce synthetic natural gas via the methanation of CO_2 together with H_2 from water electrolysis. Power to Gas (P2G) has been proposed as a very promising and versatile technology to store the surplus of renewable power. Moreover, P2G is being used as an alternative to alleviate the power transmission lines by consuming the electricity surplus generated mainly by renewable sources during periods of low demand. Solving the power balance issues caused by variations in power generation from renewable energies has been the driver to promote the integration of P2G. Also, P2G promotes

the integration of different energy sectors like renewable energy generation, CO_2 emissions reductions, electric mobility and industry process. The main advantage of this technology is that electricity can be stored for more extended periods of time when converted into fuels like hydrogen, ammonia or natural gas. A schematic representation of this process is presented in Fig. 2.12

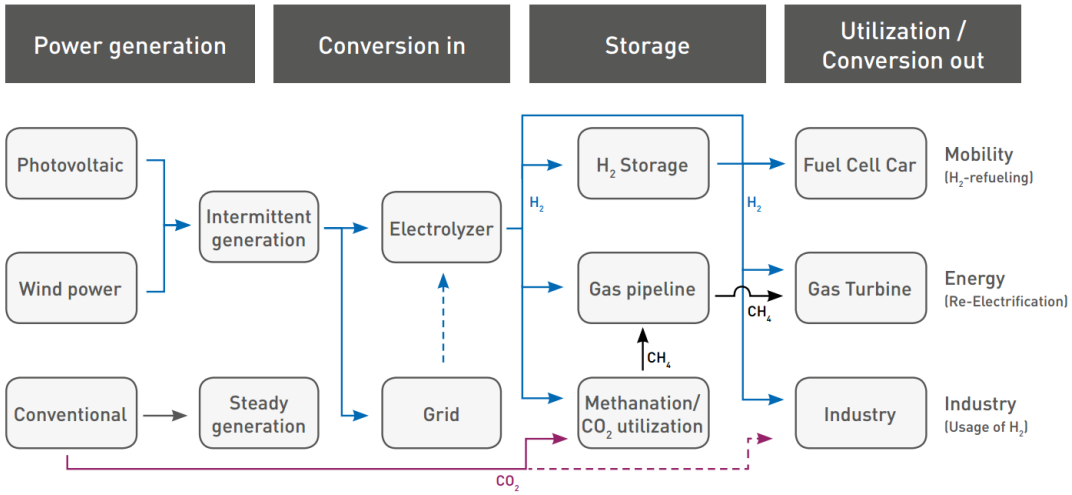

Figure 2.12: Schematic representation of power-to-gas process. [21]

In the context of fluctuating renewable energy sources and electricity surplus, Power-to-Gas (P2G) research has grown very fast in the last years. This establishes a new way to manage the electricity production from renewable energies, and match with electricity supply and demand. The advantage of this approach is that it uses the variable and excess of electricity to produce hydrogen and combined with natural gas distribution network.

Few initiatives of P2G are already operative in different locations. One example is the project "Store&Go", developed by an international joint venture of Germany, Italy and Switzerland. The overall objective of the project is to demonstrate how power-to-gas can provide synergies between electricity and gas as energy carriers for the transportation, storage, and end use of renewable energy [21]. Up to 57 Nm^3/h of synthetic natural gas (SNG) will be produced by one of the projects developed in Germany. Overall, Germany is leading the development of P2G technology with up to 17 projects [32]. The largest project is located in Werlte by "Solar Fuel GmbH", with a total capacity of 6.3 MW, generating 360 Nm^3/h of methane [30].

Along the same lines, France is developing another pilot project, referred to "Network Management by Injecting Hydrogen to Reduce Energy Carbon Content" (GRHYD). This project aims to evaluate the applicability of combining hydrogen with natural gas [33]. The project is designed to convert surplus electricity generated by wind farms in the surrounding region into green hydrogen and methane syngas. Two electrolyzers will produce the hydrogen, and a methanation reactor will combine the hydrogen with CO_2 to create methane syngas. The CO_2 used will be extracted from fumes generated by neighboring industrial plants, thereby helping to reduce local pollution. The project will have a total generating capacity of 1 Megawatt (MW) [1].

Several studies to assess the economic and technical aspects of implementing power to gas have been carried out recently. A study by Estermann et al. [28] presents the results of producing synthetic methane using solar electricity. This project bonds hydrogen produced from an electrolyzer with carbon dioxide from biomass anaerobic digestion plant in order to produce methane. The results show that the initial power capacity of the P2G plant will be 18%. However, this value will increase over time since the installed capacity of PV will also increase. Nevertheless, this implementation involves technical challenges regarding the availability of captured carbon dioxide from an anaerobic digestion plant. This research also mentions the necessity of a policy framework that establishes a more attractive electricity price for electrolysis purposes.

2.3.3. Research Work on Solar-to-Hydrogen Systems

Several studies to assess the feasibility of implementing hydrogen production via electrolysis using solar power have been carried out recently.

A small demonstration project developed by Clarke et al. [23] shows a method to integrate PV modules with a PEM electrolyzer directly. The system uses a 2.4 kW PV array connected directly with a PEM electrolyzer. The study points out the advantage of a direct coupling configuration is the cost reduction of a DC-DC converter and power electronics. However, when comparing the cost of components, the most expensive ones are related to the electrolyzer stack. The PV technology and the balance of its related components are becoming cheaper. Hence, the saving in power electronics does not balance out the costs of operation time in the electrolyzer. After approximately four months of operation, the electrolyzer stopped running due to a degradation of its membrane.

In another study performed by Homayouni et al. [36] a technical assessment and sizing of a standalone hybrid power system combining PV panels, batteries, and hydrogen storage is presented. An optimization framework model is developed to determine the optimum component sizes based on the lowest net present cost while maintaining the system reliability. By using this framework, the study concludes that the most cost-effective alternative to the energy storage is a combination of batteries with hydrogen technology. Additionally, this work concludes that the system design and sizing have an important effect on its initial cost. However, no designing rules for hybrid power systems are presented. Neither, the impact of irradiance levels or the electrolyzer operational parameters is discussed in this work. A system performance analysis is presented, but the results do not discuss the impacts of the electrolyzer switching on/off cycles due to the intermittency nature of the PV system.

Analyzing the irradiance levels is essential because it determines the sizing of the system. A significant seasonal summer-winter fluctuation of irradiance limits the capacity of a system to become self-sufficient. For instance, in Nordic countries, it becomes difficult to have self-sufficient PV system, because the combination batteries-irradiance will always be disproportional. In winter, the batteries will remain in a low state of charge, and in summer, a significant amount of energy will be curtailed. Furthermore, the switching on/off cycles are critical because every time the electrolyzer switches on, an activation overpotential is needed to start the electrochemical reaction. This overpotential, degrades the PEM membrane, by changing the properties of the membrane. The membrane's ion conductivity decreases and gas permeability increases. A control in the switching on/off cycles of the electrolyzer will help to reduce the membrane degradation and improve the lifetime of the electrolyzer at the same time.

A study of the economic assessment of a hybrid energy system PV-fuel cells is presented by Lagorse et al. [43]. In this reference, some design guidelines for a stand-alone hybrid system are tested by using a computational model in Matlab/Simulink. The analysis is based on three different configurations, as shown in figure 2.13. The goal of the study is to find the most cost-effective system configuration. Each configuration includes its specific component sizing. For configuration (c) shown in Fig 2.13, the energy management technique becomes crucial for economic optimization. A cost optimization for each configuration was presented for a 20 years lifetime. The study shows that the most cost-effective alternative is for configuration (a) with 0.519 €/kWh, followed by configuration (c) with 0.645 €/kWh and configuration (b) with 4.943 €/kWh as the least attractive option. The study concludes that relying on hydrogen as a unique storage method is currently not economically feasible. Electrolyzer and fuel cell prices need to decrease in order to make this a more attractive option in the future. Additionally, when the goal is to have a complete energy autonomous system, the configuration that combines batteries and hydrogen storage is preferred.

In general, several studies include a combination of solar and wind power technology. Almost all of them are simulation-based investigation [40]. For instance, a distributed generation system, combining solar panels and wind turbine power generation, is presented by Kabalci, [41]. In this study, the system design is developed using Matlab/Simulink. The study presents a detailed model of the main components in the system, like solar panels, wind turbine, s power converter and an inverter. The study mainly focuses on the current and voltage fluctuations. The system is optimized to provide a stable and controlled power output. The challenge for this system configuration is to provide a stable power generation and preserve the power balance with the grid. This work presents valuable insights regarding the importance of power balance when combining more than one power source. Additionally, the system was analyzed by adding a battery as energy storage unit. Understanding how such a system affects the stability of the power grid is essential because this will guar-

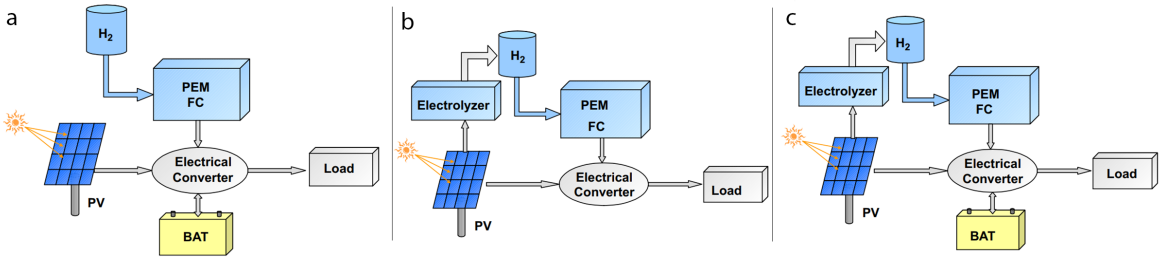

Figure 2.13: System configurations layouts. (a) PV, battery, FC is fed by an external hydrogen tank; (b) PV, FC, electrolizer and hydrogen tank and (c) PV, battery, FC, electrolizer and hydrogen tank [43]

antee high reliability to the power generator and provide a high-quality power system. Those two concepts are very important for distributed generation systems. Also, a more clear understanding of how the battery contributes to the system performance is necessary for optimizing the system size which means a significant cost reduction.

Regarding the power control management for a hybrid power system, a design and construction study combining wind, fuel cell, and a battery is presented by Fathabadi [29]. The system is designed to have an average daily energy generation of 450 kWh, completely off-grid. A vertical wind turbine WKV-10000 of 10 kW rated power and a 36 kW PV array built by 180 PV modules are the primary energy sources. The system includes a 5 kW Horizon H-5000 proton exchange membrane (PEM) fuel cell stack, which works as a secondary energy source. In this study, the power generation is optimized by implementing a highly accurate maximum power point tracker (MPPT) for both solar and wind generation. The challenge for this system configuration is to efficiently produce electricity in a remote area, even during cloudy days. This work developed a highly accurate MPPT method to efficiently tackle the intermittency problem of using solar and wind energy sources. The management control unit uses the surplus energy to run an electrolyzer and produce hydrogen. When sun and wind generators do not generate sufficient power, the control unit starts up the fuel cell. The fuel cell uses the hydrogen produced during excess power generation. This study reveals the importance of an accurate power control unit in a hybrid system to optimize the energy utilization of the system. A good power control is the core of an efficient hybrid system.

Some of the reviewed literature includes research on how to assess the performance of a hybrid power system. Luna et al. [44] presents seven performance indices to assess such a system. The parameters used to assess the quality of the system are reliability, autonomy and capital cost. Based on those three parameters, the study defines ratios to evaluate the performance of a system that includes more than one power source. The importance of those parameters is explained by the necessity to visualize and quantify the parameters of a hybrid system. A quick and fast method to assess the reliability and autonomy of a hybrid power system will help to evaluate the economic and technical feasibility of such a system.

Regarding the feasibility of energy storage for hybrid systems, Zhang et al.[65] presents a comparison between battery and hydrogen storage systems for residential buildings in Sweden. The study shows that battery systems achieve higher values of a self-sufficient ratio in comparison to other storage systems. The electrolyzer appears to be the most sensitive component when analyzing the profitability of the system. His work concludes that battery storage system is better than hydrogen storage system when comparing its profitability. The study suggests that if the electrolyzer price would drop 25%, the hydrogen storage can have a similar value of self-sufficient ratio than the battery. Comparing the feasibility of both batteries and hydrogen for energy storage is an interesting idea, but more interesting research would be on a system optimization that couples both technologies. A short-term energy storage like batteries combined with a long-term storage technology like hydrogen can easily solve the issues of the inflexibility of renewable-based power systems.

Summarizing, design, operation, and system performance are three crucial topics when using solar-to-hydrogen systems. The goal of such a system is to produce hydrogen in the most cost-effective conditions while mitigating the intermitent character of solar energy. It has been demonstrated that hybrid power systems work very well for grid-tied configurations. However, there are extra optimization challenges, for a self-sufficient energy

system, when the system operates off-grid. A more robust energy storage unit and a fine energy control management are needed to compensate the system instability. Overall, hydrogen production from electrolysis using solar power is a promising solution, but there are some challenges which need to be tackled. Thus both a detailed and more comprehensive knowledge of the system integration is necessary.

2.4. Concluding remarks

Undoubtedly, solar energy is the most important renewable energy sources. Photovoltaic solar cells have proved how easy and economic is to generate electricity from the sun. On the other hand, water electrolysis using solar electricity can potentially be a very important process for producing hydrogen as an energy carrier. Efficiencies of both technologies are a limiting factor, but it has been proven that a good match can solve the issues of energy storage, and grid flexibility on a renewable energy based power systems.

As the implementation of solar panels grows all around the world, the necessity to have proper energy management of the stochastic power generation becomes a higher priority. Alternatives for managing the power produced by renewable energy have been already developed, for instance, using batteries to store the energy surplus, increasing energy consumption to match the power generation, and producing hydrogen via electrolysis to alleviate the power systems congestion. All of these concepts have been studied independently, but there is still not much information about a holistic implementation of solar-to-hydrogen systems.

Producing hydrogen via electrolysis is a process that has been vastly researched for decades, and it has reached enough maturity level to be deployed. However, the technology is still not economically attractive to the market when competing with hydrogen production from fossil fuels. New small pilot projects are developing and providing insights into the system operation. Even though the results are promising, the technology is still not profitable enough to achieve a major hydrogen production by electrolysis using solar power. From a technical and environmental point of view, producing hydrogen from solar energy is a promising alternative to supply the world energy consumption of the future.

Previous solar-to-hydrogen systems have been developed, but there is still need of more in-depth understanding on the optimal operating conditions for each of the components. Moreover, the lack of design rules for these types of systems is a limiting factor for the faster development of such a system. More knowledge, of such a systems, will encourage the development of more projects and allow this technology to fully deploy. Hence, more investigation to fill those gaps by providing new knowledge on a solar-to-hydrogen systems is crucial for a faster implementation of flexible renewable energies.

3

Experimental Setup

This chapter describes the designed system -*Wawa*[1]- and each of its components. It also presents the process to how connect the components and let the system run. The process to startup and shutdown the system is also described. Next, the experiments to obtain the polarization curve and efficiency of the electrolyzer is presented. The chapter closes with general safety guidelines when operating the system.

3.1. System Description and Components

Wawa is the given name for the system to produce hydrogen via water electrolysis using solar electricity. Wawa consists of two PV panels (300 W each), two lead-acid batteries (70 Ah, 12 V each), and a water polymer-electrolyte-membrane (PEM) electrolyzer (120 W). Additionally, the system includes a charge controller with a maximum power point tracker (MPPT), and complementary components such as a microcontroller, a pump, tubing, flow meters, filters, gas separators and electric wires. A layout of the system and its main connections is illustrated in Fig. 3.1.

In this thesis, the first stage of Wawa was built and tested. This stage includes a direct current (DC) power source as a primary energy source. The power stability and flexibility of the power source were the reasons to first test the electrolyzer in this way. Moreover, the knowledge of the PV system design and its operation is relatively broader and more mature than the water PEM electrolysis system. Thus, the first stage included the PEM electrolyzer, power electronics, and additional components to run and test the system. In a further stage, the system will incorporate the PV modules to this initial version. A brief description of each component and its selection parameters is presented below.

PV Modules
Two BenQ-PM060MW2 PV modules of 300 W each, supply electricity to the entire system. The size and the market availability were the decisive parameters to chose these modules. Additionally, a module with a high current value (I_{sc}) is desired specially for a direct module-electrolyzer coupling. Thus, the two modules are connected in parallel to achieve a higher current.

Batteries
Two lead-acid FullRiver-DC10-12 batteries connected in series have a combined storage capacity of 1.68 kWh. The relatively low cost and its capability to deliver a high current were the reasons to opt for those batteries. The direct current generated by the PV modules charges the batteries employing an MPPT/charge controller. The batteries store the energy surplus during the day and feed to the electrolyzer when solar irradiance is low.

Maximum Power Point Tracker (MPPT)
The Victron BlueSolar 100/50 maximum power point tracker is implemented to optimize the energy generation from the PV modules. The selection of this component is based on its voltage and current limits. The MPPT has to at least support the voltage (V_{oc} = 39.9V) and the current(I_{sc} = 19.6A) delivered from the PV

[1] from the Kitchwa (indigenous Ecuadorian language), meaning the "young kid".

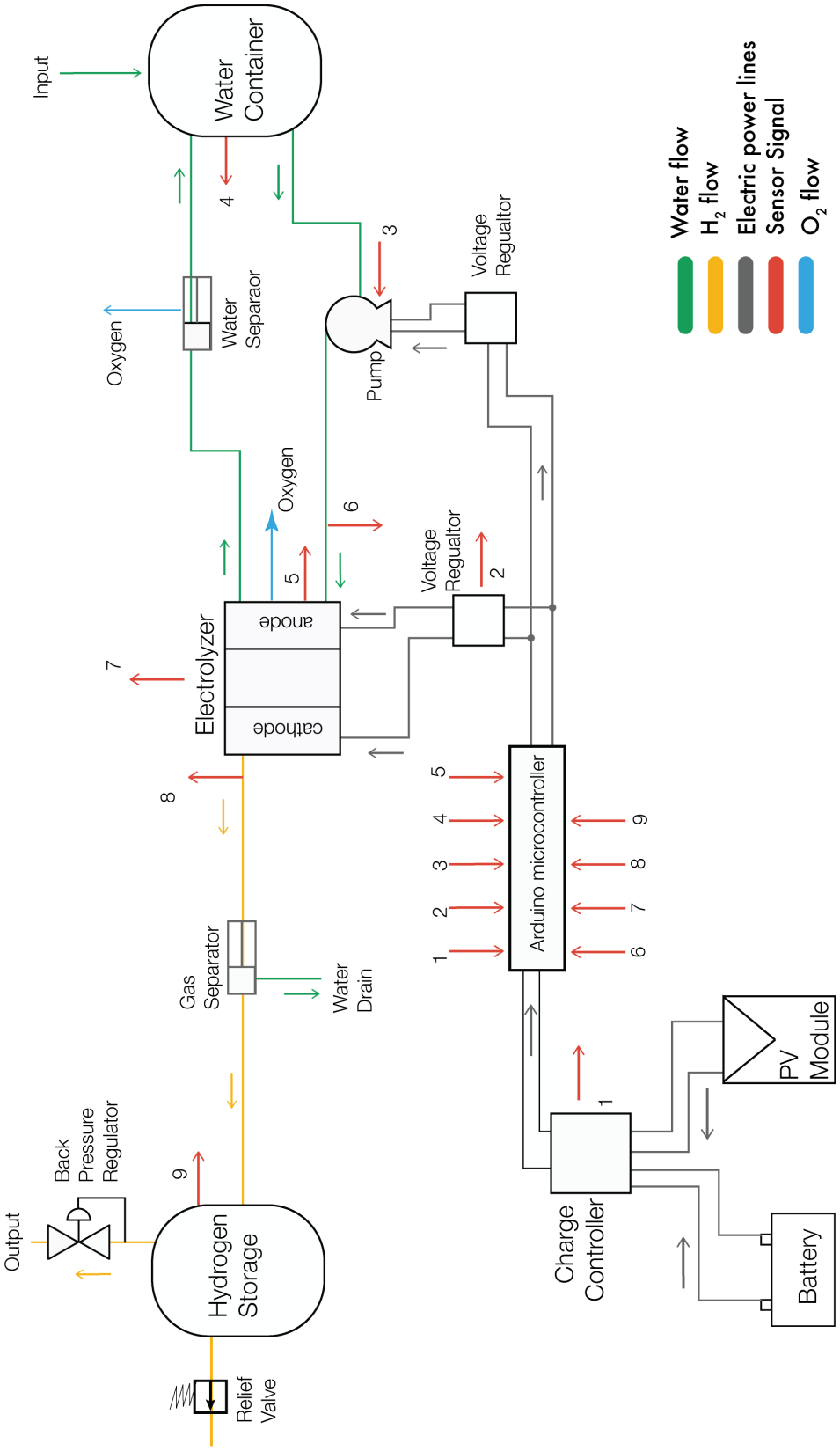

Figure 3.1: Layout diagram of the system.

modules. Similarly, the charge voltage and current have to match with the battery bank (24 V, 70 Ah) levels. Additionally, the output amperage value of the MPPT has to fit with the amperage of the load (60 A).

PEM Electrolyzer
The Giner-G5 proton exchange membrane electrolyzer is a compact, safe and straightforward hydrogen generator. With a 50 cm^2 nominal active area, no moving parts, and a 70% efficiency the electrolyzer produces 300 cm^3/min of hydrogen at nominal current, atmospheric pressure and 30^oC temperature. The component was selected based on the market availability and its suitable size for laboratory applications.

This electrolyzer has four connections for the tubes and two double connectors for each electrode. There is one inlet for the water, one outlet for oxygenated water, and two outlets for hydrogen gas. Each connection includes a stainless steel fitting to guarantee a proper sealing and avoid fluid leakage. The double connectors are included to reduce electrical losses due to the relatively high current (60 A) drawn from the electrolyzer.

Polytetrafluoroethylene (PTFE) Tubing
A Teesing 6-4x1 tube with 4 mm of internal diameter and 6 mm of external diameter is the medium used to transport the water and the hydrogen. The (PTFE) material is a synthetic flour polymer with good mechanical properties and chemical resistance to organic solvents. The tubing was selected based on its low permeability, mandatory for hydrogen gas applications. Additionally, the flexibility of the PTFE pipes give freedom for connecting the components without limiting the location for the components, as it is the case for stainless steel pipes.

Tube fittings
Tube fittings connect runs of tubing to the inlet sections in the electrolyzer, pump, and gas meter. The purpose of the fitting is to provide proper sealing and ensure leak-tight performance. The threaded fittings are suggested to provide a better grip. Additionally, it is highly recommended to use stainless steel fittings to avoid corrosion.

Water pump
A Diener Optima Series pump provides water to the electrolyzer. The selection of the pump was based on two parameters. First, a controllable and precise speed control, to adjust the water flow to the electrolyzer requirements. And second, a low-pressure pulsation to avoid damage to the electrolyzer membrane. The pump is connected to the printed circuit board (PCB) and draws a maximum current of 1.8 A at 12 V. The pump guarantees that the electrolyzer's membrane is always humidified.

Hydrogen tank
The Linde hydrogen tank is a stainless steel container of 10 liters capacity, and a maximum pressure of 200 bar (20 MPa). This tank was chosen because its relative low cost and small size. Additionally, the operational pressure of the system is relatively small (2 MPa), thus a stainless steel tank is perfectly suitable.

Water tank
The water tank is a 10 liter plastic container. The tank is filled with deionized water. This is pure water, completely demineralized with a very poor conductivity (18.2 MΩ·cm). The water is pumped towards the water inlet of the electrolyzer, and it returns to the tank after being used. Similar than for the hydrogen tank, the water tank was chosen because it is small and relatively cheap.

Gas-Water separator
Hydrogen produced by the electrolyzer contains small particles of water due to permeation through the Nafion membrane. This water content reduces the purity of hydrogen. Thus it is necessary to include a hydrogen-water separator. The output water is mixed with the oxygen produced in the anode. Oxygenated water can not be reused by the electrolyzer. Thus an oxygen-water separator is needed at the outlet of the anode of the electrolyzer before the water is recirculated to the container. Otherwise, the electrolysis efficiency is significantly reduced because the water is saturated with oxygen. The selection of this component is based on the flow rate of hydrogen produced and the required gas quality.

Electric Wires
The wires carry the electric current from the DC converter to the electrolyzer and to the rest of the electronic components. Most of the electric connection for the components requires a solid-core wire 22 AWG (American wire gauge, 0.64 mm diameter). However, the connection for the electrodes of the electrolyzer needs a thicker wire (5 AWG) since the current passing through can go up to 50 A.

Printed circuit board
The printed circuit board (PCB) is an in-house designed electronic circuit. This circuit is the interface between the power source and all the system components. The PCB includes the microcontroller, communication ports, and the necessary electronics components to run the system and monitor its parameters. Additionally, a DC/DC power converter designed to fit the voltage (2.5 V) and current (60 A) of the electrolyzer is included. Two PT-100 temperature transmitters are installed to take the signal from the temperature sensor and transmit the signal to the controller.

Microcontroller
The selected microcontroller is open source hardware known as Arduino. This component allows the system to program instructions for coordinate the sequence of system operations such as the power management. Both the startup process and the turn off process can be automatized using the microcontroller. Additionally, the algorithm to follow in case of malfunction of the system can be included in the microcontroller. The microcontroller is crucial for an efficient operation of the system.

DC power source
In this thesis, a direct current (DC) power source is used as the primary energy source to drive all the components. In this setup, two DC power sources (10 A, 32 V each) are connected in parallel to provide a constant voltage and a current of 20 A.

Current meter
The current meter is a built-in circuit that integrates a precision resistor with a minimum value. The resistor causes a voltage drop proportional to the current value passing through the circuit. Hence, the current is indirectly measured by measuring the voltage drop through the resistor. The current and voltage values are measured using a digital multimeter.

Gas meter
The gas meter is used to monitor the hydrogen production from the system.

Temperature Sensors
The electrolyzer temperature is measured using two PT-100 temperature sensors. This is a resistance temperature sensor made of a small strip of platinum with a resistance of 100 ohms at 0°C. This component measures a precise and stable temperature value by changing its resistance in function of the temperature. This sensor can be connected to the temperature transmitter placed on the PCB, and use the signal as a control variable for the system.

3.2. System Setup

This section explains how to connect the necessary components to produce hydrogen using a PEM water electrolyzer powered by a DC power source. The setup process involves the connection of all the above described components, which is summarized in the following seven steps.

- **Step 1:** Each of the four inlets/outlets of the electrolyzer should be connected to a PTFE tube, as shown in Fig. 3.3
- **Step 2:** The water inlet of the electrolyzer should be connected to the tube attached to the water pump outlet. The water pump inlet should be connected to the water container using another tube. Similarly, the output for the oxygenated water of the electrolyzer should be connected to the water container. This connection makes the water recirculate during the system operation. Figure 3.4 shows the connection for the pump.
- **Step 3:** Using a tube, the two hydrogen outputs of the electrolyzer are interconnected into a single one, as shown in Fig 3.3. This connection goes to the gas-water separator, where hydrogen and water are separated. The hydrogen production is measured by a gas flow meter connected after the water-separator. The electrolyzer tubing connections should be finished now and ready to use.
- **Step 4:** The anode of the electrolyzer should be connected with the positive outlet of the PCB. Similarly, the cathode should be connected to the negative outlet of the PCB. Polarity is important for proper operation of the electrolyzer. Figure 3.3 shows the connections for the electric cables of the electrolyzer.

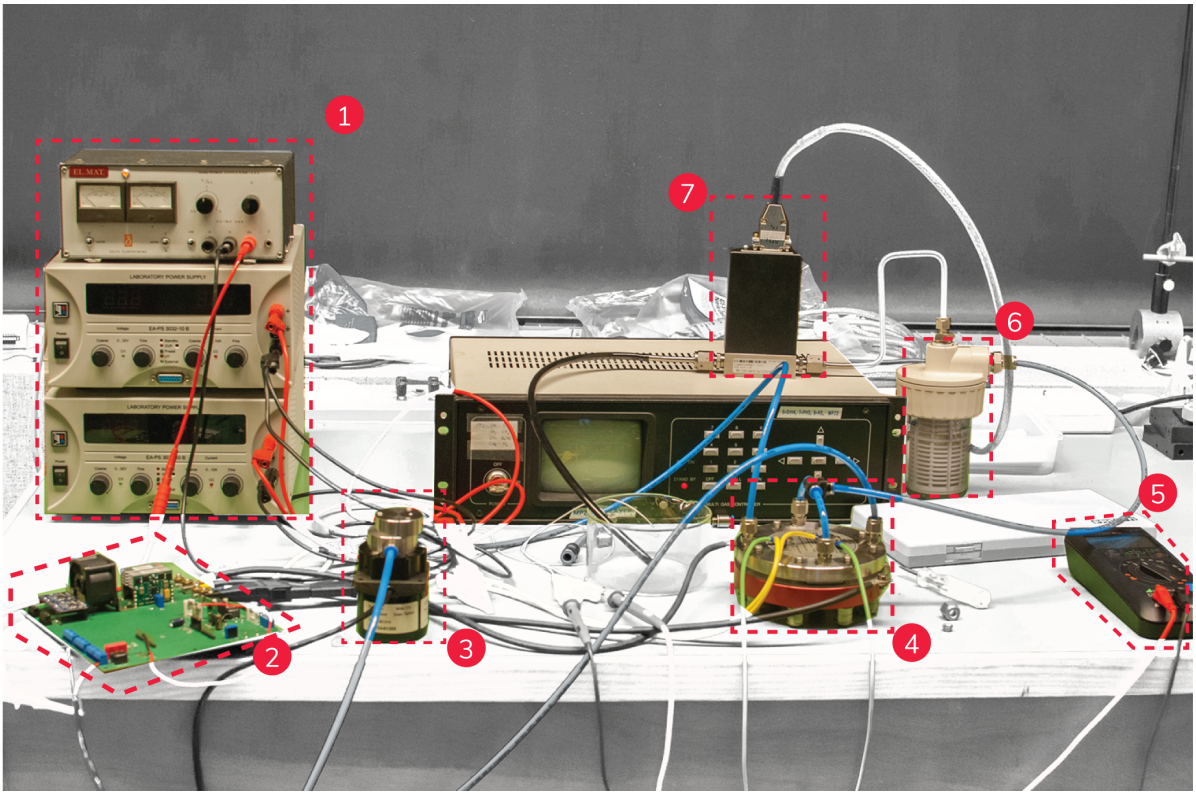

Figure 3.2: Experimental setup. [1]DC power source. [2] PCB. [3]Pump. [4]Electrolyzer. [5]Digital multimeter. [6]Gas-water separator. [7]Gas flow meter.

- **Step 5:** The PCB voltage output should be set up in a value of 1.4 V using the variable potentiometer located in the PCB, as showed in Fig. 3.5. The voltage level delivered from the PCB can be set on a range from 1.0 V to 2.5 V.
- **Step 6:** The Arduino's digital pins in the PCB should be connected to the pump wires as shown in Fig. 3.5
- **Step 7:** Finally, the controllable DC power source should be connected to the PCB.

The system is now set up and ready to be used. The interconnection of all the components is shown in Fig. 3.2.

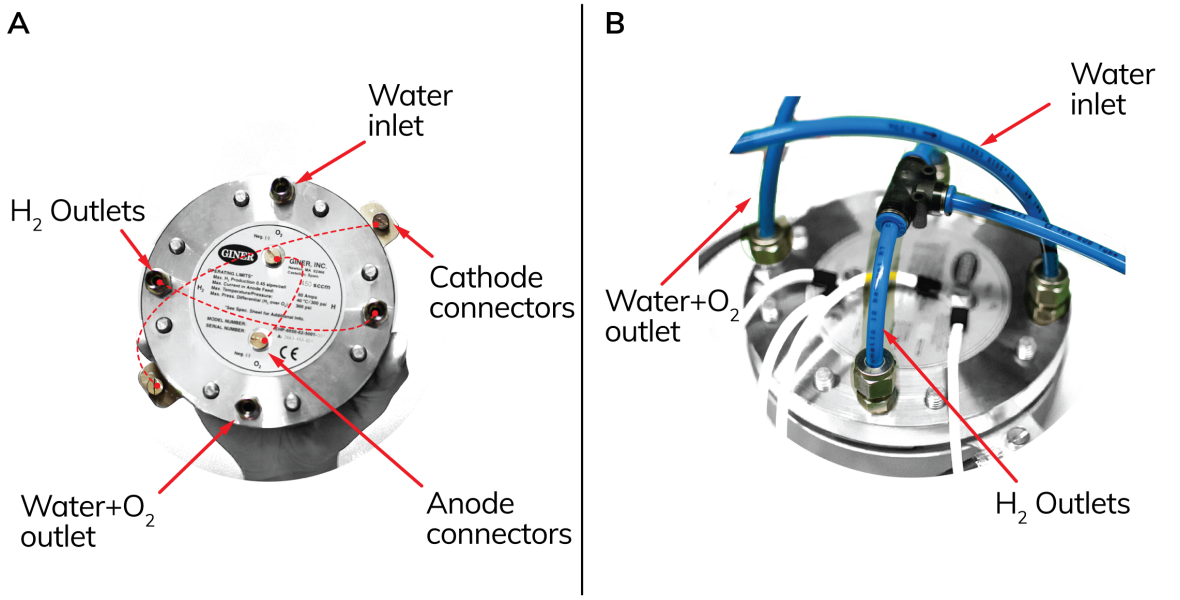

Figure 3.3: (A) Identification of each of the connectors of the electrolyzer. (B) Representation of the tube connections of the electrolyzer.

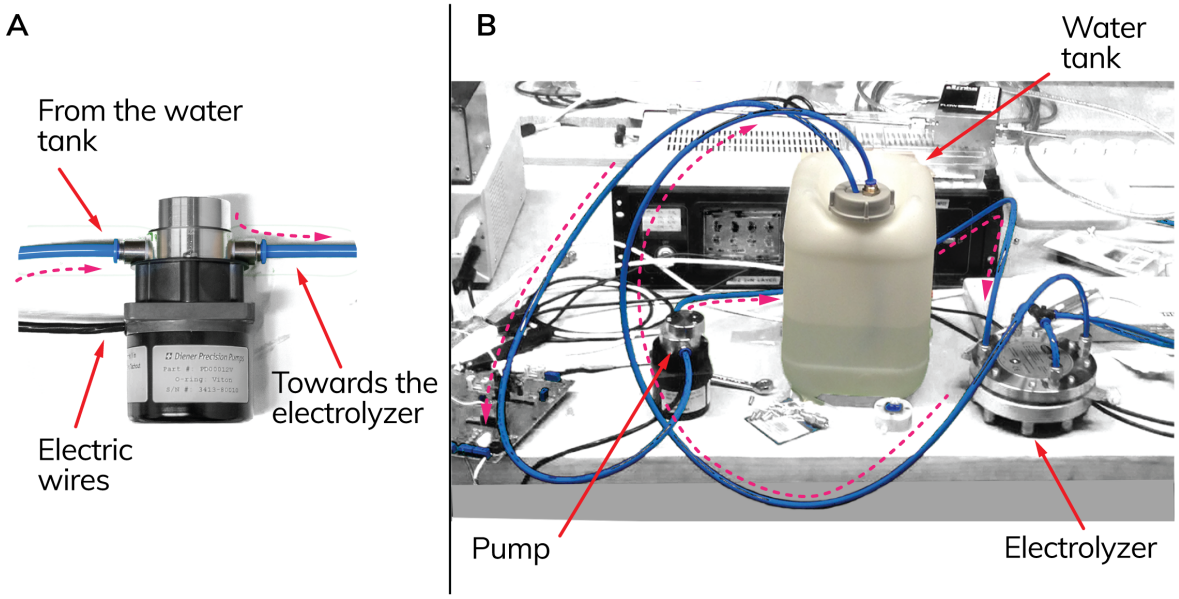

Figure 3.4: (A) Identification of the pump connectors (B) Water circuit lines for the pump, water tank, and electrolyzer.

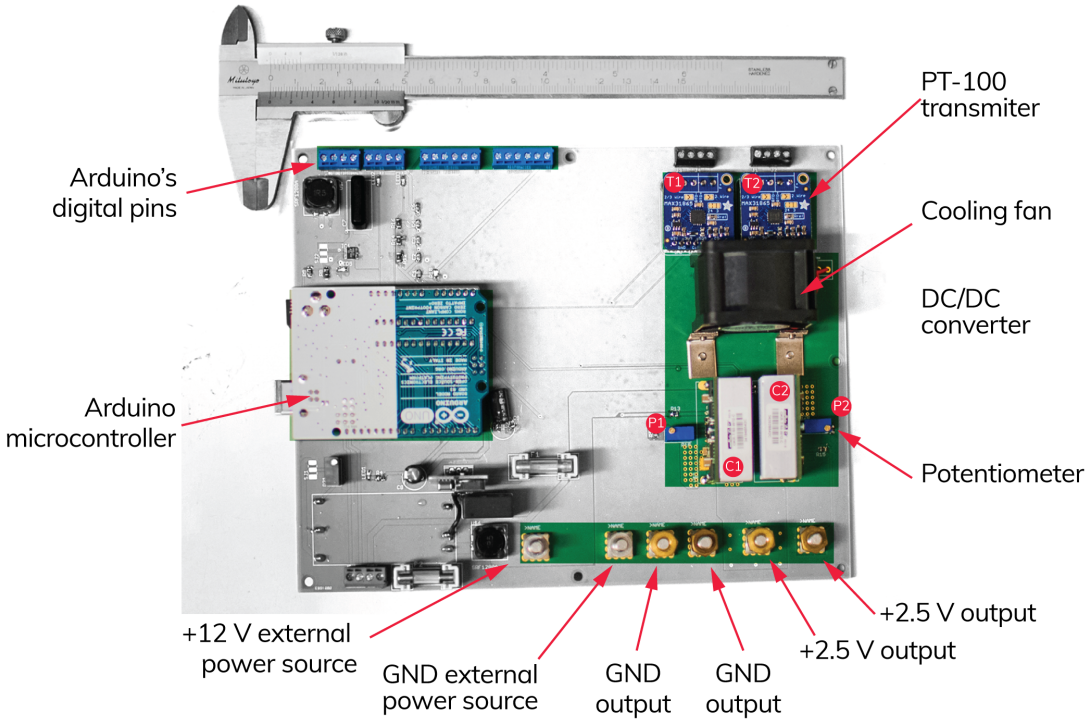

Figure 3.5: The printed circuit board (PCB) indicating main electronic components.

3.3. Operating Procedure

This section describes the two procedures to operate the system and run the experiments successfully.

Startup process

For a successful startup, all the components should be properly connected. Also, the water level in the tank should be above half its capacity. Otherwise, the electrolyzer membrane might suffer serious damage. The two basic steps to startup the system are:

- **Step 1:** The external DC power source should be plugged in and switched on. First, the pump starts sending water to the electrolyzer to humidify the membrane before applying a voltage potential. The polymer electrolyte membrane needs to be perfectly humidified before start up the electrolyzer. If the pump has not started its operation, the system should be stoped and the connection should be checked again.
- **Step 2:** The electrolyzer starts its operation by closing the circuit on the PCB. Now,the electrolyzer starts drawing current; thus hydrogen is being produced. The voltage and current values should be verified that in the correct values. If the current is higher than 60 A, or 2.5 V, the system must be stoped and the connection should be checked one more time.

The system is now operating, and ready to perform the experiments.

Shutdown process

Similar than for the startup process, there are two steps to follow to shutdown the system properly:

- **Step 1:** The electrolyzer should be turned off by unplugging the wires from the PCB. Similar than during the startup process, the pump needs to keep ruining for a couple of minutes to humidify the membrane and guarantee that all the internal gas canals are emptied
- **Step 2:** The DC power source should be switched off and the power connectors should be unpluged.

Following steps 1 and 2, the system should be turned off

3.4. Experiments and Measurements

This section describes the experiments to obtain the polarization curve of the electrolyzer and its efficiency. The polarization curve is determined by increasing the input voltage to the electrolyzer. The thermoneutral potential is the first and most important measurement of the experiment. There are five steps to follow to perform the experiment successfully.

- **Step 1:** The initial potential should be set up in 1.2 V by modifying the potentiometer in the PCB.
- **Step 2:** The steps described in Section 3.3 should be followed to set up of the system. The system start operationg after following step 1 and 2.
- **Step 3:** The initial current and voltage should be measured at the electrolyzer connectors. It is expected that at 1.2 V the electrolyzer draws no current; thus the current has a value of 0 A.
- **Step 4:** The voltage value should be increased by tuning up the potentiometer in the PCB. When the current reaches a value different than zero, mark that voltage value. This voltage is the thermoneutral voltage of the electrolyzer. The electrolyzer starts producing hydrogen by following steps 1, 2 and 3.
- **Step 5:** The voltage should be increased on steps of 0.1 V and the respective current values should be recorded. At the same time, the values of the hydrogen gas flow should be also recorded. The initial current values are significantly sensitive to the voltage variations, because it needs to overcome the activation losses.

The polarization curve of the electrolyzer results by plotting the measured values of current and voltage. The efficiency can be determined by dividing 1.48 to the thermoneutral voltage, as defined by equation (2.15) in Chapter 2.

3.5. General Safety Guidelines

This section presents some general safety guidelines to follow during the system operation. Like in any system that manages a fuel, it is necessary to keep in mind some instructions to avoid accidents. Nevertheless, working with hydrogen is safer than working with gasoline or other fuels. Hydrogen is less toxic and in case of a spill, it will immediately evaporate into the air. Because of that, a combustible situation becomes less likely. Additionally, in case of a hydrogen ignition, the flame is less likely to spread the fire. The flame will dissipate rapidly, burning itself out quickly without affecting the surroundings, like it is the case for gasoline. Hence, any gas leakage, short circuit, or operation in a enclosed environment must be avoided for safe system operation. To do so, few rules of thumb to follow are described below.

- Power cables should not be disconnected when the electrolyzer is operative; this might cause sparks due to the high current involved.
- The components should not be toched while operating. The temperature of the electrolyzer (60 ^{o}C) might cause discomfort. Additionally, the electronic components might damage because of static discharge.
- Damaged extension cords never should be used. This is a potential short circuit initiator.
- The system should be never operate over a metallic surface. This might cause an electric discharge while operating. Additionally, avoid wearing metallic jewelry.
- Do not store The electrolyzer should be stored in a ambient temperature room. The electrolyzer membrane might dry out and loose its material properties.
- The stack should be always operate in a well-ventilated area.

4

Modelling Approach

This chapter presents the modeling approach of a solar-to-hydrogen (S2H) system. Each component in the system is simulated separately, based on a model that describes the physical and chemical principles of the individual component. The model is written in the mathematical tool Matlab/Simulink, and structured on five different modules: (1) the photovoltaic module as a primary energy source; (2) the battery bank as an energy buffer; (3) the water PEM electrolyzer as a hydrogen generator; (4) the gas storage tank acting as a sink for the generated hydrogen, and (5) the control unit in charge of managing the power of the system. Lastly, six non-dimensional parameters, as a tool for designing S2H system are presented.

4.1. System Description

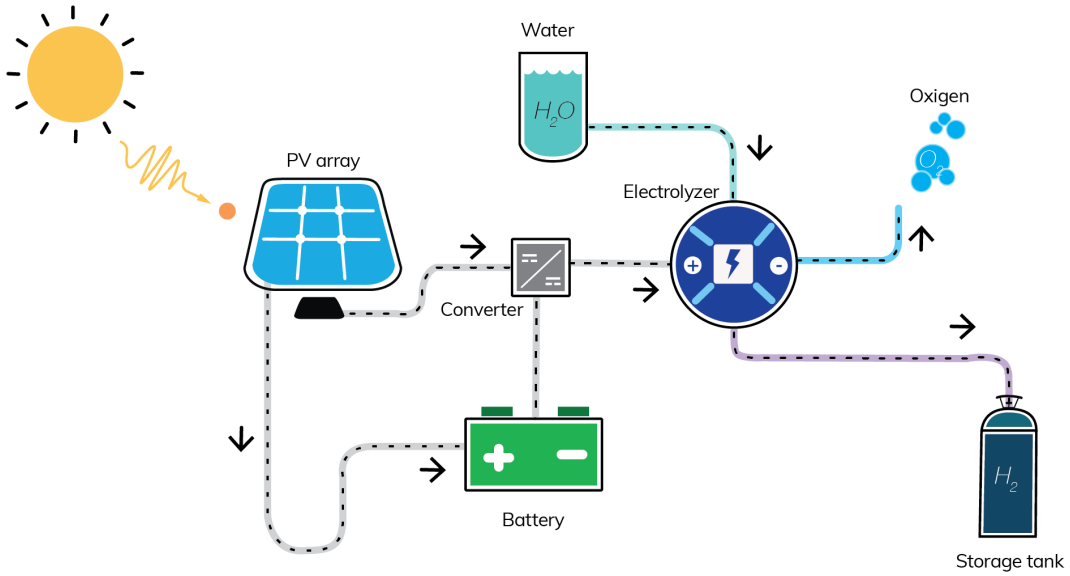

Figure 4.1: General representation of the S2H system layout

The proposed system converts energy from the sun into hydrogen. A set of two crystalline-silicon (c-Si) PV modules (300 W each one) receives the irradiance from the sun to produce electricity. The generated electricity is fed into a water PEM electrolyzer (120 W), where water is split into oxygen and hydrogen. Once the hydrogen is produced, it is stored in a tank. An MPPT charge controller is used to optimize the operation of the solar modules. Additionally, to couple the power generated from the PV modules with the electrolyzer, a DC/DC power converter is included. A lead-acid battery bank is added to store the extra energy generated by

the PV modules. The battery operates as an energy buffer in the system to deal with the intermittent nature of solar energy. A general layout of the system is presented in Fig. 4.1.

4.2. System Modeling

A model in Matlab/Simulink of the PV array, PEM electrolyzer, battery, and storage tank is presented in the following sections.

4.2.1. PV Array Model

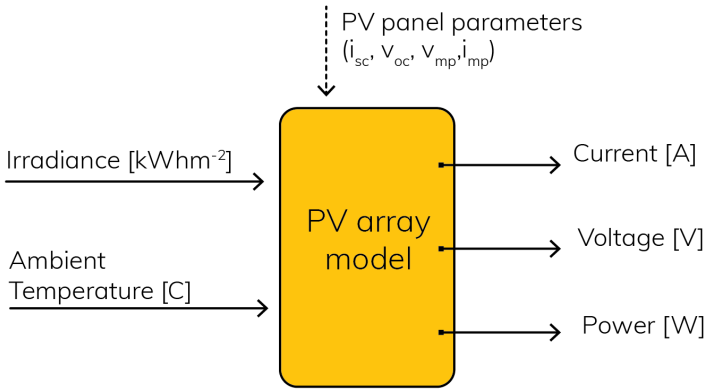

Figure 4.2: Block diagram of the PV module, representing the inputs and outputs signals of the model

The PV array model simulates the performance of the solar modules under any irradiation and temperature conditions. The developed model is flexible and allows to simulate different system configurations of the PV system. Therefore, the parameters that affect the system performance can be analyzed and then select the most optimal design. Understanding of how the solar modules operate, under certain weather conditions, and estimate the energy yield of the system, are necessary for optimal system design.

Irradiance, ambient temperature, and the PV panel parameters are taken as input variables for this model. As a result, the model outputs are the current, voltage, and the power of the PV panel. A simplified block representation of the model with the inputs and outputs variables is shown in Fig. 4.2.

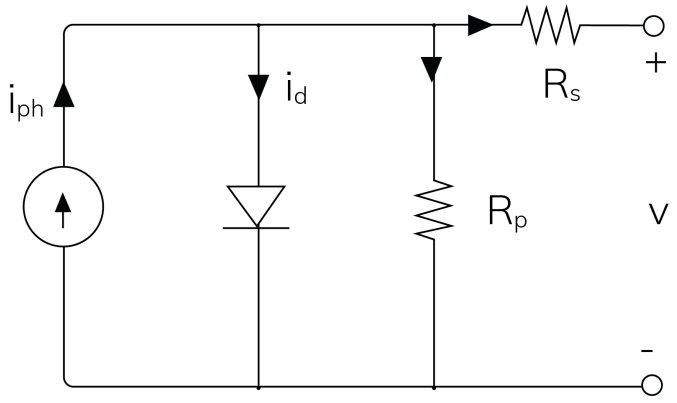

Figure 4.3: Equivalent electric circuit of a solar cell [59]

Using the fundamentals of a solar cell defined in chapter 2, and the simplified equivalent electric circuit of the solar cell, shown in Fig. 4.3, it is possible to calculate the voltage and current of the solar cell. The circuit includes a current source as the photocurrent generator, a diode branch, and two resistors. Resistor (R_s)

represents the resistance of current through the emitter and in the metal contacts. Resistor (R_p) or (R_{sh})is the shunt resistance. Applying Kirchhoff's Law to the electric circuit results in equation (4.1).

$$I_{cell} = I_{ph} - I_d - I_p \tag{4.1}$$

where I_{cell} is the total current delivered from the solar cell. I_{ph} is the photocurrent generated when the solar cell is exposed to light. I_d is the current flowing through the diode. And I_p is the shunt current due to the shunt resistor branch. Using the Shockley diode equation and the Ohm's law; expression (4.1) turns into Eq. (4.2).

$$I_{cell} = I_{ph} - I_o \left\{ \exp\left(\frac{q(V + IR_s)}{nkT_c} \right) - 1 \right\} - \left(\frac{V + IR_s}{R_p} \right) \tag{4.2}$$

where, $q = 1.602 \times 10^{-19} C$ is the elementary charge; $k = 1.38 \times 10^{-23} J/K$ is the Boltzmann constant; $n = 1.3$ [59] is the ideal constant diode factor for c-Si, T_c, is the temperature of the solar cell, I_o is the diode saturation current; and R_s, R_p are the series and shunt resistance, respectively. Solving equation (4.2), the current and voltage of a single solar cell can be determined.

A solar module is the result of various solar cells connected in series and parallel to built up its voltage and current level. Considering a number of solar cells in series N_s, and a number of cells connected in parallel N_p, equation (4.2) turns into equation (4.3)

$$I_A = N_p I_{ph} - I_o N_p \left[\exp\left(\frac{q\left(V_A + I_A \frac{N_s}{N_p} R_s\right)}{N_s nkT_c} \right) - 1 \right] - \frac{V_A + I_A \frac{N_s}{N_p} R_s}{\frac{N_s}{N_p} R_p} \tag{4.3}$$

where, I_A and the V_A are the total current and voltage respectively, generated from the PV array. I_{ph}, I_d, R_s, R_p are unknown parameters intrinsic of each PV panel. The method to calculate these values applied in this thesis is adopted from the study of Tian et al. [58], where a detailed explanation is presented. In the following sections the approach of determination of the values for I_{ph},I_d, R_s,R_p is presented.

Photo-current (I_{ph})
The photocurrent is a function of the temperature and solar irradiance. Equation (4.4) is an empirical mathematical expression that defines the behavior of the photocurrent, presented by Tian et al. [59].

$$I_{ph} = I_{ph,STC} \left(\frac{G}{G_{STC}} \right) [1 + \alpha_T (T_c - T_{STC})] \tag{4.4}$$

In equation (4.4), $I_{ph,STC}$ is the photocurrent value at standard test conditions (STC). Many studies use the approximation of $I_{ph,STC} = I_{sc}$. The relative temperature coefficient of the short circuit current α_T is a parameter given by the manufacturer. $G_{STC} = 1000 W/m^2$, is the irradiance at AM1.5 spectrum; G, is the actual solar irradiance in W/m^2; and $T_{STC} = 25^o C$, is the temperature at STC.

Consequently, the photocurrent of a solar cell under any irradiance and temperature can be determined using Eq. (4.4).

Saturation current (I_d)
The diode saturation current is a temperature dependent parameter intrinsic of a solar cell. An empirical mathematical expression defines the saturation current as equation (4.5)

$$I_d = I_{d,STC} \left[\frac{T}{T_{STC}} \right]^3 \exp\left[\frac{E_{g,STC}}{kT_{STC}} - \frac{E_g}{kT} \right] \tag{4.5}$$

where, $I_{d,STC}$, is the diode current at STC. This value can be determined using the method proposed by Tian et al. [59]. $E_{g,STC}$ stands for the bandgap energy at STC. And, E_g, is the energy bandgap of crystalline silicon, which is temperature dependent [42] and can be empirically described by Eq. (4.6).

$$E_g = 1.16 - 7.021 \times 10^{-4} \left(\frac{{T_c}^2}{T_c - 1108} \right) \tag{4.6}$$

Solar cell temperature (T_c)
Irradiance and ambient temperature modify the operational solar cell temperature. Masters et al. [45] proposes an empirical mathematical expression to determine the cell's temperature by Eq. (4.7). Where, T_{amb} is the ambient temperature, G=1000 $W \cdot m^{-2}$, is the solar irradiance and *NOCT* is the nominal operating cell temperature of the panel. The NOCT represents the temperature value reached by the solar cell when it operates at solar irradiance of $800 W/m^2$, wind speed of 1 m/s, and air temperature of $20^o C$.

$$T_c = T_{amb} + \left(\frac{NOCT - 20^o C}{800} \right) G \tag{4.7}$$

Equations (4.4),(4.5),(4.6) and (4.7) can be used to model the performance of a PV module.

The unknown parameters in equations (4.4),(4.5),(4.6) and (4.7) can be determined using the mathematical model proposed by Tian et al/ [59] and the following boundary conditions:

1. Open-circuit conditions where $I_{pv} = 0$ and $V_{pv} = V_{oc,ref}$;
2. Short-circuit condition where $I_{pv} = I_{sc,ref}$ and $V_{pv} = 0$;
3. Maximum operation point where $V_{pv} = V_{mpp}$ and $I_{pv} = I_{mpp}$;
4. The derivative of power with respect to voltage at MPP $\frac{\partial P}{\partial v} = 0$ and
5. Condition that guarantees that the temperature coefficient of the open-circuit voltage is correctly predicted by $\beta_T = \frac{\partial V_{oc}}{\partial T}$.

Table 4.1 presents the technical specifications of the SunPower-300 module, that was used for the simulations.

Table 4.1: Specification of the PV panel

Parameter	**Value**
Model	SunPower 300
Technology	Crystalline silicon
Area of each module	1.6 m^2
Peak power, Pmax	300 W
Peak power voltage, V_{mpp}	54.7 V
Peak power current, I_{mpp}	5.49 A
Short circuit current, I_{sc}	5.87 A
Open circuit voltage, V_{oc}	64 V
Temperature coeficient, V_{oc}	-176.6mV / K
Number of cells, N_s	96

Assumptions
Some assumptions concerning the physical nature of the cell behavior are necessary to establish for a more practical approach. The assumptions considered in the model of the solar cell are: the ideality factor remains constant for any irradiance and temperature condition; the impedance of the parallel resistor is infinity.

The model for the solar panel was implemented in Matlab/Simulink using the above presented equations, and the SunPower parameters of the panel. Appendix A includes the detailed representation of the Simulink model for the solar modules. Figures 4.4 and Fig.4.5 show the I-V curve of the PV panel, generated with the model. The model has the flexibility to simulate any PV module configuration using all the possible irradiance and temperature conditions.

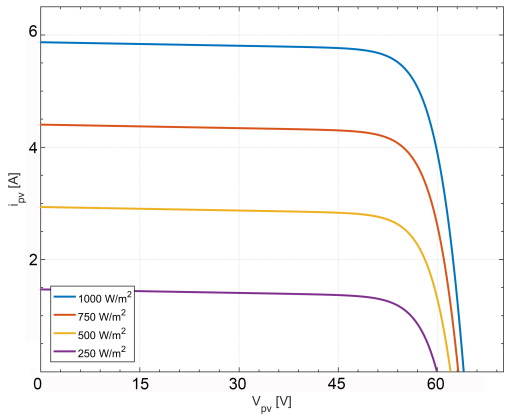

Figure 4.4: Current-voltage characteristic curve of a SunPower panel plotted by the developed model

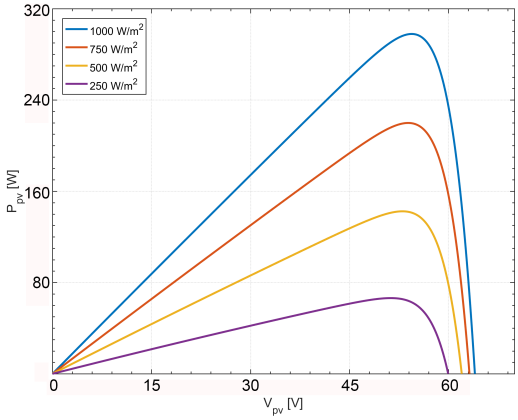

Figure 4.5: Power-voltage characteristic curve of a SunPower panel plotted by the developed model

4.2.2. PEM Electrolyzer Model

The system produces hydrogen via water electrolysis using a proton exchange membrane (PEM) electrolyzer. Chapter 2 provides the important electrochemical and thermodynamic fundamentals involved in the electrolysis process. The electrolyzer model aims to mimic the behaviour of a real component under certain voltage and current conditions. Understanding the performance of the electrolyzer is important to assess the power consumption and hydrogen production of the system. Moreover, the model provides information about the electrolyzer performance under different conditions like temperature and pressure.

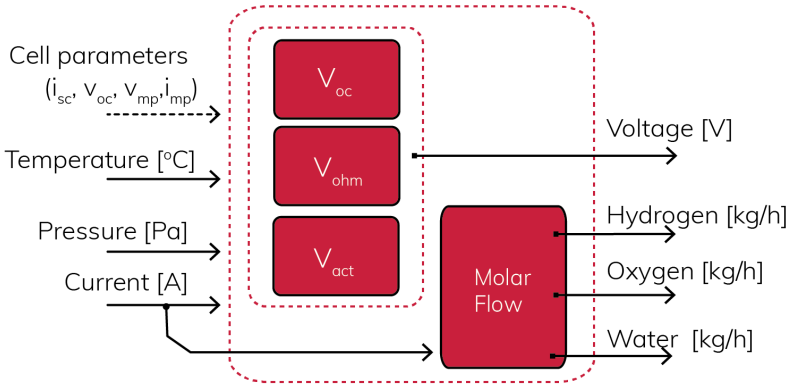

Figure 4.6: Block diagram of electrolyzer model, representing the input and output variables

The developed model of the PEM electrolyzer operation is taken from a study proposed by Awasthi et al. [18]. Current, temperature and pressure are the external parameters taken as inputs for the electrolyzer model. Additionally, the electrolyzer parameters used as input for the model. As a result, the output variables are the operational cell voltage, water consumption, oxygen, and hydrogen production. A block representation of the model with its inputs and outputs signals is presented in Fig. 4.6. A detailed water PEM electrolyzer model involves mass transfer phenomena and electrochemical reactions. Here, a more simple but practical model is used to assess the two main parameters: electrochemical potential and hydrogen production. Thus, the model is divided into two modules: (1) cell voltage module and (2) the mass flow module.

Module 1: Cell voltage

Similar to the solar cell, the electrolyzer has an I-V characteristic curve. Using the fundamentals of water electrolysis defined in chapter 2, and the simplified equivalent electric circuit of a PEM electrolyzer, shown

in Fig. 4.7, it is possible to calculate the voltage and current of the solar cell. The circuit includes a voltage source as representation of the thermoneutral voltage (V_{tn}). The two diodes connected in series, represent the reversible voltage in the anode ($\Delta E_{rev,a}$) and cathode ($\Delta E_{rev,c}$). The resistors in series represent the anode ($V_{act,a}$) and cathode ($V_{act,c}$) activation overpotential, and the ohmic overpotential (V_{ohm}). Applying Kirchhoff's Law to the circuit results in equation (4.8).

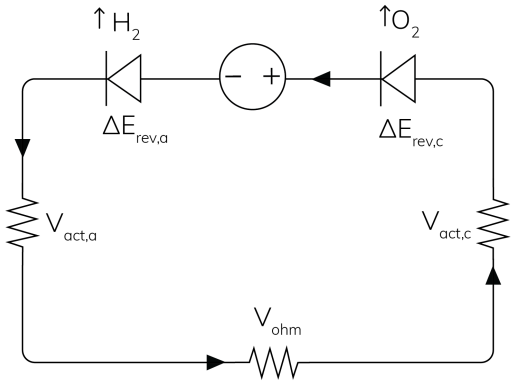

Figure 4.7: Equivalent electrical circuit of a water electrolysis cell.

$$V_{el} = E_{cell} + V_{act} + V_{ohm} \tag{4.8}$$

where E_{cell} is the open circuit voltage, V_{act} is the activation overpotential (anode and cathode) and V_{ohm} is the ohmic polarization overpotential. The open circuit voltage is a function of pressure and temperature and can be determined by the Nerst equation as shown in Eq.(4.9). Similarly, the activation and ohmic overpotentials are calculated from the empirical equations (4.11) (4.12)

$$E_{cell} = E_o + \frac{RT}{2F} \ln\left(\frac{p_{H_2} \cdot {p_{O_2}}^{0.5}}{p_{H_2O}}\right) \tag{4.9}$$

where, E_o is the standard potential, R is the universal gas constant, T is the electrolyzer temperature, F is Faraday's constant and p_x represents the partial pressure of each species inside the electrolyzer. As defined in chapter 2, the standard potential is defined by the Gibb's equation (4.10)

$$E_o = \frac{\Delta G_f}{2F} - 0.9 \times 10^{-3}(T - 298)) \tag{4.10}$$

$$V_{act} = \frac{RT}{\alpha_{an}F}\left(\frac{i}{2i_{o,an}}\right) + \frac{RT}{\alpha_{cat}F}\left(\frac{i}{2i_{o,cat}}\right) \tag{4.11}$$

$$V_{ohm} = I \times R_{ohm} \tag{4.12}$$

Assumptions
The mass transfer overpotential is neglected since it is insignificant for low current densities in PEM electrolyzers.

Using the mathematical expression above described, and the technical specification of the electrolyzer shown in the table 4.2, the voltage module for the electrolyzer was built on Simulink. A detailed representation of the model on Simulink is presented in Appendix A.

The model of the PEM electrolyzer was implemented in Matlab/Simulink using the above presented equations, and the electrolyzer parameters in table 4.2. Appendix A includes the detailed representation of the Simulink block for each component.

Figure 4.8 shows the I-V characteristic curve of the electrolyzer, generated with the model. The three main overpotential curves are included in the figure. Understanding the impact of each of the overvoltages is important to select the optimal operating condition of the electrolyzer. The model has the flexibility to simulate any number of PEM cells connected in series and different operating conditions.

Table 4.2: PEM Electrolyzer specifications

Parameter	**Value**
Power	120 W
Current	6-60 A
Operating Voltage @ 40 A	2 V
H_2 production	45-450 sccm
O_2 Production	22-220 sscm
Operating Temperature	20-50 ^oC
Weight	3 Kg
Number of cells	1
Active Area	50 cm^2

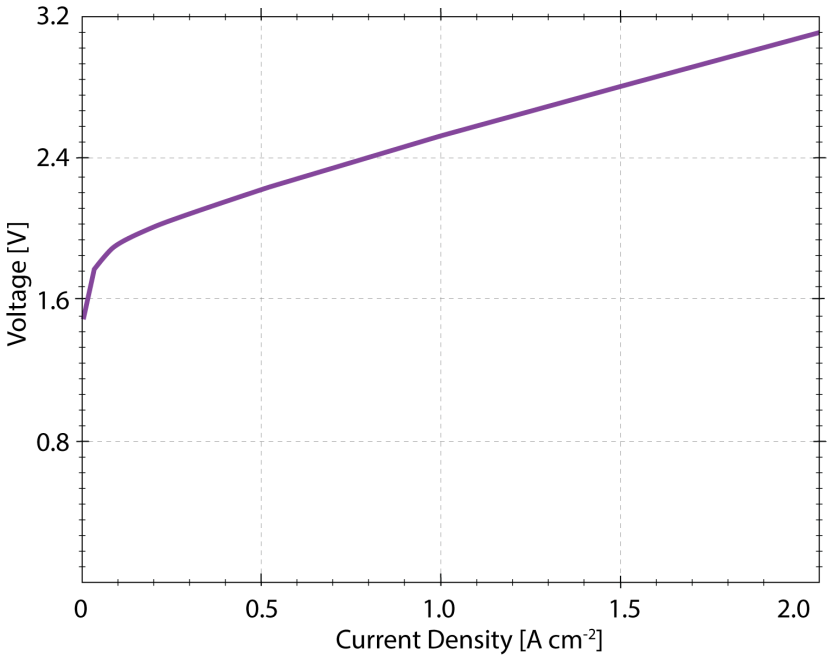

Figure 4.8: Current-voltage characteristic curve of one cell PEM electrolyzer at 300K and 1 atm

Module 2: Mass flow

According to second Faraday's law for electrolysis, the amount of substance generated by an electrode is proportional to the quantity of the electric current passing through. Chapter 2 already introduced these concepts, thus the equations to determine the molar flow of each of the species are Eq. (4.13), (4.14), and (4.15).

$$\dot{m}_{H_2} = \eta_F \frac{N_s \times I}{n \times F} \tag{4.13}$$

$$\dot{m}_{O_2} = \frac{nI}{4F} \tag{4.14}$$

$$\dot{m}_{H_2O} = \frac{nI}{2F} \tag{4.15}$$

The reaction efficiency is determined by the Faraday's efficiency (η_F) as shown in Eq. (4.16).

$$\eta_F = 96.5 \times exp\left(\frac{0.09}{I} - \frac{75.5}{I^2}\right) \tag{4.16}$$

The above equations are required to determine the molar flow of hydrogen and oxygen in the cathode and anode, respectively for a PEM electrolyzer. Similarly, with equation (4.15), the water consumption during the reaction can be determined in function of the current.

The current through the electrodes is the only external signal, that the mass flow model needs. As a result, the output of this module is the water consumption rate as well as the hydrogen and oxygen production rate. A simplified representation of the molar mass module and its input and output signals are shown in Fig. 4.6

Assumptions
The main assumption for the hydrogen production is neglecting the variation of the Faraday's efficiency. This model assumes a constant Faraday's efficiency during the electrochemical reaction. This assumption is valid since the PEM electrodes are relatively stable in operation. Thus, the electron utilization remains constant.

Consequently, the model of a PEM electrolyzer was built in two main modules. First the cell voltage module, that describes the voltage and current dependence of the electrolyzer. Second, the molar mass flow module that determines the hydrogen production and the other species involved. Both modules were built up using Simulink as represented in Appendix A.

4.2.3. Battery Model

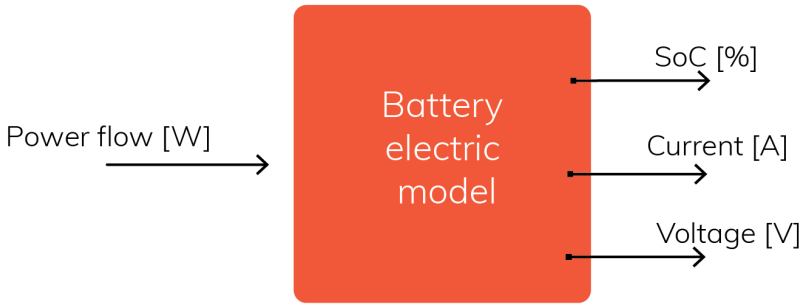

Figure 4.9: Block diagram of the battery model, representing the inputs and output signals

A detailed model of the battery involves thermodynamics, material science, and electrochemical phenomenon depending on the technology of the selected battery. For the sake of simplicity, only the power management of the battery is considered in this thesis. Thus, this model gives particular attention to the electrical behavior of the battery.

The battery model provides the energy flow during the charge and discharge process. The power flow of the battery allows assessing the number of discharge cycles, thus evaluate the lifespan of the battery. The depth of discharge is another useful parameter to assess the lifetime of the battery. The more the battery is discharged, the fewer cycles the battery will be capable of complete. Hence the proposed model for the battery has the most important variables like power flow, state of charge and deep of discharge. Those variables allow to assess the performance of the battery, and design the most optimal battery configuration

The voltage and current are the inputs for the battery model. Those input parameters are determined by the PV model. As a result, the state of charge, the discharging current, and the voltage are the outputs signals of the model. The limit of these values are set by the control unit, which is described later in this chapter.

The model is based on the simplified equivalent electric circuit of the battery, shown in Fig. 4.10. The circuit includes a controllable voltage source as the representation of the open circuit voltage (V_{oc}). This voltage is the electrochemical potential of the battery, which in this study is considered as a constant value. The resistor (r_{int}) represents the total internal resistance, experienced by the current (i_b) in the battery. The resistance includes the electronic and ionic components.

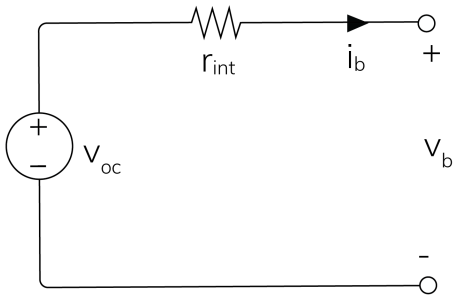

Figure 4.10: Simplified equivalent circuit of the battery

Applying Kirchhoff's Law to the circuit, the voltage flow through the battery is determined, by Eq. (4.17). The power flow in the battery can be determined using the definition of the electrical power $P_b = i_b V_b$, as expressed in Eq. (4.18). The state of charge (SOC) of the battery is defined by the relationship of the instantaneous energy inside the battery and the total battery capacity, by Eq. (4.19).

$$V_b = V_{oc} - i_b \cdot r_{int} \tag{4.17}$$

$$P_b = i_b \cdot V_{oc} - {i_b}^2 \cdot r_{int} \tag{4.18}$$

$$SOC = \frac{\int P_b \, dt}{Q \cdot V_{b,nom}} \cdot 100\% \tag{4.19}$$

Assumptions
Some asumptions were taken in the model to simplify the complexity of the battery operation and get a practical representation of the component. The temperature variations and electrochemical reaction inside the battery are neglected. The internal resistant is assumed to behave in a linear relationship independently of the temperature and chemical reactions. Those assumptions are valid since the aim of the model is to assess the components from the system perspective and not detailed.

Consequently, the battery model was built on Simulink using the above described equations and the battery specifications presented in Table 4.3. A detailed block diagram of the battery model implemented in Simulink is shown in Appendix A.

4.2.4. Storage Tank Model

The hydrogen produced by the electrolyzer is stored in a container. A steel storage tank was selected as the most suitable option because it is relatively small and cheap. This model determines the amount of hydrogen and pressure inside the tank. The amount of gas inside the tank helps to determine the optimal capacity for storage of any hydrogen production rate.

This model is developed based on the study from Al-Refai et al. [16]. Hydrogen can be considered as ideal gas, since the operational temperature and pressure are in the range where this gas behaves as an ideal gas.

Table 4.3: Battery technical specifications

Parameter	**Value**
Brand	Fullriver DC70-12
Type	AGM
Capacity	70 Ah
Rated voltage	12 V
Internal resistance	5.5 $m\Omega$
Operating temperature	25 ^oC
Dimensions (LxWxH)	260x169x211 mm
Weight	24.2 kg

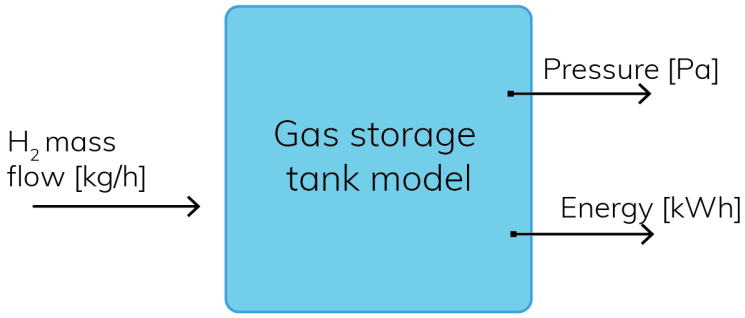

Figure 4.11: Block diagram of the storage tank model, representing the input and output signals

Assuming hydrogen behaving as an ideal gas means that the inter-molecular forces are insignificant. Thus, the pressure increase over a unit of time inside the tank is determined by Eq.(4.20).

$$\frac{\mathrm{d}P_{tank}}{\mathrm{d}t} = z\frac{\dot{m_{H_2}}RT}{M_{H_2}V_b} \tag{4.20}$$

In equation (4.20), $z = 1.0006$, is the compressibility factor for hydrogen, which corrects the deviation of a real gas from ideal gas behavior. $M_{H_2} = 2g/Mol$ is the hydrogen molar mass. And $\dot{m_{H_2}}$, is the hydrogen mass flow rate being delivered by the electrolyzer in (g/s). V_b is the volume of the tank in (m^3); T is the gas temperature in kelvin (K); and R=8.3144 $m^3PaK^{-1}mol^{-1}$ is the ideal gas constant. The pressure values is calculated by integrating dP/dt over the operation time.

Additionally, the energy stored in the tank can be determined by Eq. (4.21).

$$E_{tank} = m_{H_2} \times HHV \times 3.6 \tag{4.21}$$

Where, E_{tank} is the chemical energy in the tank in (kWh), m_{H_2} is the hydrogen mass in (Kg), and HHV=39.4 kWh/kg is the high heating value of molecular hydrogen.

Assumptions
This model assumes that the compression of hydrogen is an adiabatic process, thus temperature variations are neglected. The compression losses are not included in the model. All auxiliary power requirements such as pumps, valves and connector are not part of the model. These assumptions are made for the sake of simplicity. Nevertheless, the assumptions make this model less accurate, especially since storing hydrogen gas demands an addition of energy to reach high pressure levels.

Consequently, the hydrogen storage model was build on Simulink using the above described equations. A detailed block diagram of the hydrogen storage model implemented in simulink is show in Appendix A.

4.3. Power Control Strategy

The power control unit is responsible for managing the energy flow in the system. Energy is taken from the PV system and distributed to rest of the components. The control strategy depends on the system configuration and the optimization function. For instance, a direct coupling between the PV system and the electrolyzer will require a less sophisticated control strategy since the electrolyzer directly draws the current from the PV modules. Nevertheless, an arrangement including PV modules, batteries, electrolyzer, and auxiliary components requires a more elaborated control. Voltage levels need to be adjusted, and power needs to be optimally distributed among all the components. Overall, the hybrid systems performance depends on the control unit for an optimal operation.

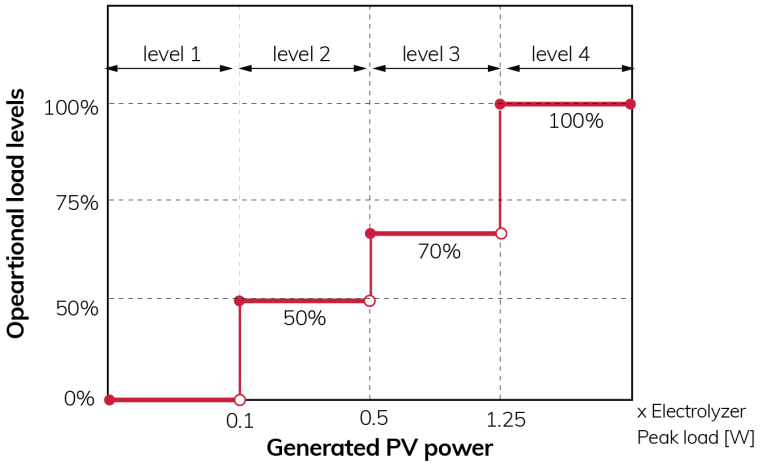

Figure 4.12: Load values in function of the amount of power delivered by the PV modules.

The proposed control strategy is designed for the system configuration that includes PV modules, electrolyzer, battery, and power electronic components. The goal is to determine the moments when the energy should be stored in the battery or consumed by the electrolyzer, minimizing the dumping of energy.

The control starts by reading the instantaneous values of: the power delivered by the PV modules (P_{pv}), the battery state of charge (SOC) and the electrolyzer power consumption (P_{load}).

Four operational levels have been defined for the electrolyzer, to safeguard its lifetime, and optimize the energy consumption of the system. This means that the electrolyzer power consumption (P_{load}) is defined by the power delivered from the PV system (P_{pv}). Based on the PV generated power, the electrolyzer might operate at 0%, 50%, 70%, or 100% of its capacity. For instance, when the generated power -from the PV system- is more than 1.25 times the electrolyzer rated power (P_{pv}>1.25P_{el}^{max}); the electrolyzer operates at its maximum capacity ($P_{load} = P_{el}^{max}$). In the next level, the electrolyzer works at 70% of its capacity when the generated PV power is between 0.5 and 1.25 times the electrolyzer rated power. When the PV system generates between 0.1 and 0.5 times the electrolyzer peak power (P_{el}^{max}); the electrolyzer runs at 50% of its capacity. For a PV power less than 0.1 of P_{el}^{max}; the electrolyzer does not operate. Figure 4.12 illustrates the four operation levels of the electrolyzer as a function of the power delivered by the PV system.

Once the load value (P_{load}) is defined, the control unit determines how much power should be provided to the electrolyzer, or stored in the battery or dumped. The decision is determined by subtracting the PV power and the fixed load value ($P_{diff} = P_{pv} - P_{load}$). Based on the irradiance level, the result might be either positive or negative. In other words, this value tells when there is a surplus or deficit of energy in the system. For either situation, the next step for the control unit is to verify the battery state of charge (SOC).

Similarly to the electrolyzer, the battery has two levels for the state of charge (SOC). These levels are established to safeguard the battery lifetime. For lead-acid batteries, the literature suggests that the state of charge should not be lower than 40% and higher than 90%. Hence, when the state of charge reaches a value of SOC=90%, the battery will be considered fully charged. Likewise, the discharging process stops when SOC=40%.

For the condition when $P_{diff} > 0$ and SOC<90, the power is used to charge the battery. In contrast, the power will be dumped if the battery is fully charged (SOC=90%). This situation is not desirable, yet the control algorithm has to include this possibility to avoid undefined control errors.

When there is an energy deficit on the system $P_{diff} < 0$, but the battery has enough energy stored (40%<SOC<90%), the electrolyzer draws energy from the battery, thus the battery discharges. Lastly, the system will experience a power shortage when both conditions $P_{diff} < 0$ and SOC<40% are reached, thus the systems blacks out . The described system control is illustrated in a flow diagram by Fig. 4.13.

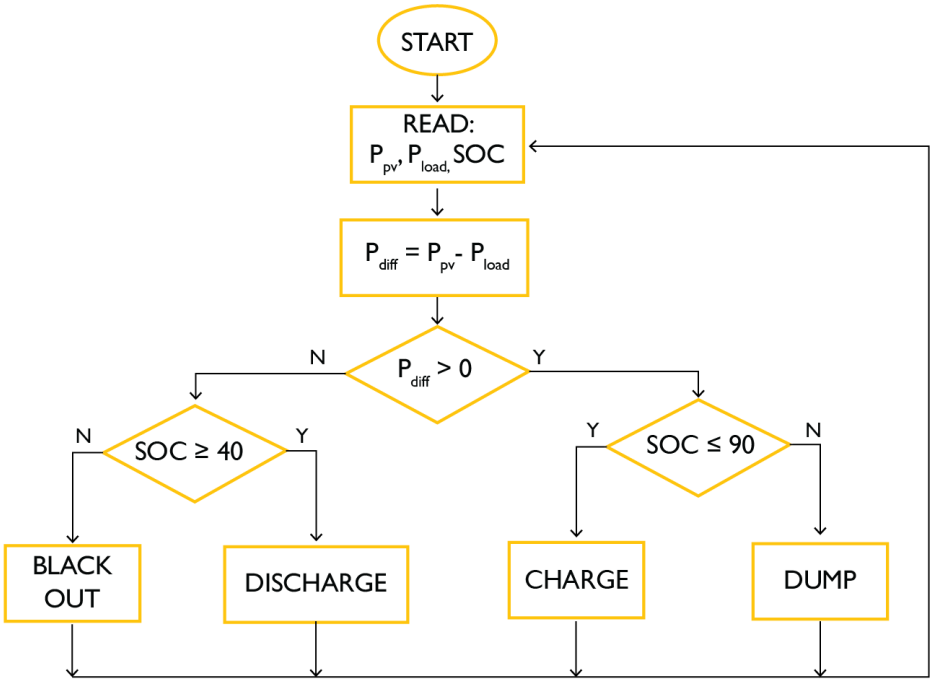

Figure 4.13: Flow diagram of the system control

4.4. Performed Simulations

Three system configurations were tested, in order to assess the performance of the hybrid system. The first configuration is a direct coupling between the PV modules and the electrolyzer. The second configuration includes a maximum power point tracker (MPPT) between the PV modules and the electrolyzer optimizing the electricity production from the solar panels. The third configuration includes the same components from the second one, plus a battery bank. Figure 4.14 illustrates the three system configurations tested in this thesis. The next chapter describes in more detail each configuration along with the performed analysis.

Additionally, scaling of the system components is analyzed, using the third system configuration. Understanding how each component size affects the performance of the system, is essential for the design of such a system. Hence, a total of one-hundred combinations of component sizes were simulated. Table 4.4 shows the sizes for the PV modules, batteries, and electrolyzer utilized. The combinations were done as shown in Fig. 4.15

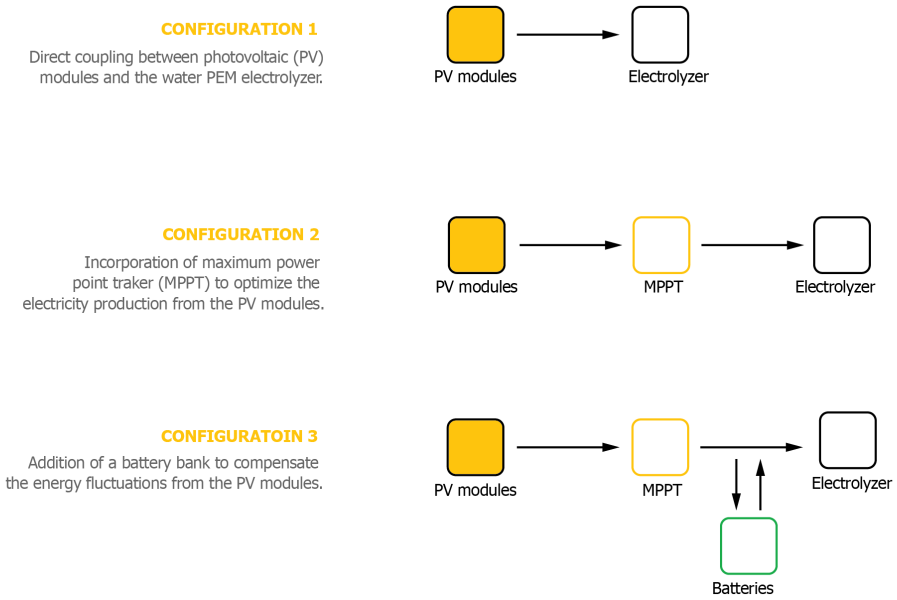

Figure 4.14: Schematic representation of the three system configurations

Table 4.4: Size components utilized for the performed simulations

PV modules (W)	Battery bank (Ah)	Electrolyzer (W)
600	70	120
1200	140	240
1800	210	480
2400	280	960
	350	1200

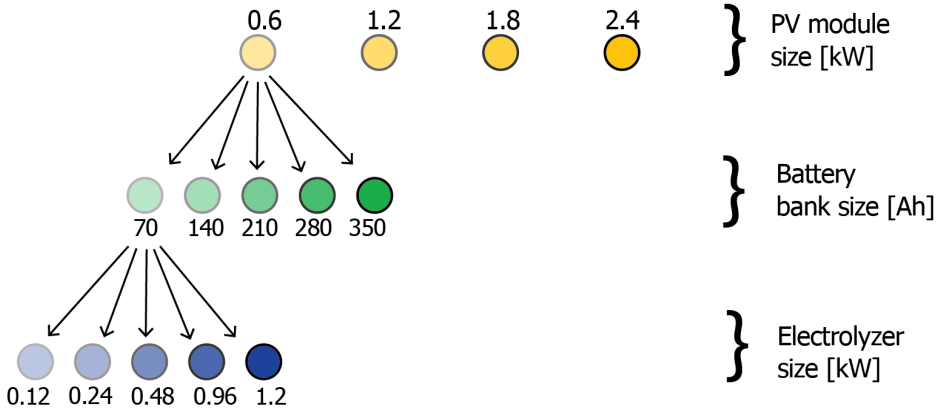

Figure 4.15: Illustrative representation of the combinations used to asses the impact of component size.

4.5. Non-dimensional Sizing Factors

In order to analyze and explain the simulation results in a more comprehensive way, six non-dimensional factors are proposed. The factors relate the three main variables of the system: the PV modules, the battery bank, and the electrolyzer. The proposed factors aim to provide a criterion for the system design. The following section introduces each factor.

Battery energy factor (BEF)

The battery energy factor (BEF) is equal to the installed battery capacity (in Wh) of the system divided by the total annual energy delivered from the modules (in Wh) Eq. (4.22). This factor provides a relative comparison between the battery and PV modules size. Ideally speaking, having a BEF=1 means that the PV generated energy over a year can be stored in the battery bank. Since batteries have a low energy density (60 Wh/l), storing large amounts of energy means a large volume of batteries. For instance, using 2 solar modules (300 W each) will approximately generate 600 kWh/year in Delft. This means a storage container of 10 m^3. Additionally, since batteries naturally self discharge over time (6% per month), a big amount of energy (216 kWh) will be lost. Hence, practically speaking having a system with BEF=1 is far from an optimal design.

$$BEF = \frac{battery\ energy\ capacity\ [Wh]}{annual\ PV\ energy\ generated\ [Wh]} \tag{4.22}$$

PV to load factor (PVL)

The PV to load factor (PVL) is a relative size comparison between the nominal PV module power (in watt peak W_p) and the yearly average load value (in watts) Eq.(4.23). The last one is defined as the energy consumed by the electrolyzer over a year divided by the number of hours in a year. For example, an energy consumption of 876000 Wh during a year represents an yearly average load value of 100 W. This value is related to the electrolyzer utilization. For instance a averange load of 100 W might represent a 120 W (rated power) electrolyzer operating most of the time at 83% of its capacity.

$$PVL = \frac{averange\ annual\ load\ [W]}{PV\ installed\ capacity\ [W_p]} \tag{4.23}$$

Energy deficit factor (EDF)

The energy deficit factor (EDF) is equal to the annual energy deficit (in Wh) divided by the annual PV energy output (in Wh) Eq.(4.24). As explained in Section 3.3, the system experiences an energy deficit when neither the PV modules nor the battery can deliver power to the electrolyzer. The electrolyzer needs a minimum amount of power to start its operation which is defined by the power control unit. The minimum amount of power needed to run the electrolyzer is defined to be 10% of its rated power, according to in figure 4.12

$$EDF = \frac{annual\ energy\ deficit\ [Wh]}{annual\ PV\ energy\ generated\ [Wh]} \tag{4.24}$$

Surplus energy factor (SEF)

In contrast to the energy deficit factor, the surplus energy factor (SEF) is proposed. This is equal to the energy dumped by the system (in Wh) divided to the total PV generated energy (Wh) Eq. (4.25). The energy dumped might occur during high irradiance periods and small storage capacity. The higher the value the higher the amount of energy dumped. An optimal system operation should have a SEF value as close as possible to zero.

$$SEF = \frac{annual\ energy\ dumped\ [Wh]}{annual\ PV\ energy\ generated\ [Wh]} \tag{4.25}$$

Load factor (LOF)

The load factor is defined as the fraction between the yearly average load consumption (in watts) and the installed load capacity (in watts) Eq. (4.26). This factor evaluates the electrolyzer utilization over a year. A value of LOF=1, means the electrolyzer is operating at its maximum capacity during the entire year. Indeed, the value can not reach a higher value than LOF=1.

$$LOF = \frac{averange\ annual\ load\ [W]}{maximum\ rated\ load\ [W]} \tag{4.26}$$

Energy consumption factor (ECF)

The difference between the surplus and the deficit energy is defined as the energy consumption factor (ECF). This index shows the relationship between the actual energy used and the total PV generated energy Eq.(4.5). A value of ECF=0 can indicate two situations.

First, the same amount of energy is dumped by the system as the amount of energy to run the electrolyzer over a year is lacking. Secondly an ECF=0 can also mean that the system is effectively managing all the energy. Both dumped and deficit energy are equal to zero. The last case is the most desired one. Having values of ECF<0 represent a lack of energy for the system. The more negative the value, the bigger the energy deficit is. This value can be corrected by either adding more solar modules ore reducing the load value. On the other hand, when the ECF>0, it means that the system is dumping more energy than the deficit energy. This situation might be corrected by both increasing the battery capacity of the system or increasing the energy utilization.

$$ECF = \frac{\text{annual energy dumped [Wh] - annual energy deficit [Wh]}}{\text{annual PV generated energy [Wh]}}$$

$$ECF = SEF\text{-}EDF \tag{4.27}$$

5

Model Results and Discussions

This chapter presents the simulation results of the solar-to-hydrogen (S2H) system operation. The results are presented in three parts. Each section corresponds to a different system configuration : (I) direct coupling, (II) including an MPPT, and (III) including a battery bank. The first section presents the results of a tailored PV module directly connected to the PEM electrolyzer. In the second section the results of hydrogen production using a PEM electrolyzer powered by a commercial PV module attached to a MPPT are discussed. The third section, presents two designs. The initial design includes a set of PV modules, MPPT and batteries, operating for the entire year. The final design includes two set of components. One designed for summer and another for winter. For all the configurations, the results of the PV energy yield, the hydrogen production, the electrolyzer lifetime, and the system efficiency are discussed. All simulations were run for irradiance data over a year with a resolution of one hour from Delft.

5.1. System Configuration I: Direct Coupling

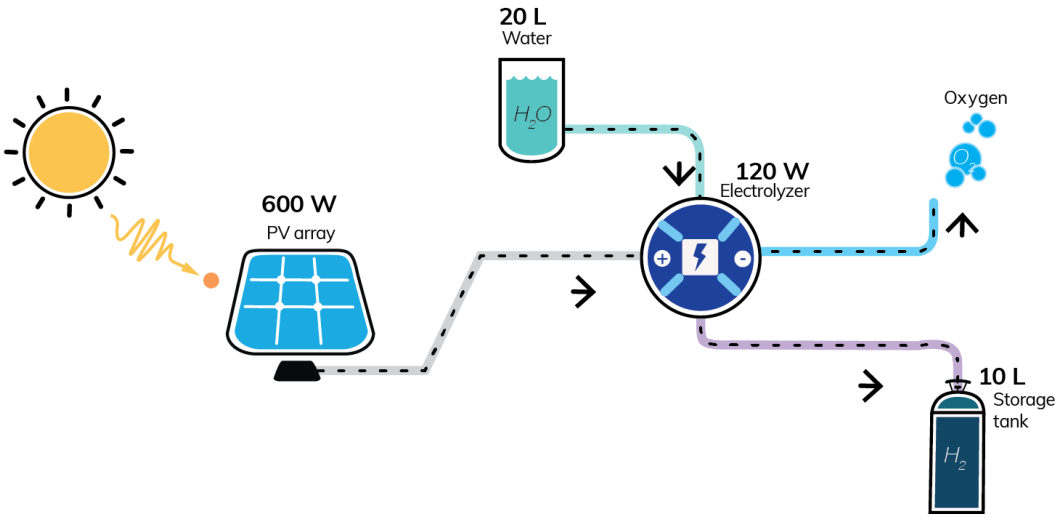

Figure 5.1: Schematic representation for system configuration I: Direct coupling.

System configuration I is the most straightforward system set up between the PV modules, as the primary energy source, and the electrolyzer as the load. The initial design consists of one solar panel connected directly to a polymer electrolyte membrane (PEM) electrolyzer of a single cell of 120 W rated power. The PV module delivers direct current (DC) power to the electrolyzer. The electrolyzer uses this energy to split water into oxygen and hydrogen gas. A water tank of 20 liters is connected to the electrolyzer using a pump, to guarantee a

constant water flow during the system operation. This configuration does not include extra power electronic components. Because of that, the configuration becomes a simple and relatively low-cost system. Fig. 5.1 shows the schematic representation of the system configuration.

The optimal operation between the PV modules and the electrolyzer is achieved when all the available solar power is used to produce hydrogen. The optimal operating point for the PV modules is known as the maximum power point (MPP). In this thesis, the optimal operating point of the electrolyzer is defined by the nominal operating point (60% rated power). Thus, the optimal operating point of the system is the combination of both conditions.

The operating point of the system can be identified using the current-voltage (I-V) characteristic curve of both components. Using the data of a SunPower-300 module, and the model implemented in Simulink, the I-V curve for the solar panel is obtained. Figure 5.2 shows the I-V curve of the PV module for different irradiance conditions. Similarly, the P-V characteristic curve in Fig. 5.3 shows the irradiance dependence of the maximum power point. The MPP of the PV module is irradiance and temperature dependent. Any operating point of the system different than the MPP involves energy losses in the system. In other words, the harvesting of the available solar energy is not optimal.

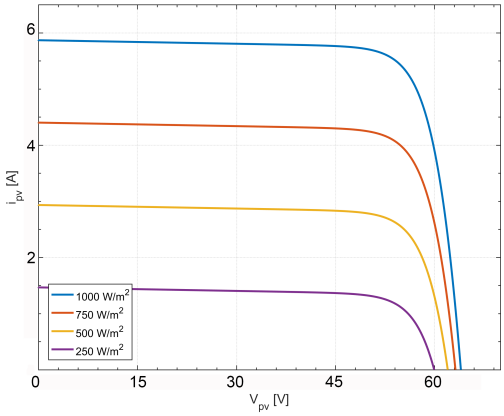

Figure 5.2: Current-voltage characteristic curve of a SunPower panel plotted by the developed model

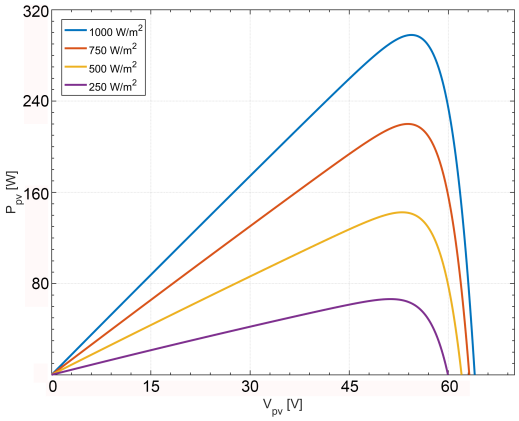

Figure 5.3: Power-voltage characteristic curve of a SunPower panel plotted by the developed model

Figure 5.4 shows the I-V curves of both components the electrolyzer and the PV module. Several electrolyzer configurations curves are included in the figure. Each curve of the electrolyzer represents new cells connected in series. The more PEM cells connected in series, the closer the operating point it gets to the MPP of the solar panel. Each intersection point in the I-V curve defines the operating point for the whole system. Unfortunately, the crossing point for a single cell electrolyzer working with the SunPower-300 module is far distant from the MPP of the module. This means significant energy losses during the system operation.

When the electrolyzer and the PV modules are connected, the operating point is limited by the load value of the electrolyzer. This means that the PV module only delivers the power that the electrolyzer can consume. When the PV modules can produce more solar power than the possible power to be consumed by the electrolyzer, the solar power is wasted; thus the configuration is not optimal.

The MPP of the solar modules is located at a relatively high voltage (48 V) and low current (5.8 A). The reason for that is because the PV modules are designed to achieve higher voltages than current values. Generally, a solar panel is made of several single solar cells connected in series; this causes that the voltage builds up. On the other hand, the PEM electrolyzer operates at a relatively low voltage (2 V) and high current (50 A). The reason for that is because of the thermodynamics and electrochemistry principles that govern the water splitting process. These concepts were already introduced in Chapter 2.

The mismatch of voltage and current between the electrolyzer and the PV module represents a limitation for easy and direct coupling of the components. A direct connection between the commercial module (SunPower-300) and the electrolyzer represents a significant amount of energy losses. Then, this thesis explores two alternatives to find the optimal direct configuration between the PV modules and the electrolyzer. The first

alternative is increasing the number of PEM electrolyzers connected in series to achieve a higher voltage closer to the MPP of the PV module. The second alternative is tailoring a PV module that satisfies the voltage and current levels of the electrolyzer. Both alternatives are discussed in the following sections.

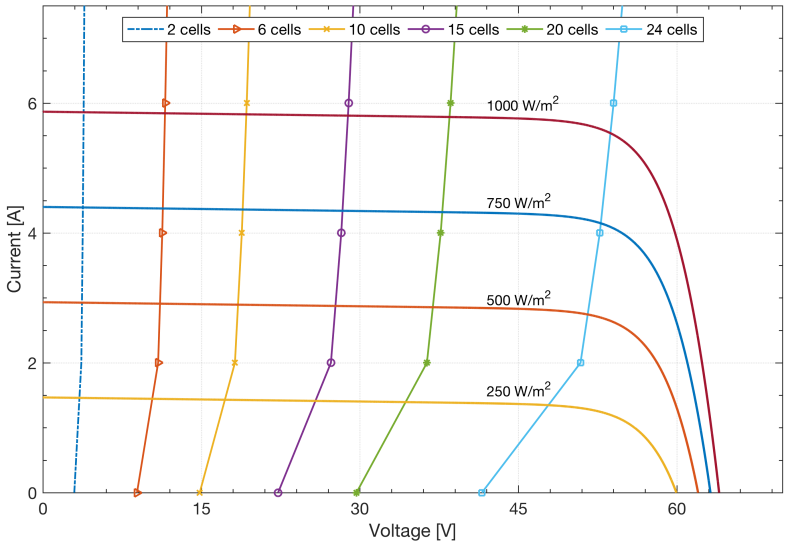

Figure 5.4: Current-voltage characteristic curve of SunPower-300 solar panel exposed at different irradiance values, and electrolyzer with several cells connected in series.

Connecting PEM cells in series

When more than one PEM cells are connected in series, the operating voltage of the electrolyzer increases. The voltage increases because each PEM cell needs an equal potential to split water. Hence, the operating voltage of the whole stack increases proportionally to the number of cells connected in series. Figure 5.4 shows the I-V curve of the SunPower-300 module exposed at different irradiance levels and an electrolyzer with different cells connected in series. The simulations were run for 2, 6, 10, 15, 20 and 24 identical PEM cells connected in series. Each configuration adds up the voltage level and the power consumption of the electrolyzer. For a single PEM electrolyzer, a voltage of approximately 2 V is needed. Then, to achieve a voltage of 48 V, the electrolyzer needs 24 PEM cells connected in series. The achieved voltage is closer to the MPP of the PV module. Consequently, the operating voltage of the system is optimized.

Connecting several PEM cells in series increase the operating voltage of the electrolyzer. Nevertheless, the current delivered by the PV module remains relatively low (6 A). The current value of 6 A, represents less than 15% of the electrolyzer's rated current (40 A). The hydrogen production related to that current is significantly low. Low current value means that the electrolyzer is not being optimally used. Hence, the current from the PV module needs to adapt to the electrolyzer requirements.

The current value can be increased by connecting more solar panels in parallel. The electrolyzer utilized in this thesis draws a maximum current of 50 A. Hence, using nine solar modules connected in parallel (6 A×9=54 A), the current and voltage of both components are satisfied.

Consequently, the system for an optimal direct configuration needs an electrolyzer stack made of 28 cells in series, and nine solar modules connected in parallel. The electrolyzer reaches a power of 2400 W (48 V×50 A), and the PV modules built up a power of 2700 W (300 W×9). These results show that the voltage and current are limiting factors when sizing an S2H system for a direct configuration.

Tailoring a PV module

The second alternative to match both voltage and current of the components is by customizing a PV module. The PV module is designed to provide a relatively low voltage (2 V) and higher current (50 A). In order to achieve that, the solar module is customized with several single solar cells connected in parallel and only few cell connected in series. In this way, the voltage remains low and the current builds up.

The I-V curve of a single cell can be plotted in a graph by using the implemented model in Simulink. The

parameters of the solar cell are shown in table 5.1. Figures 5.6 and 5.7 show the generated current and voltage of several solar cells connected in series and parallel. A tailored solar module made of 5 × 7 (series× parallel) solar cells, reaches an open circuit voltage of 3.1 V and short-circuit current value of 60.2 A. The power peak of the tailored PV module is approximately 150 W. The customized PV module satisfies the voltage, current and power levels for the electrolyzer. Consequently, the final system configuration consists of a single cell PEM electrolyzer of 120 W, and a tailored PV module of 150 W.

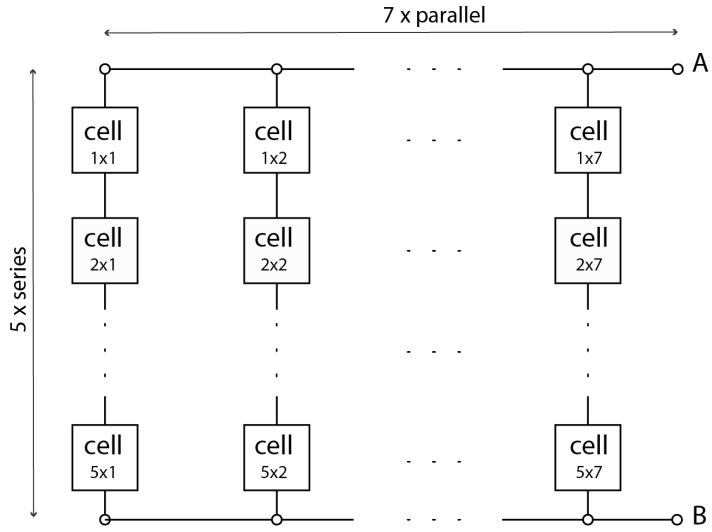

Figure 5.5: Solar cell configuration for the tailored PV module.

Table 5.1: Single solar cell specifications

Parameter	**Value**
Manufacturer	BSolar Ltd.
Material	Monocrystalline P-Type Silicon
Mean power	4.30 W
Peak power voltage, V_{mmp}	0.50 V
Peak power current, I_{mmp}	8.60 A
Open circuit voltage, V_{oc}	0.620 V
Short circuit current, I_{sc}	8.88 A
Short circuit temperature coefficient	3.14 mA/K
Ideality factor, n	1.3
Dimensions	156 × 156 mm

Regarding size, the second alternative is the smaller option. The size of the system is related to the PV module and the single cell electrolyzer. Additionally, the second alternative is more straightforward than the first alternative since it implies fewer components. A system with two components, one PV module and one electrolyzer, is relatively less expensive than a system with 28 PEM cell electrolyzer and nine PV modules. Consequently, the most cost-effective alternative for a direct connection between the PV module and a PEM electrolyzer is by customizing a PV module that suits the electrolyzer operating characteristics. The next sections discuss the performance of the system using the tailored PV module and the single cell PEM electrolyzer.

5.1.1. PV Energy Generation

The simulation run in this section, and in the rest of this chapter uses irradiance data on an hourly basis from Delft, as shown in Fig. 5.8. The highest level of irradiance happens during summer, with values up to 900 Wh/m^2. Over the entire year, the amount of irradiance in Delft is 1030 kWh/m^2. The power generation by the system for the period of a year is shown in Fig. 5.9. Using the tailored module of 150 W_p (Watt-peak) the annual power production is 143.9 kWh/year. The efficiency of the module is 16.4% ($143.9/(0.156^2 \times 35 \times 1030)$).

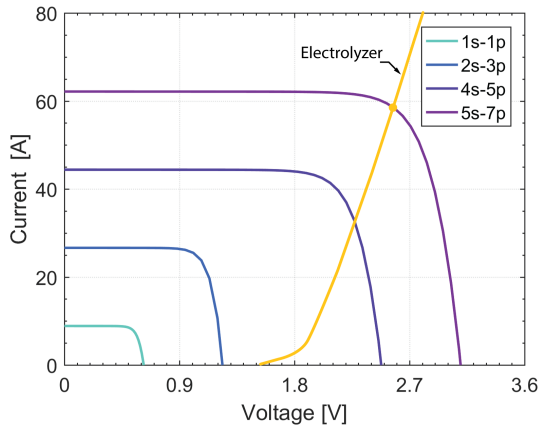

Figure 5.6: I-V characteristic at STC for various solar cell connected in series (s) and parallel (p).

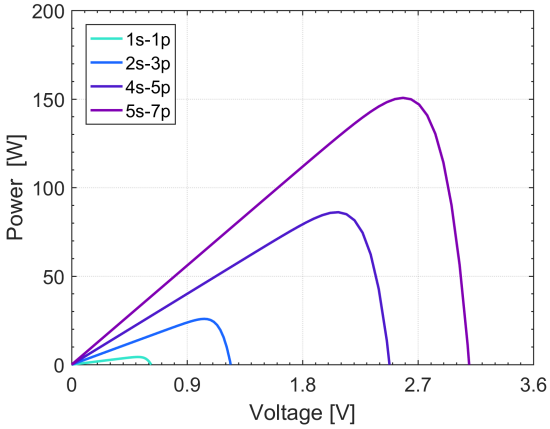

Figure 5.7: P-V characteristic at STC for various solar cell connected in series (s) and parallel (p).

The efficiency value is calculated only considering the actual production of energy, but not including the cable losses or any other kind of energy losses in the system. The fact that the tailored PV module fits the current and voltage of the electrolyzer reduces the electric losses for a direct configuration.

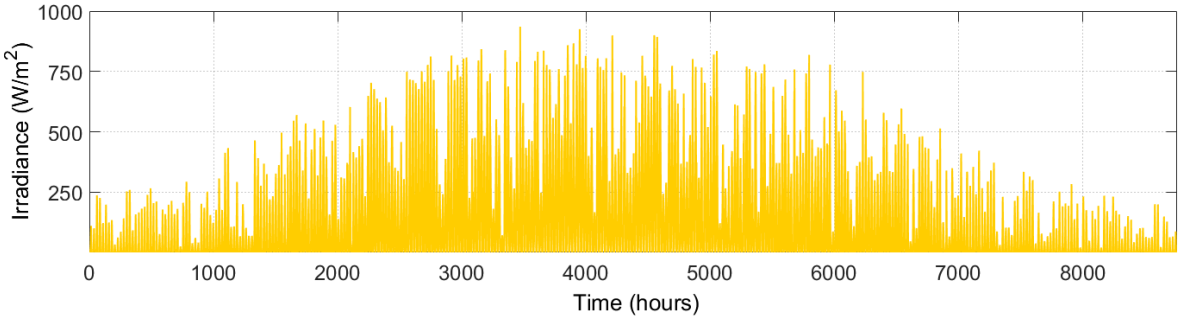

Figure 5.8: Irradiance data from Delft over the period of a year.

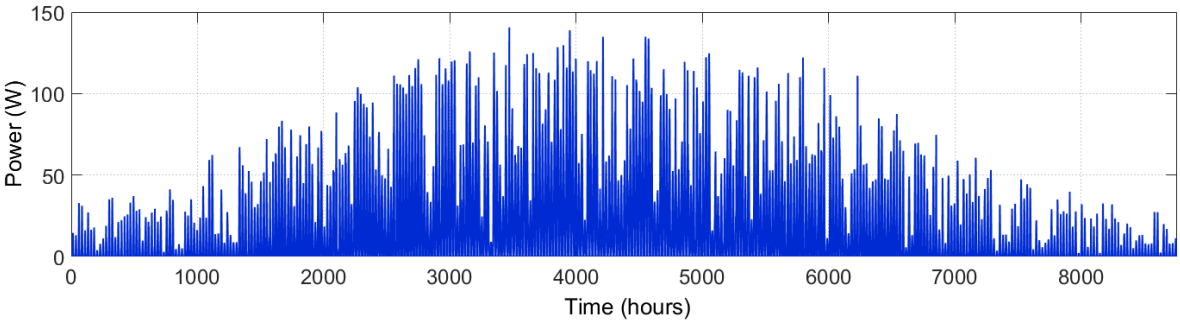

Figure 5.9: Power generated from the tailored PV module exposed to the yearly irradiance of Delft.

5.1.2. Hydrogen Production

For a direct configuration system, all the generated power by the PV module is used to produce hydrogen. The tailored PV module provides the current and voltage to the electrolyzer without the need for any extra electronic components. The production of hydrogen is proportional to the current delivered by the PV module. The more current delivered by the PV module, the higher the hydrogen production from the electrolyzer. Over the period of a year, the system produces 1.831 kg of hydrogen, as shown in Fig. 5.10. This production means that for each kilogram of hydrogen, the system consumes 78.59 kWh. For an ideal hydrogen produc-

tion (100% efficiency), the energy to produce one kilogram of hydrogen would be 33.33 kWh/kg. Thus, the efficiency of the electrolyzer in this system configuration is 42.41%.

The hydrogen production in the system is limited to the electrolyzer capacity. The electrolyzer capacity is 120 W. All the power production higher than 120 W cannot be used to produce hydrogen. Hydrogen cannot be produced with the energy surplus because it oversaturates the electrolyzer's capacity. Hence the component sizing is crucial for an optimal system design. This issue can be solved by over-sizing the electrolyzer capacity or by adding an energy storage component to the system.

The hydrogen production is directly proportional to the irradiance levels. During summer when there are higher irradiance levels, the hydrogen production increases. Figure 5.10 shows how the rate of hydrogen production increases significantly during the period when there is more solar power available. During winter (left/right area in Fig. 5.10) the hydrogen production is minimal.

Additionally, as part of the electrolysis process, oxygen is produced in a total amount of 13.76 Kg. The water consumption corresponding to the generated hydrogen is 16.48 Kg of water. Understanding the electrolysis process is essential because both water and oxygen are substances that are always present during the hydrogen production. Oxygen can be reused for medical applications or to generate electricity when combining with hydrogen using a fuel cell.

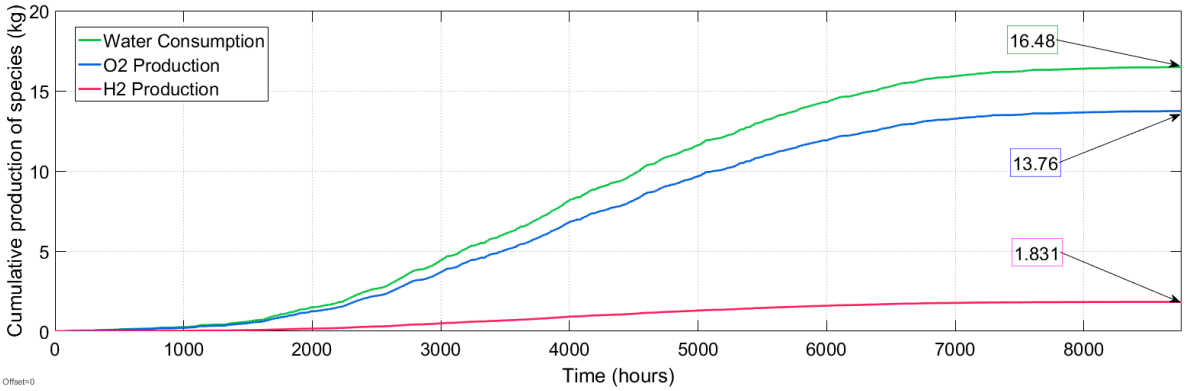

Figure 5.10: Cumulative hydrogen production over a year using a direct coupling configuration of a tailored PV module and a PEM electrolyzer.

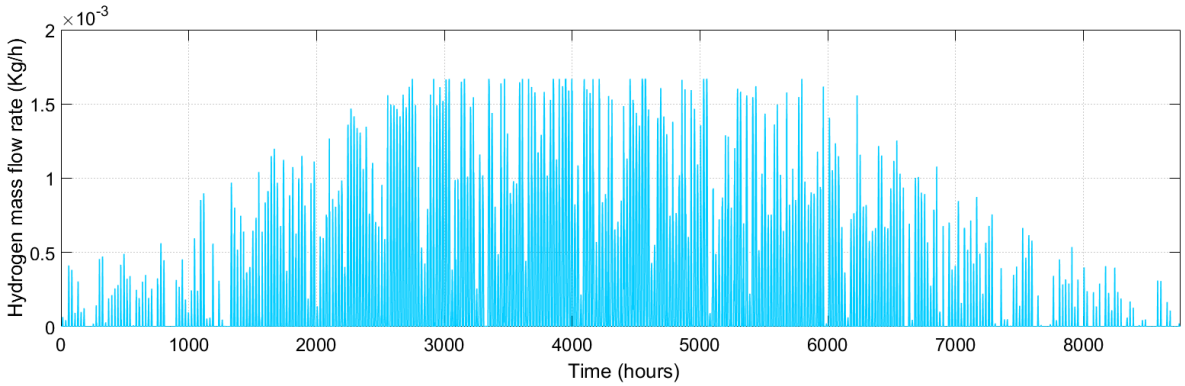

Figure 5.11: Hydrogen production using the direct coupling system configuration of a tailored PV module and a PEM electrolyzer.

5.1.3. Electrolyzer Lifetime Impact

The electrolyzer is the most sensitive component of the system. Electrochemical, mechanical and electrical stress during its operation reduce teh lifetime of this component. Additionally, this is the most expensive component of the system. The material properties of the membrane in the electrolyzer are affected by the voltage applied during operation. For instance, every time the electrolyzer starts its operation, there is an

overpotential needed to initiate the reaction. The ion conductivity and the gas permeability are the properties more susceptible to decay. The more frequent this overpotential needs to be applied, the more likely the membrane properties deteriorate. Every time the electrolyzer shuts down and turn on again, a high activation overpotential is delivered to the membrane. This operation condition induces a local overpotential in the cathode higher than 1.4 V which degrades the membrane, reducing the permeability of hydrogen ions through the membrane. Therefore, the assessment of the electrolyzer's lifetime in this thesis is indirectly done by assessing the number of start-stop cycles.

The optimal operating strategy would be when the system operates with zero number of start-stop cycles. The electrolyzer stops running, every time the voltage from the PV module is less than the thermoneutral voltage of the electrolyzer. In theory for a 100% efficient electrolyzer, the thermoneutral voltage would be 1.48 V. In practice, a 74% efficient electrolyzer would need a potential of 2.0 V. In this thesis, the electrolyzer model works with a thermoneutral voltage of 1.6 V. This value is defined based on the overpotentials defined in the model. Hence, every time the PV module delivers a voltage lower than 1.6 V, the electrolyzer stops running.

Figure 5.12 shows the voltage fluctuation of the electrolyzer for a year. For the periods of lower irradiance (left/right side of the figure), the voltage reaches an average value of approximately 1.8 V. During summer, the tailored panel generates voltages up to 2.8 V. Figure 5.13 shows a detail of the voltage and current of the electrolyzer during winter days. The daily intermittency of sunlight generates fixed start-stop cycles for the electrolyzer.

Over the time of 160 hours, there are seven periods when the electrolyzer receives a voltage value less than 1.6 V, as shown in Fig. 5.13. Below the level of 1.6 V, the electrolyzer does not draw current. This means the electrolyzer does not produce hydrogen because there is not enough energy to make it operate. Over the period of a year, the electrolyzer switches on-off 365 times. In practice, the electrolyzer might experience a higher frequency of on-off times because the second-to-second irradiance data might have moments when the irradiance crosses zero. Additionally, it is important to mention that 365 times of on-off cycles for the electrolyzer is because of the use of a tailored PV module. When using a commercially available module for direct coupling, the electrolyzer will receive relatively high voltages and low current values. Thus, for a direct coupling PV module-electrolyzer it is strongly suggested to use a tailored PV module to achieve an optimal operation.

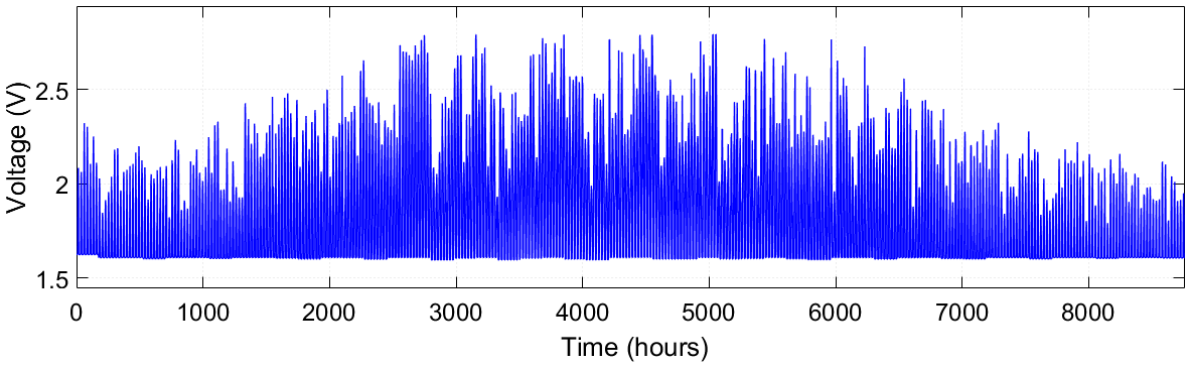

Figure 5.12: Voltage of the electrolyzer directly coupled with the tailored PV module for the period of a year.

5.1.4. System Efficiency

The efficiency of the system is calculated by multiplying the efficiency of each component. The energy utilization of the system is calculated by measuring how much solar energy is actually converted into hydrogen. First, the PV module efficiency is equal to the energy yield of the module divided by the solar energy falling into the module. Second, the efficiency of the electrolyzer is obtained by dividing the energy content in the produced hydrogen to the energy being consumed by the electrolyzer. The heat losses in the electrolyzer and the voltage losses in the cables are not taken into account in this analysis. Then, the efficiency of the system is calculated by the expression below.

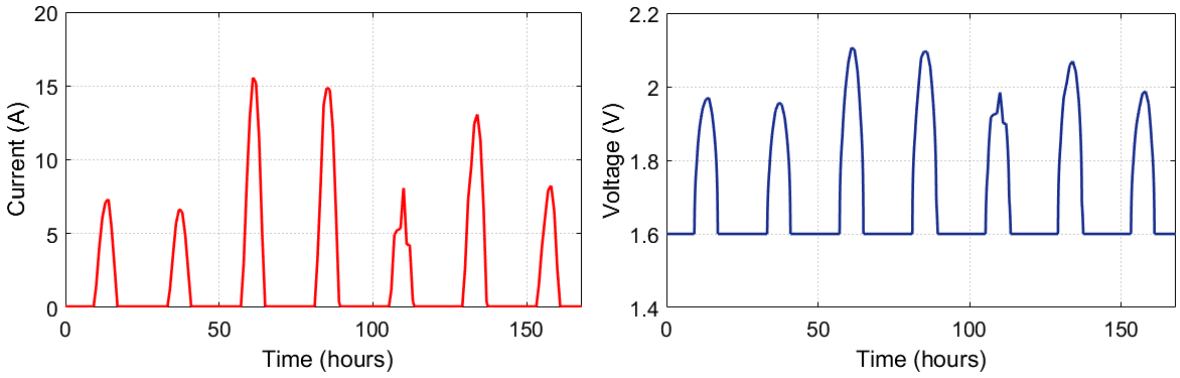

Figure 5.13: Voltage and current of the electrolyzer operationg wit a tailored PV module

$$\begin{aligned}\eta_{sys} &= \eta_{pv} \cdot \eta_{el} \\ &= \frac{P_{pv}}{G_{in} \times n_{sc} \times A_{pv}} \cdot \frac{E_{H_2,theory}}{E_{H_2,real}} \\ &= \frac{143.9}{1030 \times 35 \times 0.156^2} \cdot \frac{33.33}{78.59} \\ &= 6.95\%\end{aligned}$$

where, P_{pv} is the annual energy delivered by the module in kWh. G_{in} is the annual irradiance falling into the module in kWh/m^2. The effective area of the module is equal to the area of a single solar cell A_{pv} multiplied by the number of solar cells n_{sc} in the module. The theoretical energy content in one kilogram of hydrogen is $E_{H_2,\text{theory}} = 33.33$ kWh/kg. And the actual energy in kWh used by the system to produce one kilogram of hydrogen is $E_{H_2,\text{real}}$.

5.1.5. Remarks for System Configuration I

A direct coupling of a PV module and a PEM electrolyzer to produce hydrogen is possible. The challenge for a direct configuration is to adjust the I-V curves of the components to find the optimal operating point. There are two alternatives to adjust the I-V curve in a direct system configuration. The first option is by connecting more than one PEM cell in series to build up the operating voltage of the electrolyzer. Additionally, this alternative needs few solar panels connected in parallel to reach the current value that satisfies the electrolyzer current. The second alternative and the most effective for a direct configuration is by tailoring a solar module that satisfies both the current and voltage of the electrolyzer. For a 120 W electrolyzer, the most optimal PV module consists of 5×7 (series×parallel) solar cells. The hydrogen production is proportional to the irradiance falling in the PV module. The higher irradiance, the more hydrogen the system produces. Overall, the system efficiency has a value of 6.95%.

The optimal design of the system is achieved when the energy yield of the PV module is a bit higher than the electrolyzer capacity. The downside of the direct system configuration is the start-stop cycles of the electrolyzer because of the daily irradiance fluctuations. Reducing the start-stop cycles will safeguard the electrolyzer lifetime. A solution for this issue is including an energy storage component that stores the energy excess during the day and feeds it during the night. Another alternative to explore might be the operation of the electrolyzer only during summer. These alternatives are discussed further in this chapter.

5.2. System Configuration II: Including an MPPT

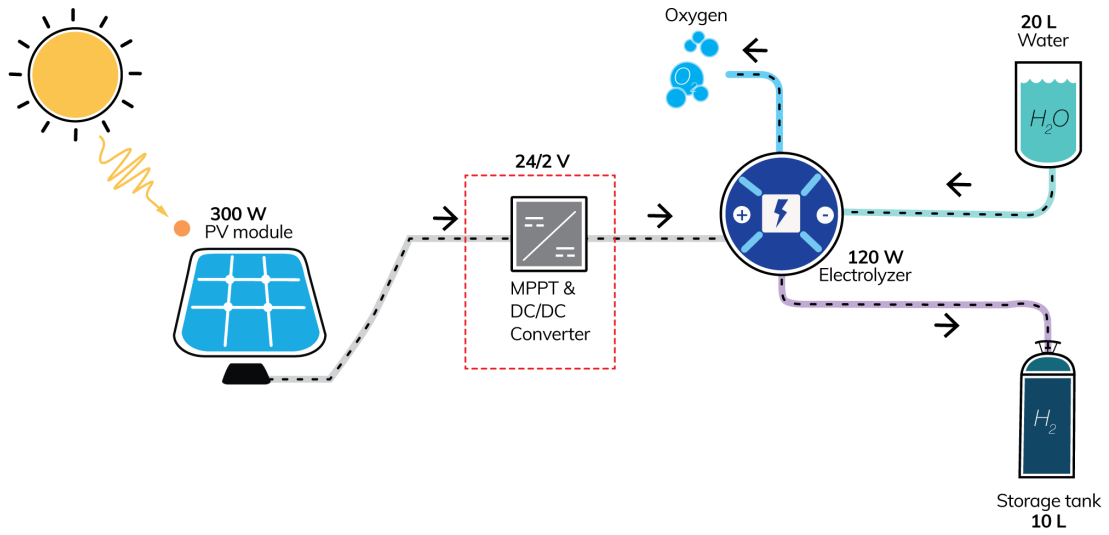

Figure 5.14: Schematic representation of system configuration II: Coupling including a MPPT.

The system configuration II includes a direct current (DC/DC) power converter and a maximum power point tracker (MPPT) between the electrolyzer and the PV module. One SunPower-300 module converts the sunlight into electricity to power the entire system. Table 5.2 shows the characteristics of the SunPower-300 module. The size and parameters of the electrolyzer (120 W) remain the same as in the previous configuration. The power converter adjusts the voltage and current from the PV modules to the electrolyzer. Figure 5.14 shows a schematic representation of the system configuration II. The following sections discuss the results of the system performance.

Table 5.2: Specification of the PV panel

Parameter	**Value**
Model	SunPower 300
Technology	Crystalline silicon
Area of each module	1.6 m^2
Peak power, Pmax	300 W
Peak power voltage, V_{mpp}	54.7 V
Peak power current, I_{mpp}	5.49 A
Short circuit current, I_{sc}	5.87 A
Open circuit voltage, V_{oc}	64 V
Temperature coefficient, V_{oc}	-176.6mV / K
Efficiency, η_{pv}	18.4%
Number of cells, N_s	96

5.2.1. PV Energy Generation

Over the entire year, the solar panel generates a total energy equal to 303.1 kWh/year, as shown in Fig. 5.15 Given that the annual irradiance in Delft is 1030 kWh/m^2, and the area of the module is 1.6 m^2, the efficiency of the PV module is 18.39%. The efficiency value is almost equal to the theoretical efficiency of the module (18.4%). For comparison purposes, the system was run without the MPPT. Then, the total energy produced is 13.9 kWh/year. The power generation of the PV module without the MPPT is illustrated in Fig. 5.16. The MPPT significant affects the energy harvesting in approximately 22 times larger than a system without MPPT. The reason for this behavior is because, without the MPPT, the operating point of the PV module is defined by the electrolyzer, as shown previous system configuration in figure 5.4. The MPPT adjusts the electrical

characteristics of the load to let the PV modules operate at its maximum power point for all the irradiance levels. Consequently, the use of an MPPT benefits the system by efficiently harvesting the maximum energy possible from the PV modules.

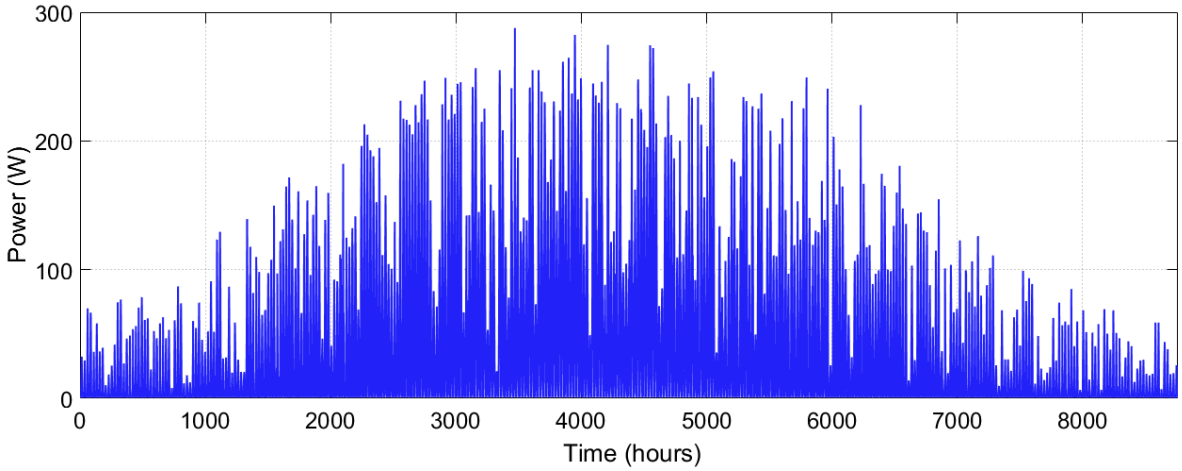

Figure 5.15: Power generated by the SunPower-300 module using an MPPT.

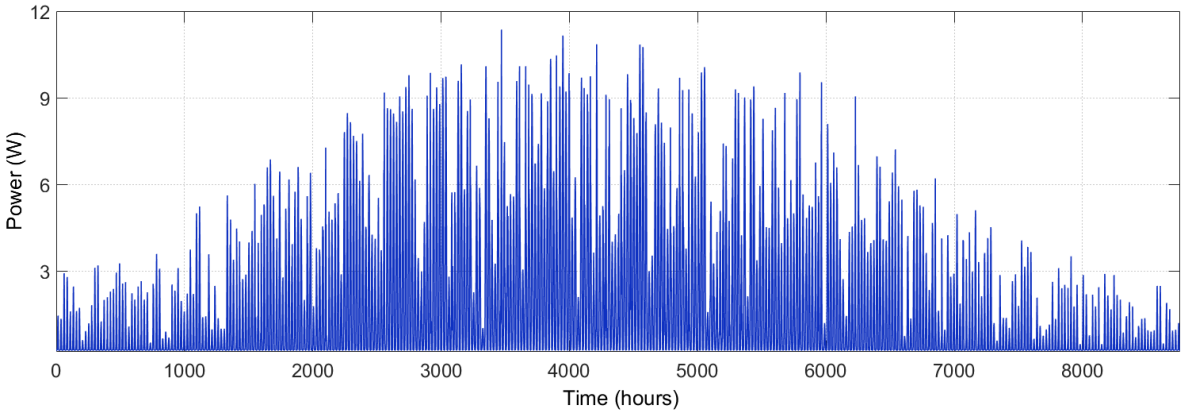

Figure 5.16: Power generated by the SunPower-300 module without using an MPPT (Used for contrasting purposes).

5.2.2. Hydrogen Production

Over the period of a year, the system generates a total amount of 3.703 Kg of hydrogen, as shown in Fig. 5.17. The electrolyzer consumes 266 kWh/year to produce that amount of hydrogen. Thus, each kilogram of hydrogen produced by the system needs 71.83 kWh. The energy consumption to produce one kilogram of hydrogen is lower than the one on system configuration I. This result can be explained looking at figure 5.18. There are two clear limits for the hydrogen generation. The upper limit is determined by the maximum capacity of the electrolyzer. The PV module can deliver a maximum power of 300 W. Then, all the power delivered by the module, higher than the 120 W is practically wasted. The solution for this issue is using a higher electrolyzer capacity. Then the challenge for an optimal configuration is to find the perfect combination size between the electrolyzer and the PV modules.

5.2.3. Electrolyzer lifetime impact

Corrosion in the electrodes, short circuit damage, and membrane degradation are some of the main causes that affect the electrolyzer lifetime. The membrane degradation is severely impacted by the rapid load changes, operating voltages close to the thermoneutral voltage, and the high number of start-stop cycles. In this research, the analysis is more focused on the system operation. Hence, similarly than for the system configura-

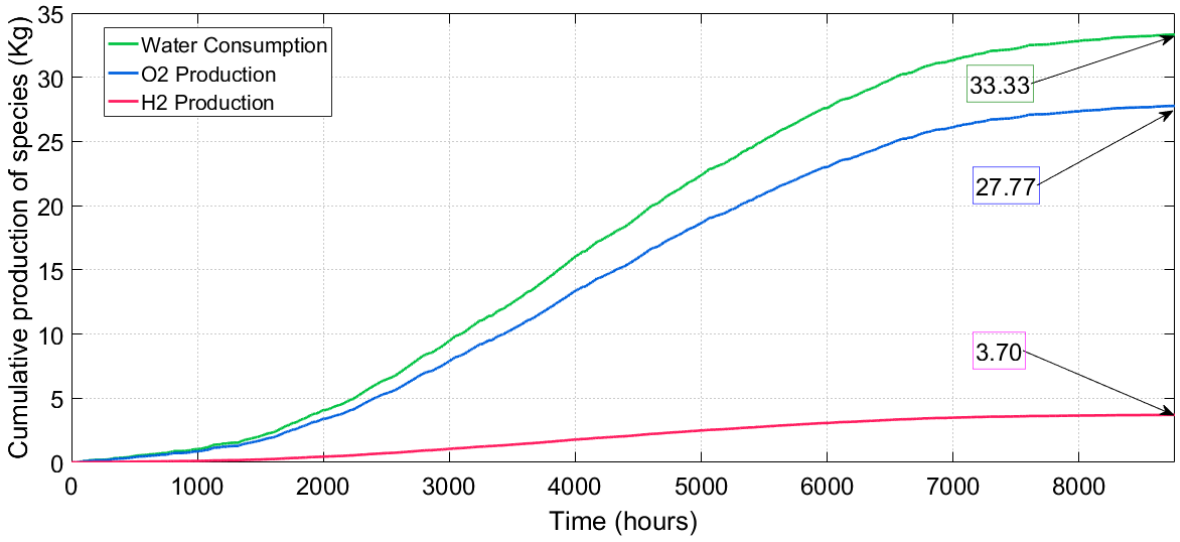

Figure 5.17: Cumulative hydrogen production over a year by the electrolyzer powered with one Sun-Power-300 attached to an MPPT.

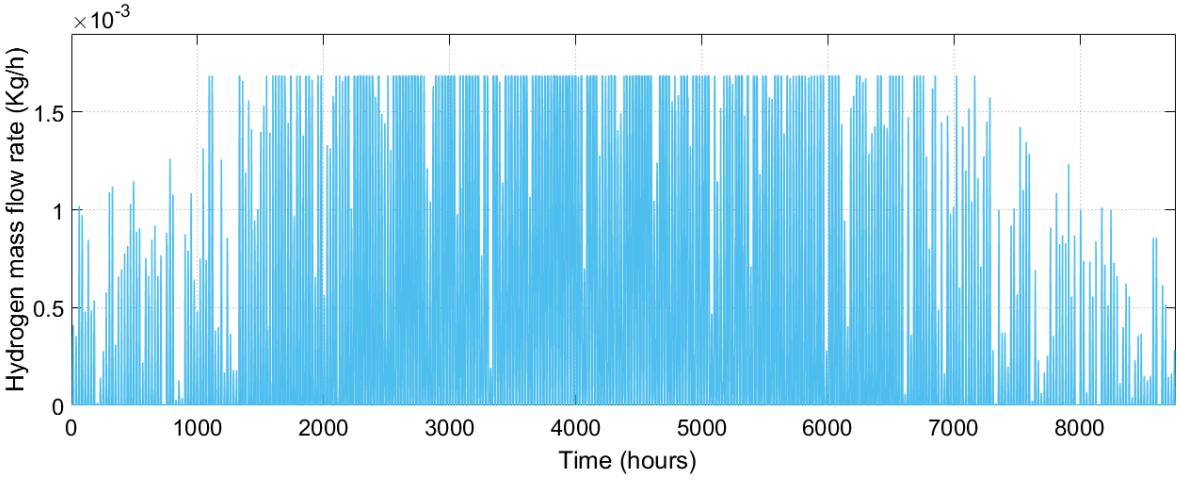

Figure 5.18: Hydrogen production by the electrolyzer powered with one Sun-Power-300 module attached to an MPPT.

tion I, the electrolyzer lifetime is indirectly assessed by the number of start-stop cycles.

The electrolyzer stops running when the voltage from the PV module is lower than the thermoneutral voltage (1.6 V). Figure 5.19 shows the voltage fluctuation of the electrolyzer operating during a year. There are two relevant points in the figure. The point on the bottom which represents the minimum voltage at which the electrolyzer operates (1.6 V). The point on the upper side (2.4 V) represents the cut-in voltage of the electrolyzer. The voltage of 2.4 V is the maximum voltage limit the electrolyzer can handle. Looking closely at the voltage fluctuations of the electrolyzer shown in figure 5.20, the number of start-stop cycles can be identified. There are seven times when the electrolyzer does not operate in a period of approximately 170 hours. This means, the electrolyzer powers on and off 365 times during a year. Essentially, the off-moments represent the night times, when there is no sunlight. Comparing to the previous system configuration, there is the same number of start-stop cycles.

Another simulation without the MPPT was performed for comparison purposes. Figure 5.21 shows the voltage fluctuations for the electrolyzer without the MPPT. The results show that the MPPT clearly, increases the operating voltage of the electrolyzer. This is because the power delivered by the PV modules is optimally harvested by the MPPT. Thus, the use of an MPPT in the system configuration does impact in the start-stop cycles of the electrolyzer.

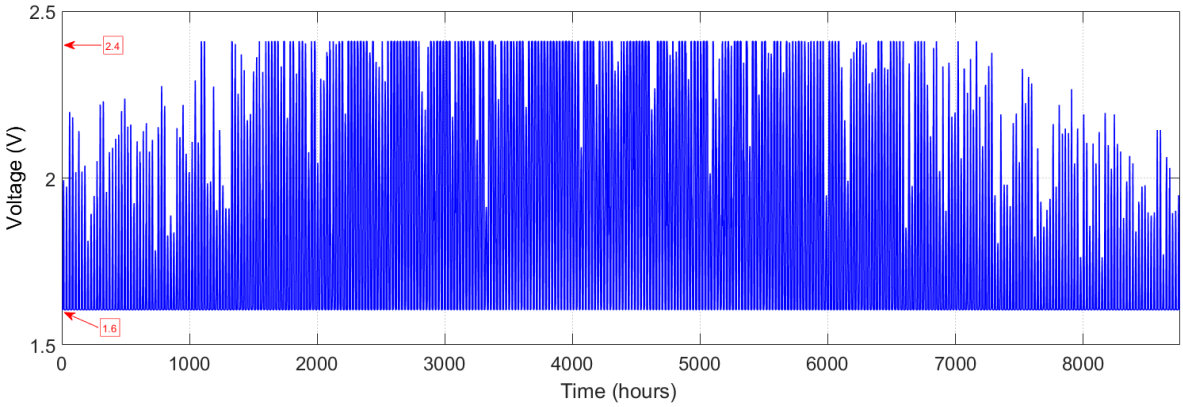

Figure 5.19: Electrolyzer's voltage for the system configuration II (using an MPPT).

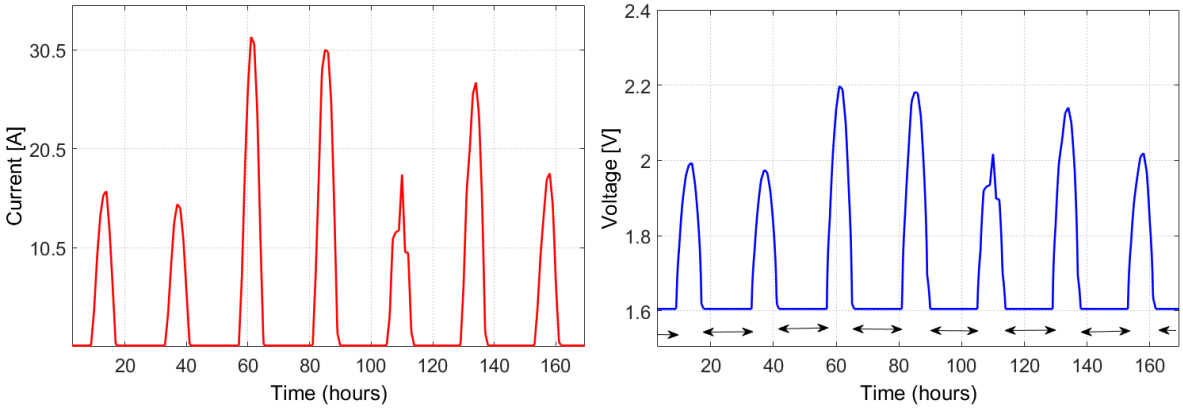

Figure 5.20: Voltage and current values of the electrolyzer working with the system configuration II (including an MPPT).

5.2.4. System Efficiency

Similar than in the previous section, the system efficiency is calculated by multiplying the efficiency of each component. The efficiency of the PV module is the ratio of the output power to the solar energy falling into the module. Similarly, for the electrolyzer, its efficiency is the ratio of the energy consumed by the electrolyzer to produce one kilogram of hydrogen to the theoretical energy value to produce one kilogram of hydrogen with

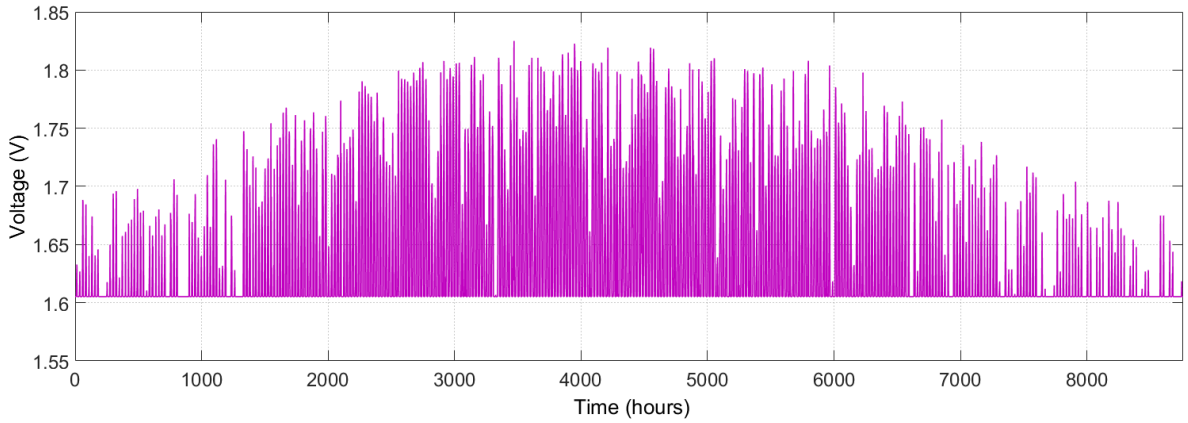

Figure 5.21: Electrolyzer's voltage operation without the MPPT (showed for contrasting purposes).

a 100% efficiency electrolyzer. The efficiency of the MPPT is neglected in this analysis because, in practice, the MPPT consumes a minimal amount of energy compared to the rest of the components. Additionally, the system experiences heat losses in the electrolyzer. The heat losses in the system are also neglected because the analysis is out of the scope of this thesis. Nevertheless, we are aware that the system in real operation needs a special analysis of the heat losses. Then, the efficiency of the system configuration II is calculated as shown below.

$$\begin{aligned}\eta_{sys} &= \eta_{pv} \cdot \eta_{el} \\ &= \frac{303.1}{1030 \times 1.6} \times \frac{33.33}{85.38} \\ &= 0.1839 \times 0.3909 \\ &= 7.18\%\end{aligned}$$

5.2.5. Remarks for System Configuration II

A system to produce hydrogen via a PEM electrolysis using solar panels profits by the implementation of an MPPT. The main impact of the MPPT is the automatic adjustment of the current and voltage from the PV modules to the electrolyzer. The MPPT improves the system by more efficient energy harvesting. In fact, the connection of a commercial solar module with the electrolyzer is strongly advised not to use it without the MPPT. The energy losses are significant when the system operates without the MPPT. Regarding the hydrogen production, there is not a direct connection between the use of the MPPT and the hydrogen production rate. Nevertheless, the electrolyzer performance is significantly increased by the voltage delivered by PV module when using an MPPT. The key for an optimal configuration is the correct sizing of the components. Using a 300 W module and 120 W electrolyzer, there is a significant waste of energy during high irradiance because the system can only consume 40% of the energy production. The optimal system design must include equal capacity for the PV module and electrolyzer. Furthermore, the start-stop cycles are not affected by adding the MPPT into the system. The system configuration needs an energy buffer to reduce the start-stop cycles caused by the daily solar intermittency.

5.3. System Configuration III: Including an MPPT and Batteries

This section presents the results of the last system configuration analyzed in this thesis. Two system designs are discussed here. (1) initial design, and (2) final design. The initial design is similar to the design presented in the previous section. One set of components running over the entire year. The final design combines two sets of components. Each set is used for different times in the year. Both designs are presented in the following sections.

5.3.1. Initial Design

The system configuration in this section includes the PV modules, the electrolyzer, the MPPT and batteries. The initial simulation includes one SunPower-300 solar panel connected to a 120 W PEM electrolyzer. The battery is a lead-acid technology of 24 V and 70 Ah capacity. The system layout of configuration III is shown in Fig. 5.22.

New in this configuration is the power control unit. The unit manages the power in the system, deciding where and when to feed the right amount of power to each component. The control unit is a key component for optimal system operation. Overall, the optimal operation of the system is when all the energy is used for hydrogen production, and there is zero energy wasted. Additionally, an optimal system design utilizes the battery along its entire deep of discharge. Regarding the electrolyzer, the most wanted operating mode is a constant operation with very soft voltage fluctuations. In the following sections the results of the PV power generation, the electrolyzer power consumption, the battery state of charge and the hydrogen production are presented for the initial design for system configuration III.

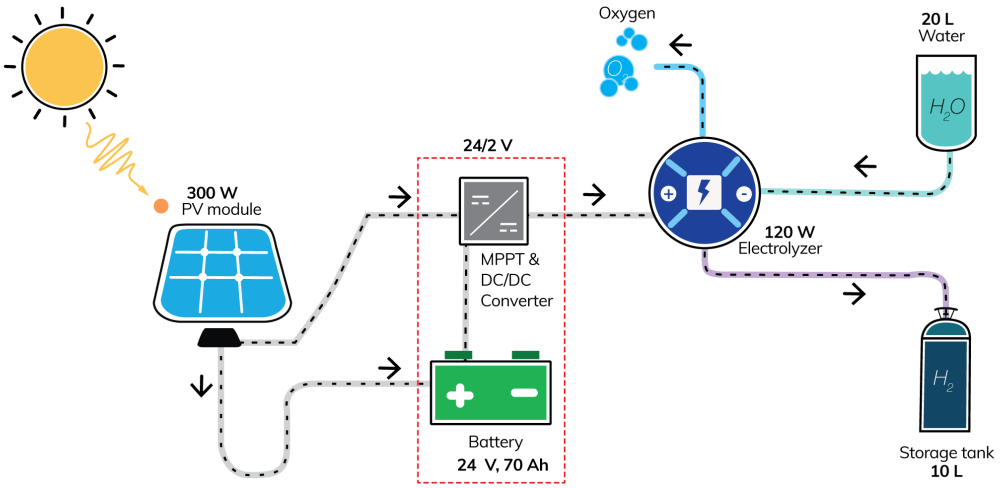

Figure 5.22: Schematic layout of the system configuration for Case III.

PV Energy Generation

The generated power in the first configuration is the result of a 300 W PV module exposed to the irradiance data from Delft. Figure 5.23 shows the generated power of the panel during a year. The curve follows the bell shape from the irradiance with a maximum generation during summer (center of the figure) and minimum generation during winter. Over the entire year, the PV module generates 303.1 kWh. Given that the module has an area of 1.6 m^2 and the yearly irradiance in Delft is 1030 kWh/m^2. The efficiency of the panel becomes 18.39%.

The generated power is distributed to the electrolyzer and the battery. The electrolyzer operating point is defined based on the level of power generated by the module. The algorithm to define the operating point is included in the power control unit. A variable operating point of the electrolyzer is important to create flexibility in the operation of the electrolyzer. Additionally, the variable operating point helps to minimize the number of start-stop cycles of the electrolyzer. There are four operating points for the electrolyzer. Those

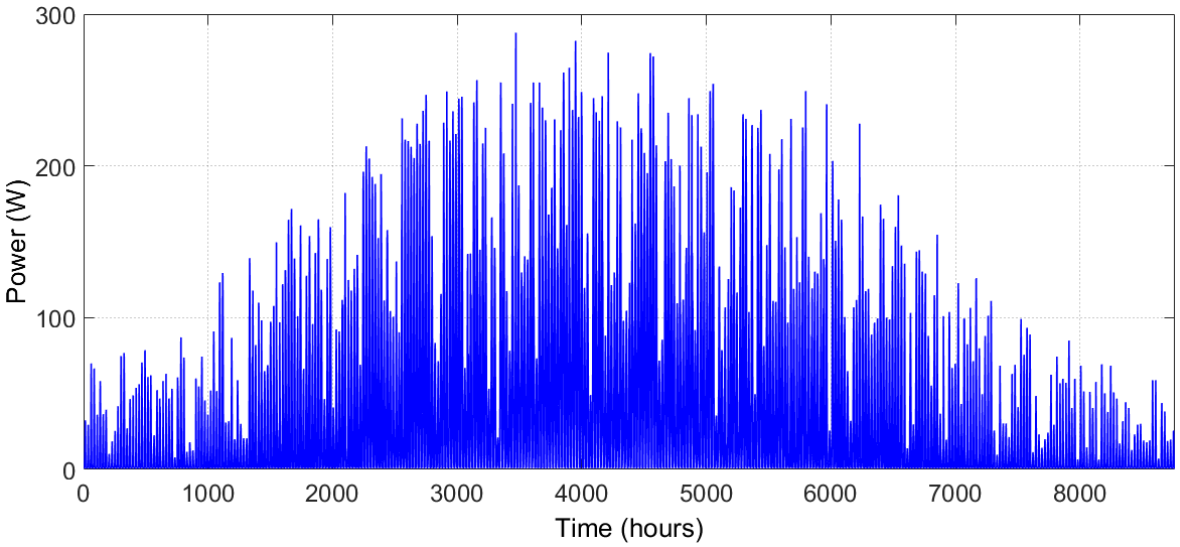

Figure 5.23: Power generated by the PV module using the initial design for the configuration III.

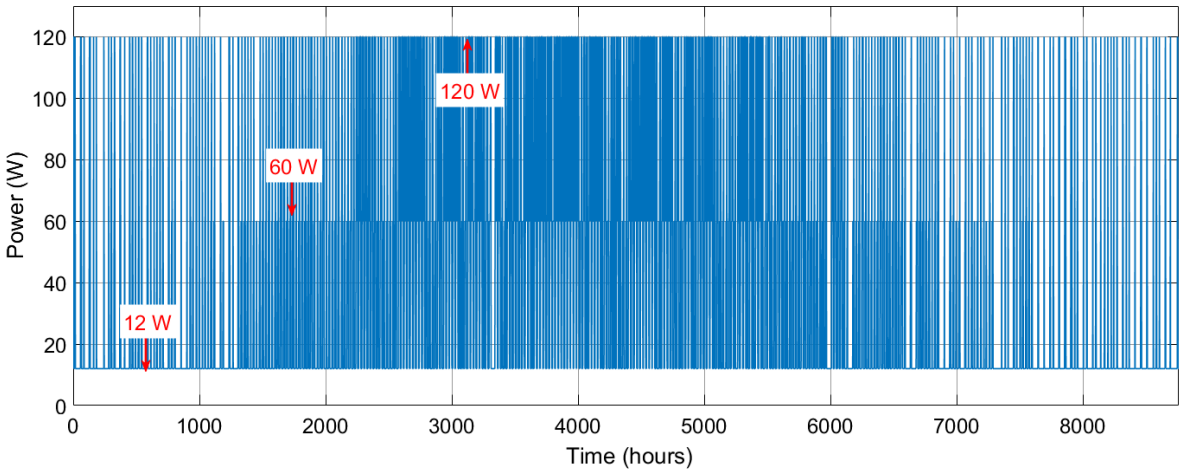

Figure 5.24: Power consumed by the electrolyzer using the initial design for the configuration III.

points are set at 0%, 10%, 50% and 100% of its capacity. The selection of these points was made to safeguard the electrolyzer. Figure 5.24 shows the electrolyzer power consumption where three operating points are marked. The minimum value of 12 W (10%) prevails during the low irradiance periods. Making the electrolyzer operates at 10% of its capacity reduces its energy consumption to prevent stopping its operation. Hence, the electrolyzer can still work during low irradiance periods or even during the night. The highest operating point appears more in the center area of the figure. This point belongs to the summer irradiance. During the mid irradiance levels (like in the spring and fall), the electrolyzer operates at 50% of its capacity.

Even though the electrolyzer has several operating points to optimize the energy consumption, the system has moments of energy surplus and deficit. The energy surplus happens when the electrolyzer cannot consume more power to produce hydrogen, and the battery can not store more energy. Opposite to that, the system has an energy deficit when there is no irradiance, and the energy in the battery is not sufficient to power the electrolyzer. Figure 5.25 and 5.26 show the energy deficit, and the energy surplus of the system, respectively. Over the entire year, the system has a total energy deficit of 16.820 kW, and an energy surplus of 5.119 kW. The reason for this energy mismatch is the big irradiance difference between summer and winter, typical from northern countries. Including more solar panels and batteries can solve this issue, but it will lead to a oversized system.

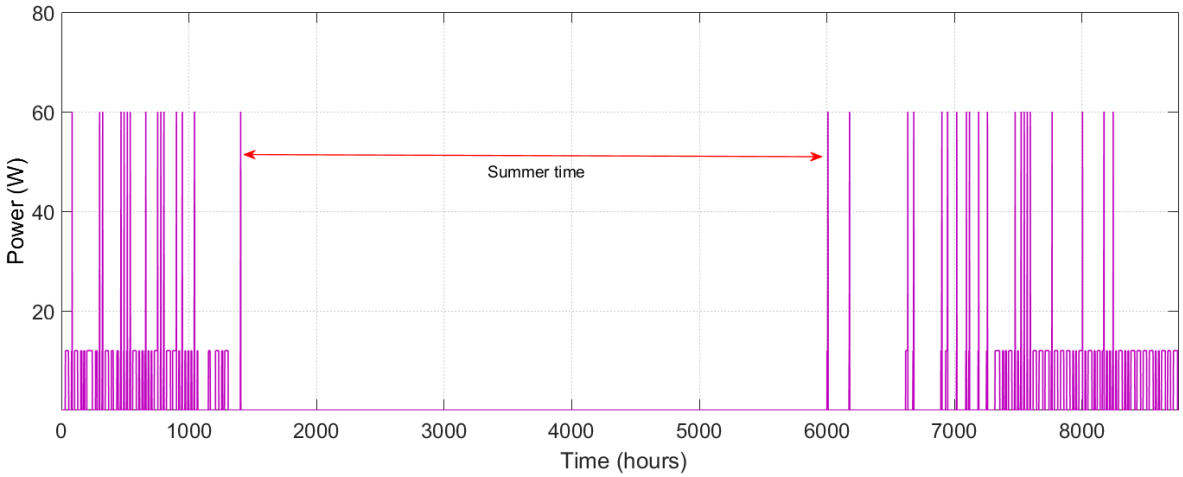

Figure 5.25: Energy deficit of the system using the initial design for the configuration III.

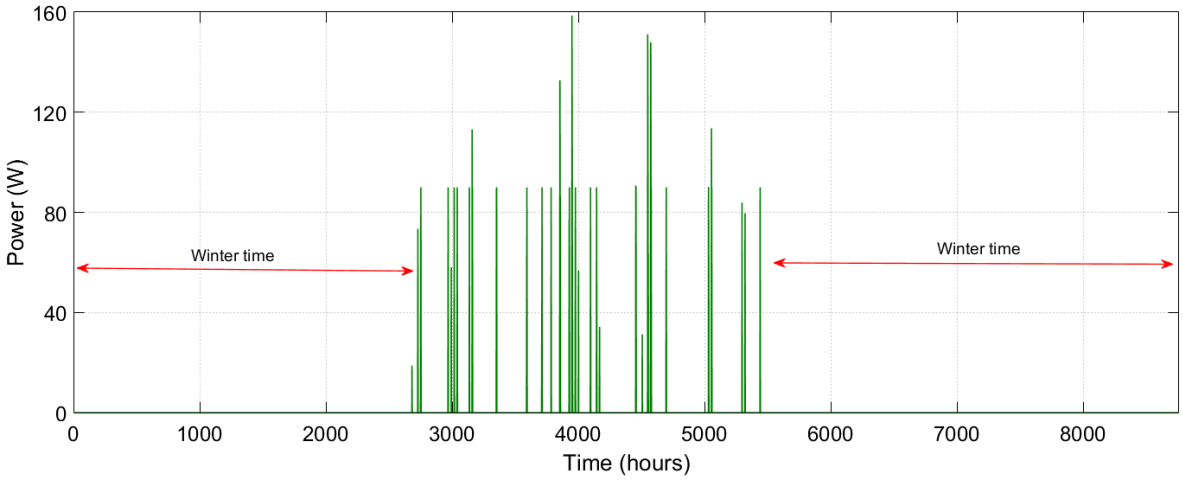

Figure 5.26: Energy surplus of the system using the initial design for the configuration III.

Hydrogen generation

Regarding the hydrogen production, the system generates a total amount of 4.815 kg of hydrogen in a year as shown in Fig. 5.27. The energy consumption by the electrolyzer for this amount of hydrogen is 303.1 kWh. Hence, the energy-hydrogen ratio of the system is 62.95 kWh/kg. Comparing the hydrogen production of the configuration without a battery unit, the system generates 1.11 kg of additional hydrogen. Hence, implementing a battery into the system increases the hydrogen production by 30%.

Electrolyzer Lifetime Impact

Similar than in the previous configurations, the electrolyzer lifetime impact is indirectly assessed by the number of start-stop cycles during its operation. Figure 5.28 shows the current and voltage of the electrolyzer during 170 hours. Even the system now includes a battery, the electrolyzer still has moments when it turns off. Those moments correspond to the times when there is no irradiance. Nevertheless, the off-moments are shorter than in previous configurations, as shown in Fig. 5.28. The reason of shorter off-moments is because the energy stored in the battery powers the electrolyzer. Instead of letting the electrolyzer stop working, the electrolyzer sets up its operating point at its minimum level (12 W), which is approximately equivalent to 6.2 A and 1.95 V. In order to achieve a constant operation of the electrolyzer, two things can be done. First, modify the electrolyzer limits in the control unit. And second, increase the number of solar panels to store enough energy in the batteries to run the electrolyzer during the night. On the one hand, the first option reduces

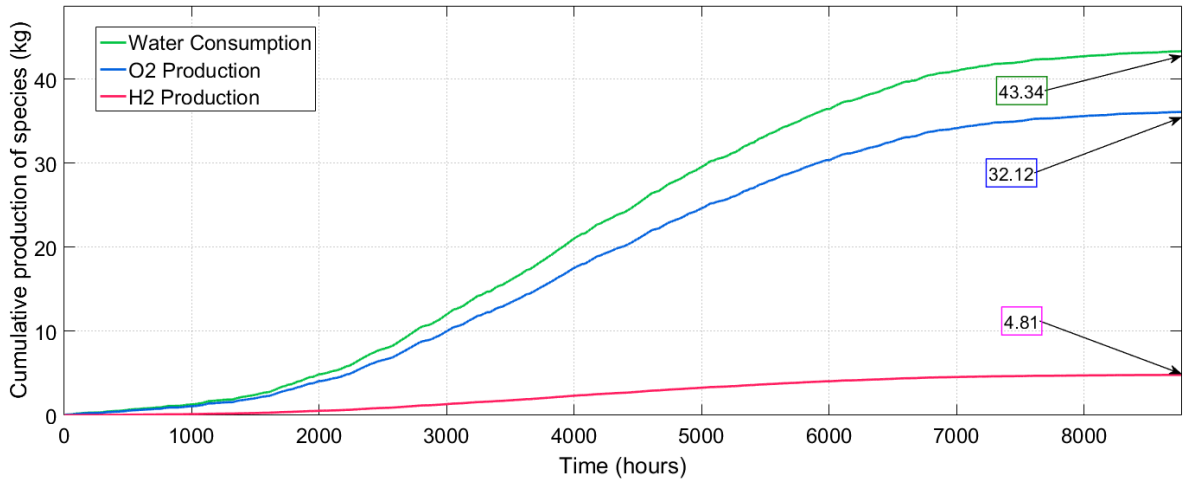

Figure 5.27: Cumulative hydrogen production using the initial design for the configuration III.

the hydrogen production by the electrolyzer. On the other hand, the second option generates more energy surplus during summer.

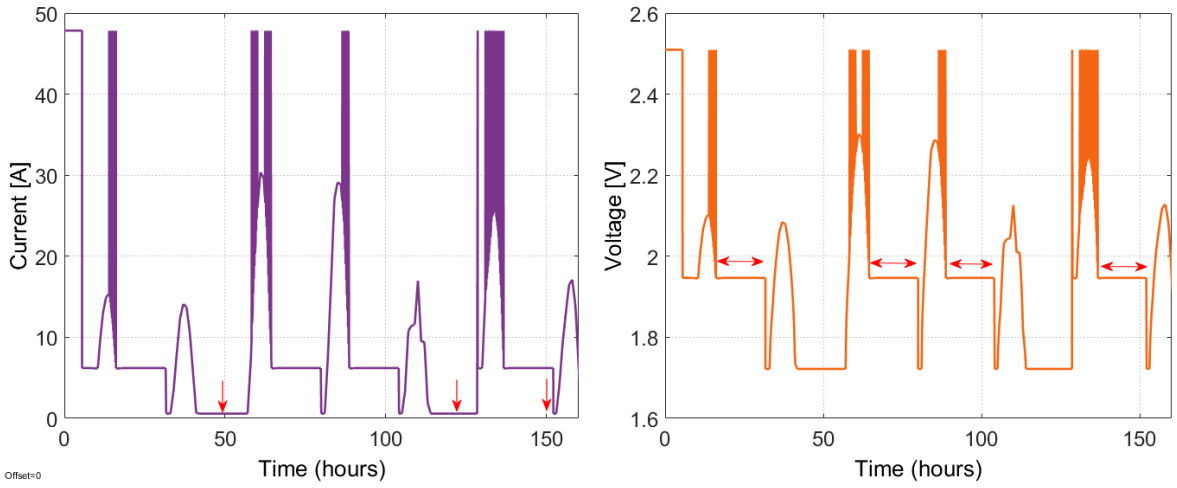

Figure 5.28: Current and voltage of the electrolyzer using the initial design for the configuration III.

Battery State of Charge

Similar than the electrolyzer, the battery has also operating limits to optimize its performance. The lower limit (40%) and the upper limit (90%) are defined to safeguard the battery lifetime. When the battery reaches 40%, the battery stops discharging. On the contrary, when the battery reaches 90% the battery cannot charge anymore. Figure 5.29 shows that during winter, the battery is not efficiently used. The low irradiance levels do not allow the PV module to generate enough energy to charge the battery fully. During winter time, the battery is using only 10% of its capacity. The problem can be solved by adding more solar modules to generate more power and store it in the batteries. However, during summer there will be more excess of energy that can be neither consumed or stored. The battery improves its capacity utilization during summer. The battery charges and discharges over its full range capacity. An optimal system design has a battery size that can periodically fluctuate between its minimum and maximum state of charge.

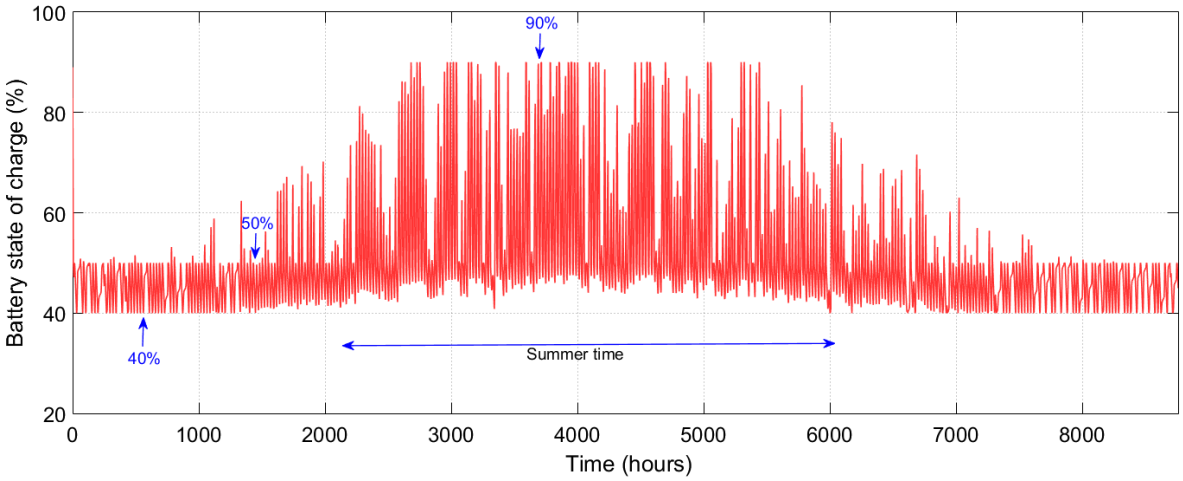

Figure 5.29: Battery state of charge using the initial design for the configuration III.

System Efficiency

The efficiency of the system is equal to the product of each component efficiency. The efficiency of the module and the electrolyzer are calculated in the same way than in the previous configurations. New to this configuration is the battery efficiency, which in this thesis is considered constant and equal to 85%. Nevertheless, in real operation, the efficiency depends on some factors like temperature, the rate of charging and discharging. Similar than in the previous configurations, the efficiency of the MPPT is neglected for practical reasons. Hence, the efficiency of the system is calculated by the expression below.

$$\begin{aligned}\eta_{sys} &= \eta_{pv} \cdot \eta_{el} \cdot \eta_{bat} \\ &= \frac{303.1}{1030 \times 1.6} \times \frac{33.33}{62.95} \times 0.85 \\ &= 0.1839 \times 0.5295 \times 0.85 \\ &= 8.28\%\end{aligned}$$

Remarks from the initial design

Adding a battery into the system configuration profits the hydrogen production using PV modules. The battery works as an energy buffer to supply power to the electrolyzer during low irradiance moments. However, the irradiance difference between summer and winter creates a mismatch of energy in the system. Energy deficit during winter and energy surplus during summer are the two pitfalls of the system. A power control unit is necessary for an optimal system operation. The hydrogen production increases by adding a battery into the system. Also, the start-stop cycles are significantly reduced. Overall, the system efficiency has a value of 8.28%.

5.3.2. Final Design

The system configuration in this section includes a small variation from the initial design. This configuration is divided in two, a system configuration for winter and another for summer. In this simulation, winter uses the irradiance data from January to March, and from October to December. Summer uses the irradiance date from April to September. The configuration for winter includes two SunPower-300 modules attached to an MPPT, one battery of 24 V, 70 Ah, and the electrolyzer of 120 W. The configuration for summer includes one SunPower-300 module attached to an MPPT, two batteries of 24 V, 70 Ah, and the electrolyzer of 120 W. This combined design is proposed in order to minimize the surplus and deficit of energy in the system. The results in this section are presented in two parts, one for summer and another for winter. The PV power

generation, the energy surplus/deficit, the hydrogen production, the battery state of charge, and the current-voltage fluctuations results are presented in the following section.

Winter System Configuration

The generated energy using two modules of 300 W during winter is 137.660 kWh. Figures 5.30 and 5.31 show the generated power during this period. The system has a minimal energy deficit of 5.937 kWh and an energy surplus of 3.222 kWh.

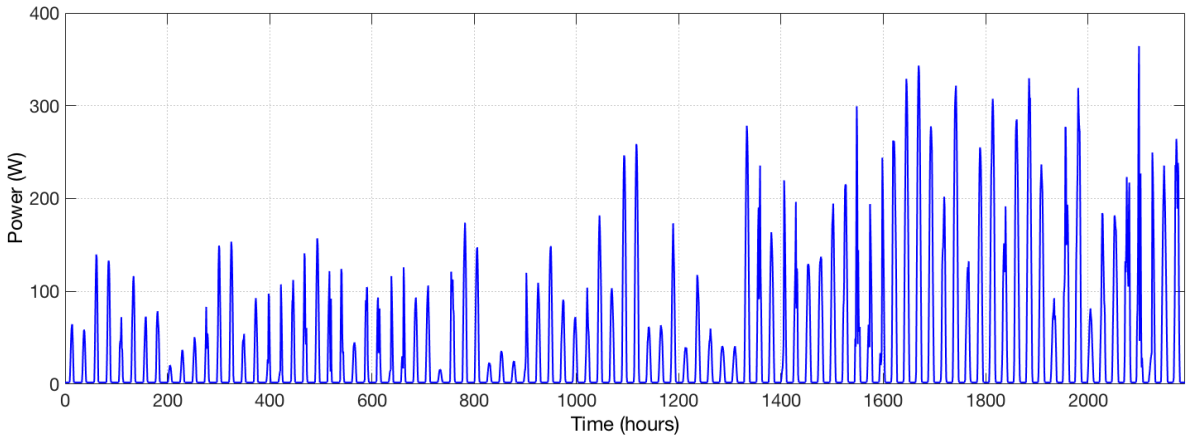

Figure 5.30: Power from the PV using the final design (from January to March) for the configuration III.

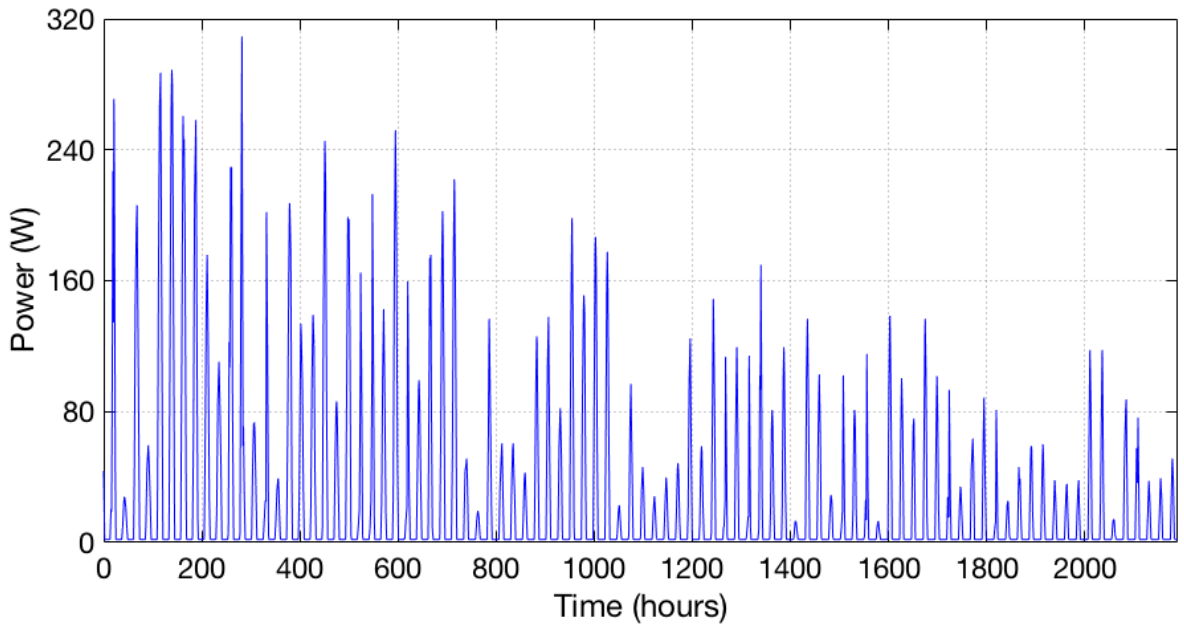

Figure 5.31: Power from the PV using the final design (from October to December) for the configuration III.

Figures 5.32, 5.33, 5.34 and 5.35 show the energy surplus and deficit generated by the system for this configuration. Additionally, the hydrogen produced by the system reaches a value of 1.987 kg. Figures 5.36 and 5.37 show the cumulative hydrogen production during this period. The energy needed to generate one kilogram of hydrogen is 69.28 kWh/kg. Thus, the electrolyzer efficiency for this configuration results in 48.11%.

The battery state of charge fluctuates in the lower limit range. However, the battery stores enough energy to run the electrolyzer during the night at its minimum operating level. Figures 5.38 and 5.39 show the state of charge of the battery during winter. Additionally, current and voltage levels fluctuate along with the irradiance but always above the minimum operating levels. Figures 5.40 and 5.41 show the current and voltage levels

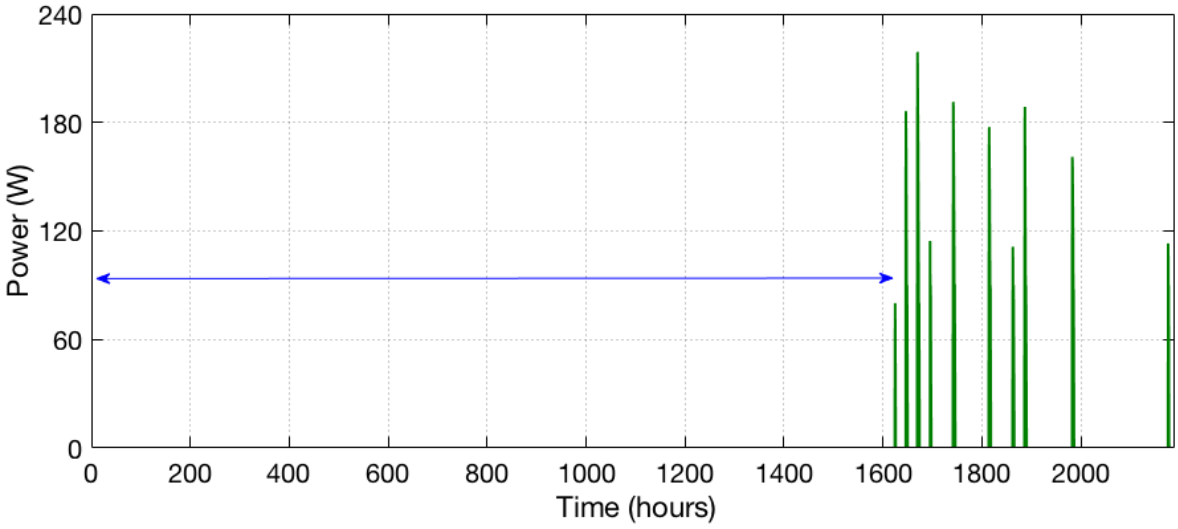

Figure 5.32: Energy surplus of the system using the final design (from January to March) for the configuration III.

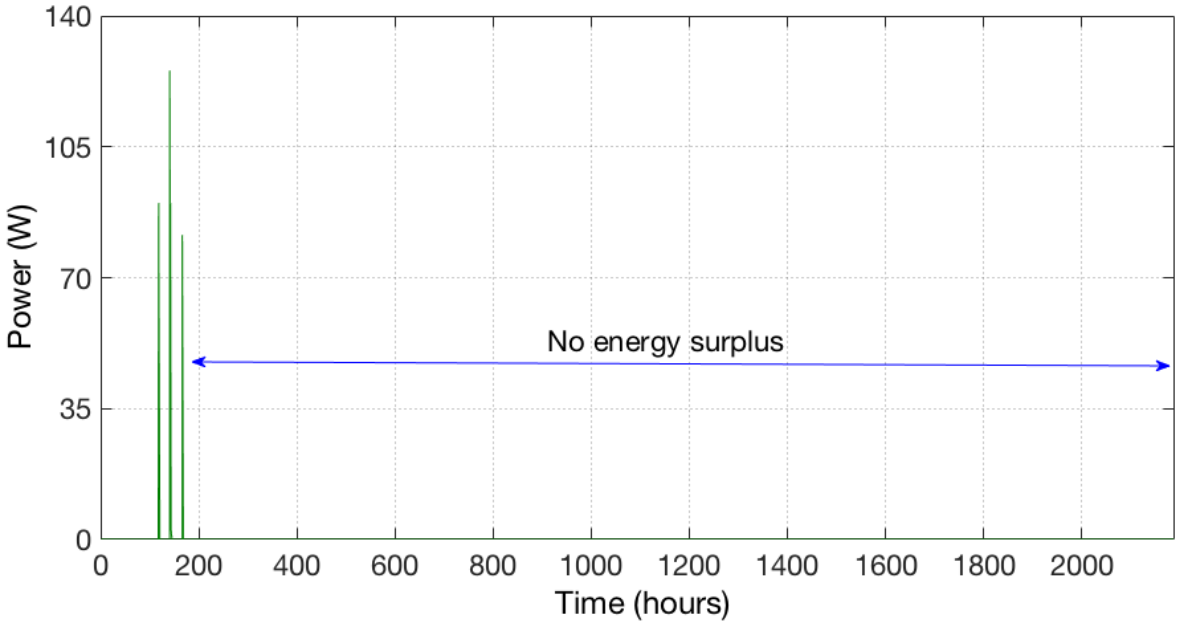

Figure 5.33: Energy surplus of the system using the final design (from October to December) for the configuration III.

of the electrolyzer during this period. Important to mention is that the electrolyzer continually runs over the entire summer period, except during the very few times of energy deficit in the system.

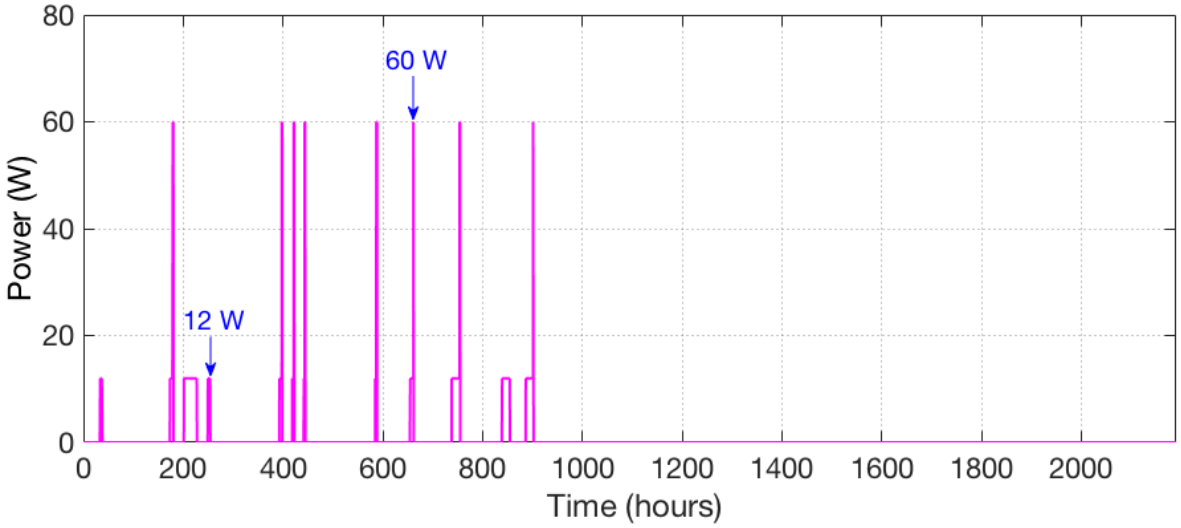

Figure 5.34: Energy deficit of the system using the final design (from January to March) for the configuration III.

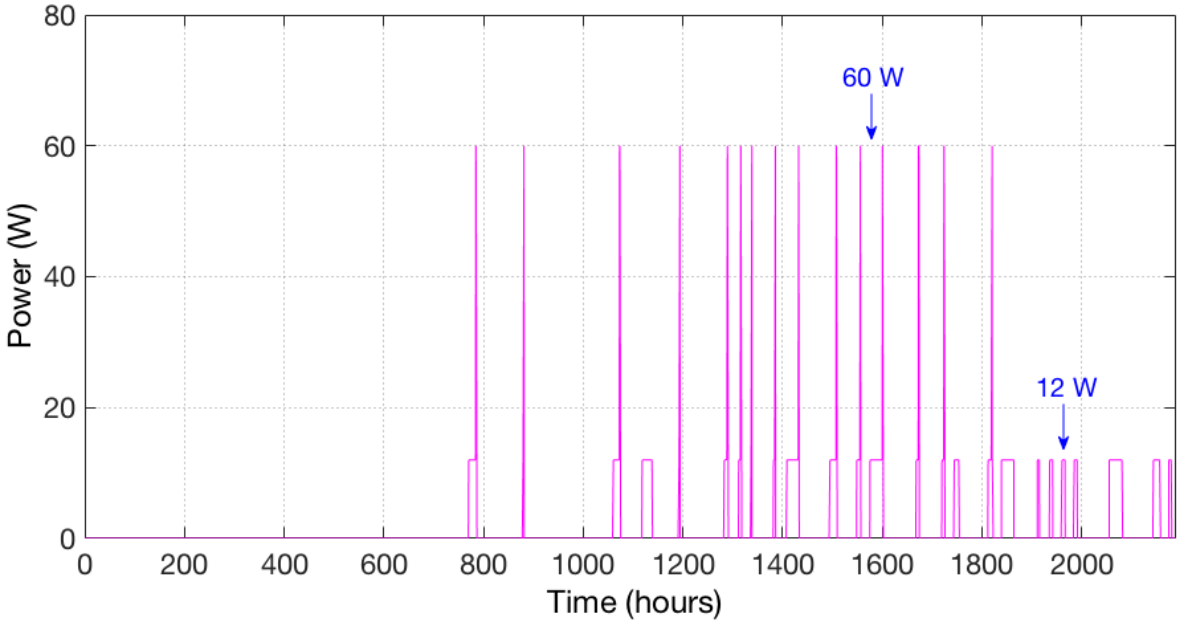

Figure 5.35: Energy deficit of the system using the final design (from October to December) for the configuration III.

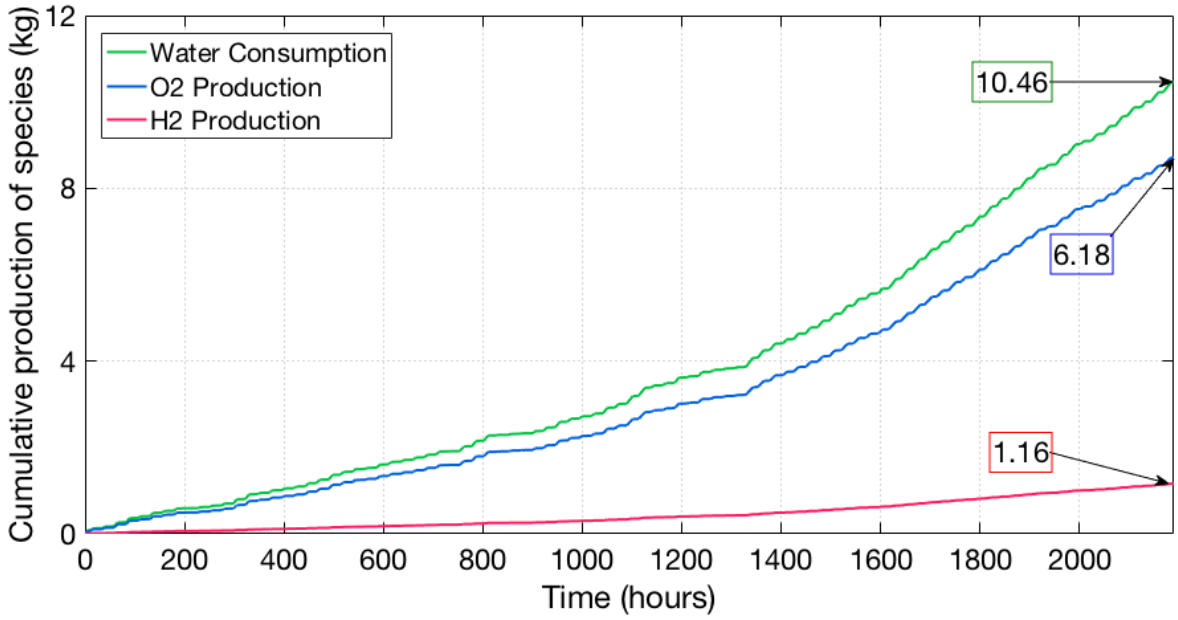

Figure 5.36: Cumulative hydrogen production by the system using the final design (from January to March) for the configuration III.

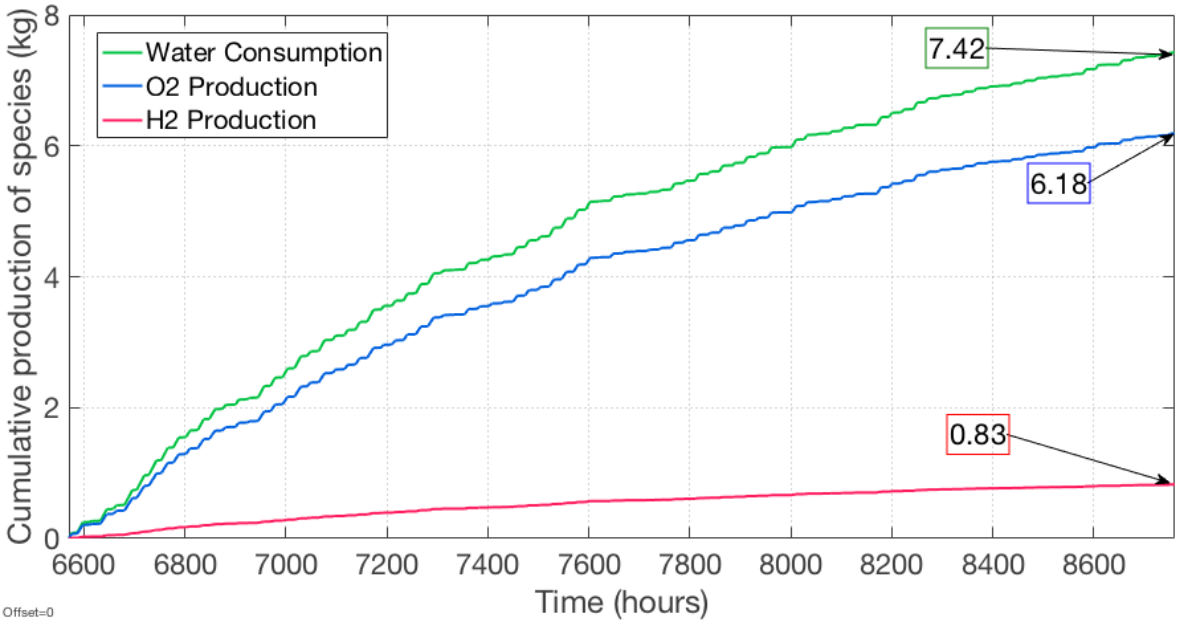

Figure 5.37: Cumulative hydrogen production by the system using the final design (from October to December) for the configuration III.

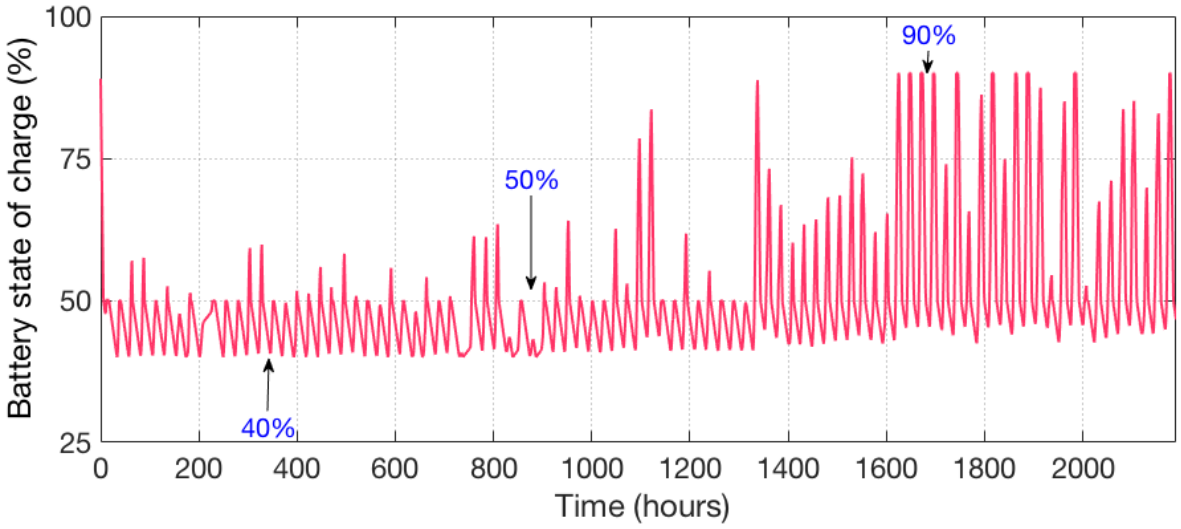

Figure 5.38: Battery state of charge using the final design (from January to March) for the configuration III.

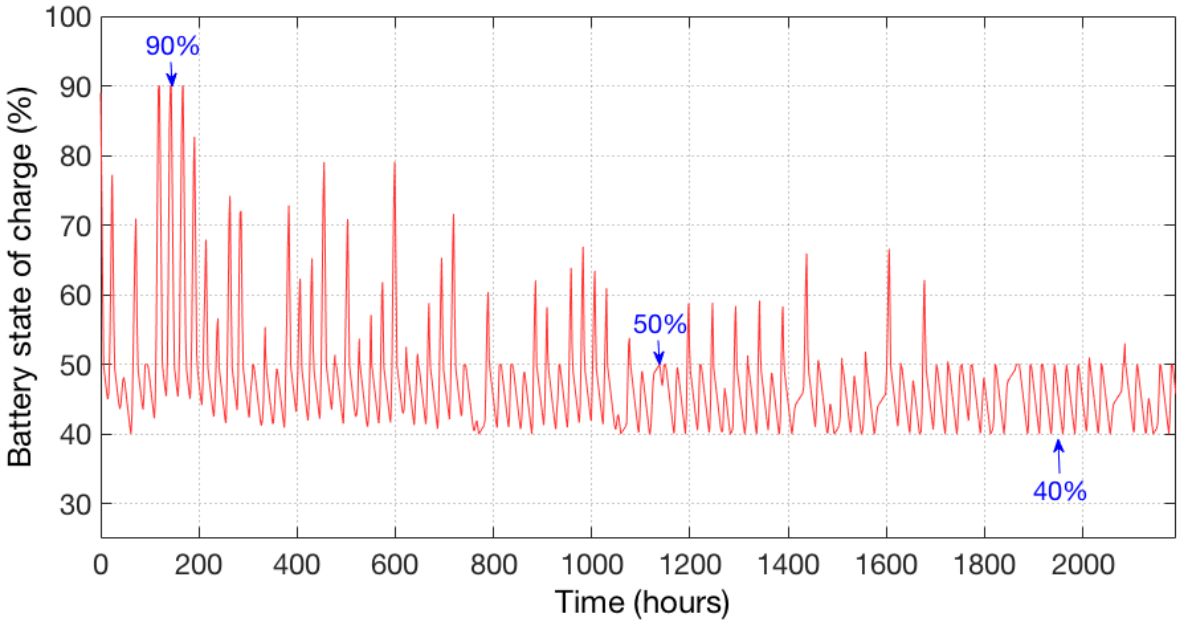

Figure 5.39: Battery state of charge using the final design (from October to December) for the configuration III.

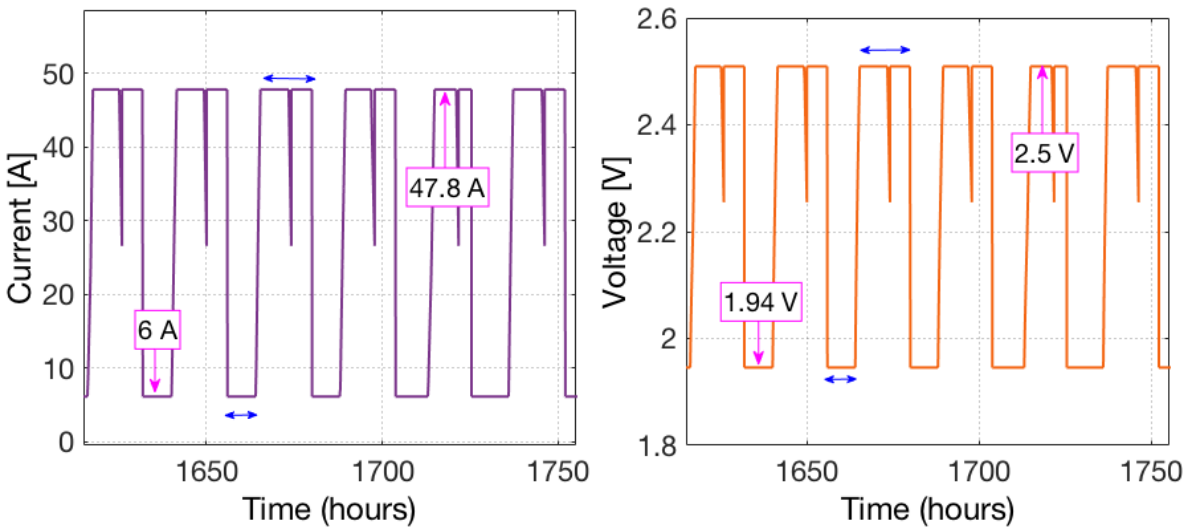

Figure 5.40: Current and voltage of the electrolyzer using the final design (from January to March) for the configuration III.

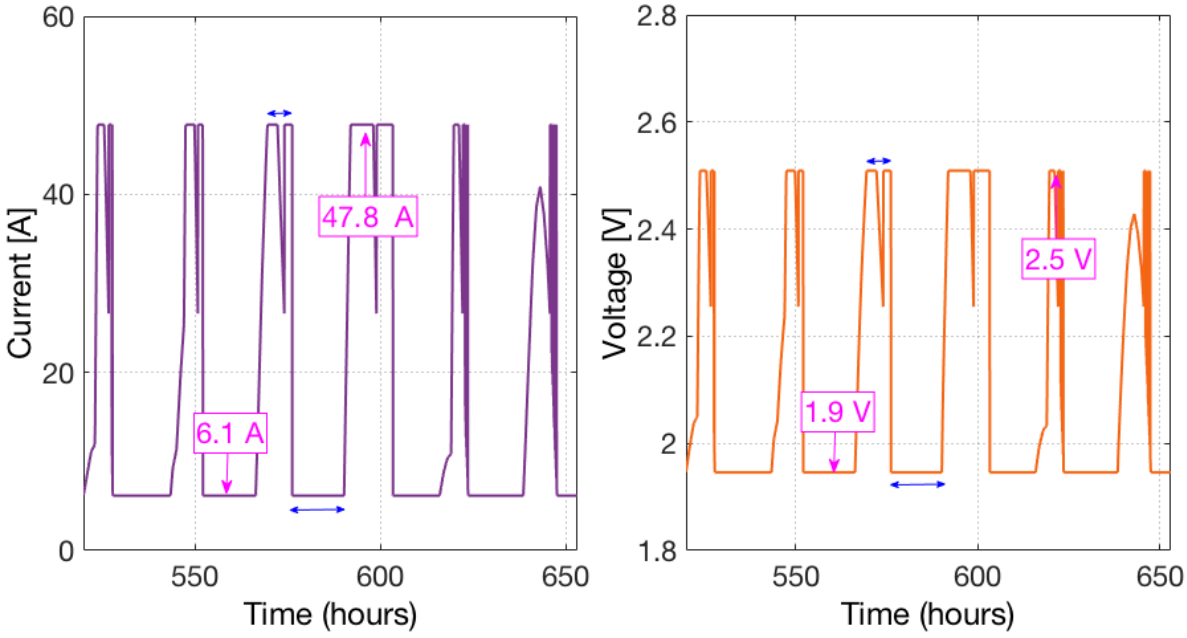

Figure 5.41: Current and voltage of the electrolyzer using the final design (from October to December) for the configuration III.

Summer System Configuration

The generated energy using one module of 300 W during summer is 243.300 kWh. Figure 5.42 shows the generated power during this period. The system has a null energy deficit and minimal energy surplus of 93.4 Wh. Additionally, the hydrogen produced by the system reaches a value of 3.863 kg. Figures 5.43 shows the cumulative hydrogen production during this period. The energy needed to generate one kilogram of hydrogen is 62.98 kWh/kg. Thus, the electrolyzer efficiency for this configuration results in 52.92%.

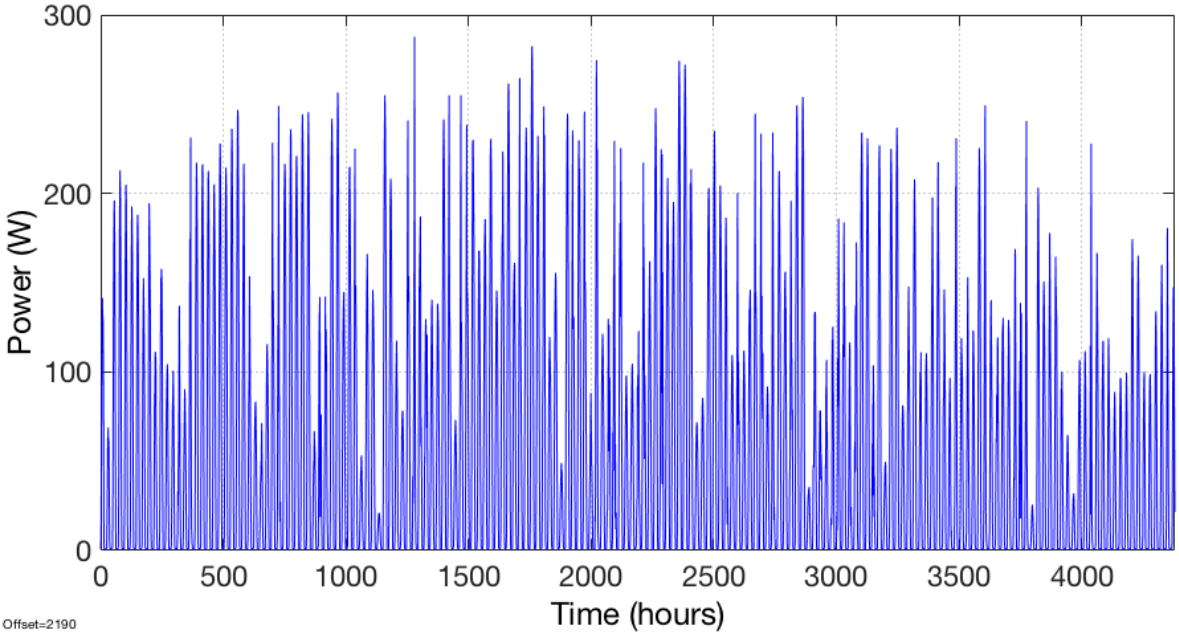

Figure 5.42: Power from the PV using the final design (from April to September) for the configuration III.

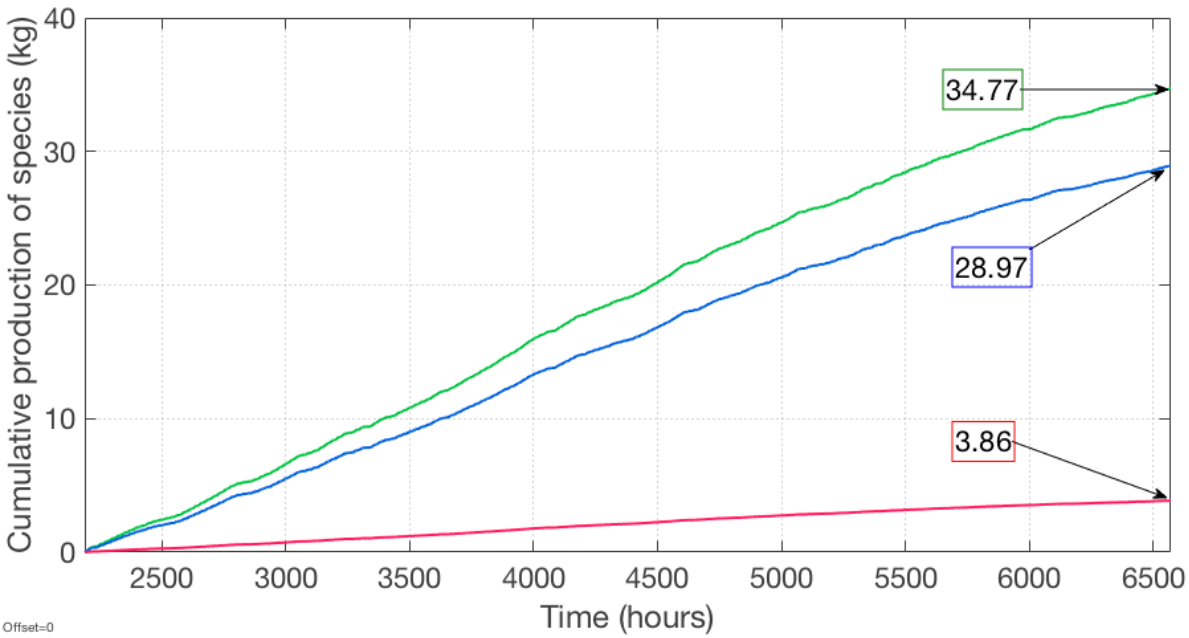

Figure 5.43: Hydrogen production using the final design (from April to September) for the configuration III.

In contrast to the winter configuration, the battery state of charge fluctuates along all its capacity range. Figure 5.44 shows the state of charge of the battery during winter. Additionally, current and voltage levels fluctuate along with the irradiance but always above the minimum operating levels. Figure 5.45 shows the

current and voltage levels of the electrolyzer during this period. Important to mention is that the electrolyzer is operating during the entire year, except during the very few times when there is energy deficit in the system.

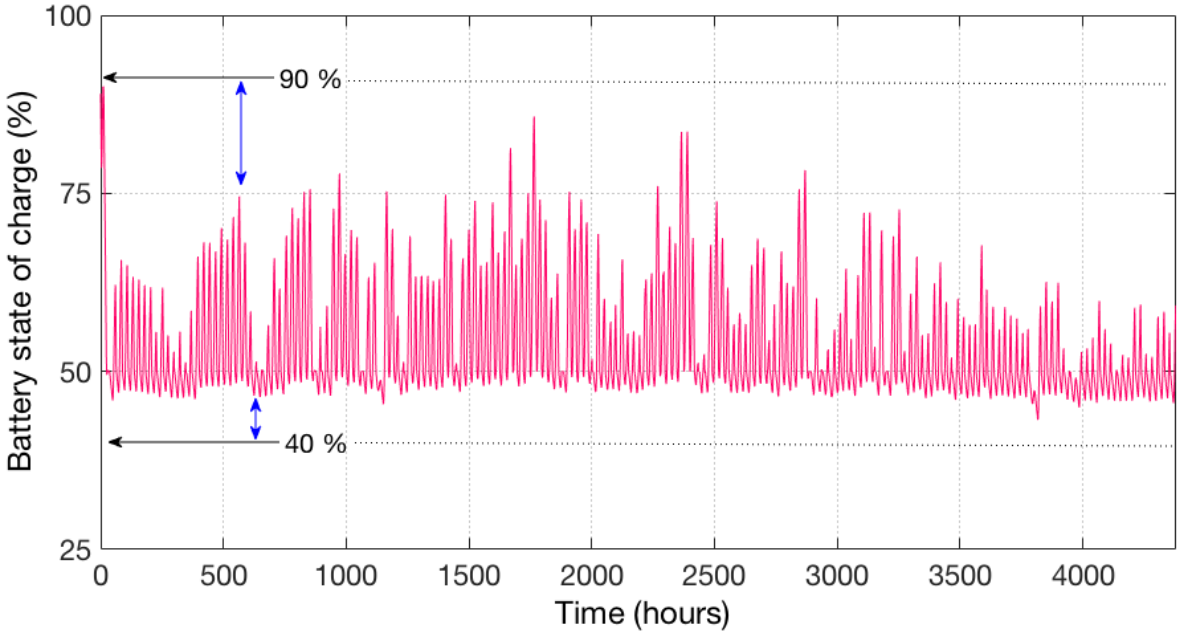

Figure 5.44: Battery state of charge using the final design (from April to September) for the configuration III.

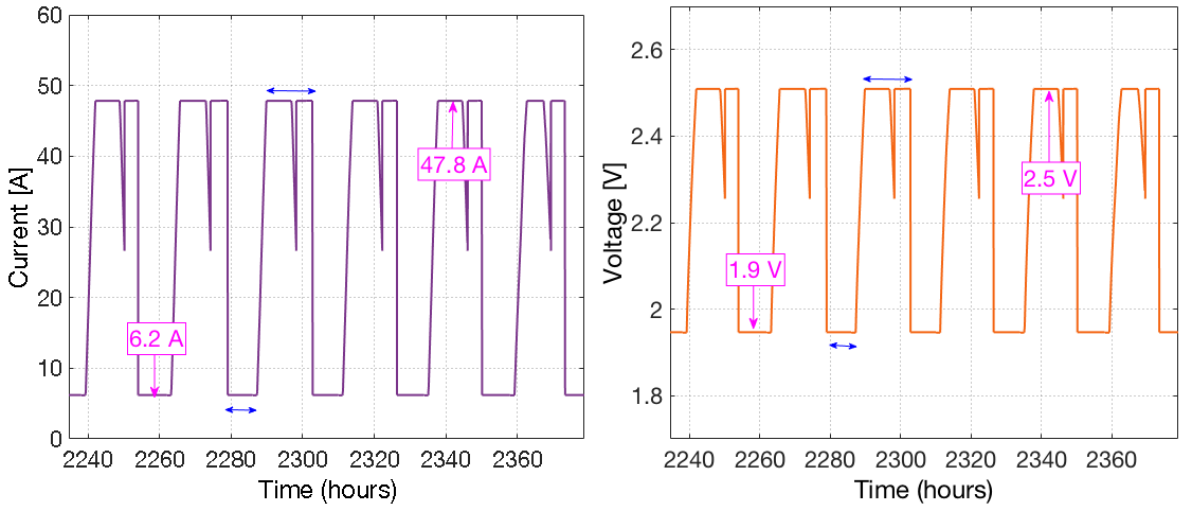

Figure 5.45: Current and voltage of the electrolyzer using the final design (from April to September) for the configuration III.

5.3.3. Remarks for System Configuration III

A system to produce hydrogen via a PEM electrolysis using solar panels profits very much by the implementation of an MPPT and batteries. The MPPT helps to harvest the solar energy available from the PV modules in an efficient way. The battery works as an energy buffer to supply power to the electrolyzer during zero irradiance moments. A single configuration for the entire year is not the most efficient when combining solar modules and batteries for cities located in the northern hemisphere like Delft. The big irradiance difference between summer and winter creates a mismatch of energy in the system. This mismatch generates energy surplus during summer and energy deficit during winter. Adding more solar modules is a solution to solve the energy deficit during winter, but it creates an excess of energy problem during summer. A power control unit is crucial when including batteries in the system. The right control power management allows to effi-

ciently use the energy in the system and distributed among each component at the right moment. The most optimal design is a hybrid configuration for summer and winter. The total system configuration consists of two solar modules of 300 W each; two batteries of 24 V, 70 Ah each; and a PEM electrolyzer of 120 W rated power. Regarding the hydrogen production, there is a notable increment in the system by adding a battery unit. The hydrogen production increase from 39.09% without the battery to 52.95% using the batteries. Regarding the electrolyzer, it operates almost the entire year, except for very few moments when the irradiance is extremely low during winter. Adding the battery in the system allows reducing to almost zero start-stop cycles over a year. The reduction of the number start-stop cycles means additional operating lifetime for the electrolyzer. Hence, the most optimal configuration to generate hydrogen using a PEM electrolyzer powered by PV modules is by using a hybrid seasonal combination of PV modules attached to an MPPT and a battery unit.

6

Conclusions

6.1. Concluding Remarks

The central research question, of how to gain a fundamental understanding of the design, operation, and assessment of the hydrogen production using solar power and a PEM electrolyzer has been answered in three parts. First, a model of a solar-to-hydrogen system was developed using Matlab/Simulink. Three system configurations have been performed to analyze the effects of operating parameters in the system behavior. Second, *Wawa*, the demonstrator system to produce hydrogen using solar panels has been designed, built and tested. Finally, some designing rules based on six non-dimensional factors for a solar-to-hydrogen system were presented.

Answering the first research sub-question (RQ1), this thesis has shown that the components to be considered when designing a solar-to-hydrogen system are mainly three the PV modules, the PEM electrolyzer, and the battery. However, an optimal design of such a system involves extra components like the power control management unit, and the power electronic components. The system demands of sensors, pumps, tubing, and electric wires. All those components combined make the solar-to-hydrogen system. The proposed computational model allows emulating all the components in different sizes and operational conditions. As explained in Chapter 4, current, voltages and hydrogen production are determined using the PV modules and electrolyzer model. For the battery model, the model provides the state of charge, current, and voltage fluctuations. The control unit manages the energy of the system and distributes it to the rest of the components.

To understand how does the irradiance affect the system performance, and thus answer the second research sub-question (RQ2), three different configurations were studied to analyze the performance of the system. As discussed in Chapter 5, first, the most straightforward configuration is a direct connection between the modules and the electrolyzer. In the second configuration, the system includes a maximum power point tracker (MPPT) attached to the PV modules. Finally, the third configuration includes a battery to store the surplus of energy generated by the PV modules.

A direct coupling of one PV module and one PEM electrolyzer to produce hydrogen is possible. The challenge for a direct configuration is to adjust the I-V curves of the components to find the optimal operating point. There are two alternatives to adjust the I-V curve in a direct system configuration. The first option is by connecting more than one PEM cell in series to build up the operating voltage of the electrolyzer. Additionally, this alternative needs few solar panels connected in parallel to reach the current value that satisfies the electrolyzer current. The second alternative and the most effective for a direct configuration is by tailoring a solar module that satisfies both the current and voltage of the electrolyzer. For a 120 W electrolyzer, the most optimal PV module consists of 5×7 (series$\times$parallel) solar cells. Overall, the system efficiency has a value of 6.95%. The downside of the direct system configuration is the start-stop cycles of the electrolyzer because of the daily irradiance fluctuations.

A system to produce hydrogen via a PEM electrolysis using solar panels profits by the implementation of an MPPT. The main impact of the MPPT is the automatic adjustment of the current and voltage from the PV modules to the electrolyzer. The MPPT improves the system by more efficient energy harvesting. In fact, the

connection of a commercial solar module with the electrolyzer is strongly advised not to use it without the MPPT. The energy losses are significant when the system operates without the MPPT. Regarding the hydrogen production, there is not a direct connection between the use of the MPPT and the hydrogen production rate. Nevertheless, the electrolyzer performance is significantly increased by the voltage delivered by PV module when using an MPPT. When using a 300 W module and 120 W electrolyzer, there is a significant waste of energy during high irradiance because the system can only consume 40% of the energy production. The optimal system design must include equal capacity for the PV module and electrolyzer. Furthermore, the start-stop cycles are not affected by adding the MPPT into the system.

The third research sub-question (RQ3) involved the assessment the system performance including a battery. A system to produce hydrogen via a PEM electrolysis using solar panels profits very much by the implementation of an MPPT and batteries. The MPPT helps to harvest the solar energy available from the PV modules efficiently. The battery works as an energy buffer to supply power to the electrolyzer during zero irradiance moments. A single configuration for the entire year is not the most efficient when combining solar modules and batteries for cities located in the northern hemisphere like Delft. The big irradiance difference between summer and winter creates a mismatch of energy in the system. This mismatch generates energy surplus during summer and energy deficit during winter. A power control unit is crucial when including batteries in the system. The right control power management allows to efficiently use the energy in the system and distributed among each component at the right moment. The most optimal design is a hybrid configuration for summer and winter. The total system configuration consists of two solar modules of 300 W each; two batteries of 24 V, 70 Ah each; and a PEM electrolyzer of 120 W rated power. Regarding the hydrogen production, there a notable increment in the system by adding a battery unit. The hydrogen production increase from 39.09% without the battery to 52.95% using the batteries. Regarding the electrolyzer, it operates almost the entire year, except for very few moments when the irradiance is extremely low during winter. Adding the battery in the system allows reducing to almost zero start-stop cycles over a year. The reduction of the number start-stop cycles means additional operating lifetime for the electrolyzer. Hence, the most optimal configuration to generate hydrogen using a PEM electrolyzer powered by PV modules is by using a hybrid seasonal combination of PV modules attached to an MPPT and a battery unit.

To find the critical parameters of the hydrogen production via PEM water electrolysis, and thus answer the fourth research sub-question (RQ4), *Wawa* was designed and built as a demonstrator system. *Wawa* consists of two PV panels (300W each), two lead-acid batteries (70 Ah, 12 V each), and a water polymer-electrolyte-membrane (PEM) electrolyzer (120 W). Additionally, the system includes a charge controller with a maximum power point tracker (MPPT), and complementary components such as a microcontroller, a pump, tubing, flow meters, filters, gas separators and electric wires. The first stage of Wawa was built and tested. Using a direct current (DC) power source and a water PEM electrolyzer, the hydrogen generation was successfully achieved. As discussed in Chapter 2 and 5, the experimental results have shown that the critical parameters for such a system can be categorized into three parts: electrical, mechanical and chemical. Regarding the chemical parameters, water composition plays a key role in the performance of the system. A direct recirculation of the water from the electrolyzer reduces its efficiency because of lack of hydrogen and the excess of oxygen in the water. Regarding the mechanical parameters, water flow, temperature, and pressure are critical to the operation system. By changing any of those parameters, the electrolyzer performance is affected. Regarding the electrical parameters, the voltage is crucial in the operation of the system. Voltages lower than the thermoneutral potential can not run the electrolyzer. In contrast, high and unstable voltages generate energy losses.

To find what are the sizing guidelines for a solar-to-hydrogen system, and thus answer the fifth research sub-question (RQ5), six non-dimensional sizing factors were presented in Chapter 4. The factors relate the three primary variables of the system: the PV modules, the battery, and the electrolyzer. These factors provide a criterion for the system design by a relative comparison between each component. Several simulations were run with different components size, to later plot the data using the non-dimensional factors, as presented in Appendix B. The results show that the proposed factors can be used as a designing tool for solar-to-hydrogen systems in a more methodical way.

It is the hope of the writer that the world installed capacity of solar modules keeps growing, and eventually, solar electricity prices become significantly lower. Thus, the hydrogen generation via PEM electrolysis will become more attractive and less polluting than the production based on fossil fuels. For utility companies, the concept of the solar-to-hydrogen system is a promising alternative to alleviate the congestion of distri-

bution of the grid in highly dense urban areas. A compact and decentralized solar-to-hydrogen system is a promising alternative to have abundant clean energy all the time.

Furthermore, humankind needs to stop increasing the CO_2 emissions now. Solar-to-hydrogen systems are serious candidates to provide clean, reliable and stable power generation. More importantly, hydrogen production using solar power means less use of natural gas and oil. Solar-to-hydrogen systems promote the increase of solar energy generation, and reduction CO_2 emissions. Undoubtedly, using solar energy to produce clean fuels is an excellent opportunity to make a critical change in the history of humanity.

6.2. Recommendations for Future Research

This thesis project demands a holistic knowledge in different technical fields. Each component can be further analyzed to provide a more realistic simulation of the system. This thesis presented a computational model to assess the performance of the system which can be customized to any configuration and operational conditions. A more fine control management model can enhance the system response by making the control more accurate and secure for any power fluctuation in the system. Also including a detailed model of the power electronic components in the system can provide a more precise behavior of the charge controller, and power converter. Nevertheless, the complexity of the modeling might not necessarily improve the results of the model.

Future research can explore the system performance under different irradiance conditions by using the non-dimensional factors. Investigating the relationship of location, component sizes and capacity factor of the system can be done by using the proposed of the non-dimensional factors.

Regarding *Wawa*, the demonstrator system, the next research stage includes the assessment of the system with the PV modules in situ. Additionally, the microcontroller installed in the PCB can be programmed to have an automated operation of the system as well as the collection of the data in real time. Researching the actual performance of hydrogen production, temperature, and pressure fluctuation by using the demonstrator system might provide more insightful results than the simulations.

This project did not dive into the economic aspects of such a system because there are already several studies stating that such a system requires a significant capital investment. Nevertheless, for a big scale implementation of a solar-to-hydrogen system, the situation might change. Calculating the economic impact of such a system to investigate under which conditions the it becomes economically feasible could be included in future research. Further research in solar-to-hydrogen systems is crucial to promote and showcase the potential and benefits of such a promising technology.

A

Simulink Block Diagrams of the System

A.1. Simulink Model of the PV Module

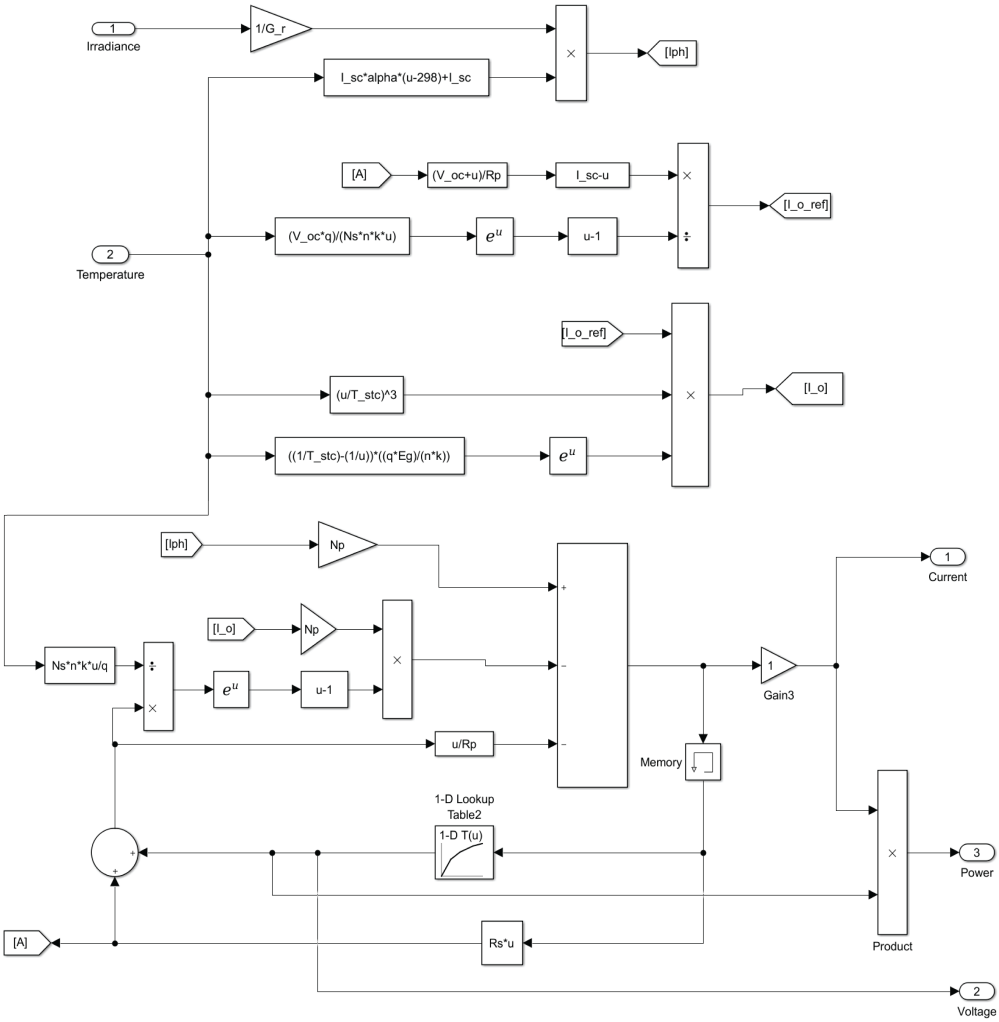

Figure A.1: Simulink block diagram representing the photovoltaic module.

A.2. Simulink Model of the Battery

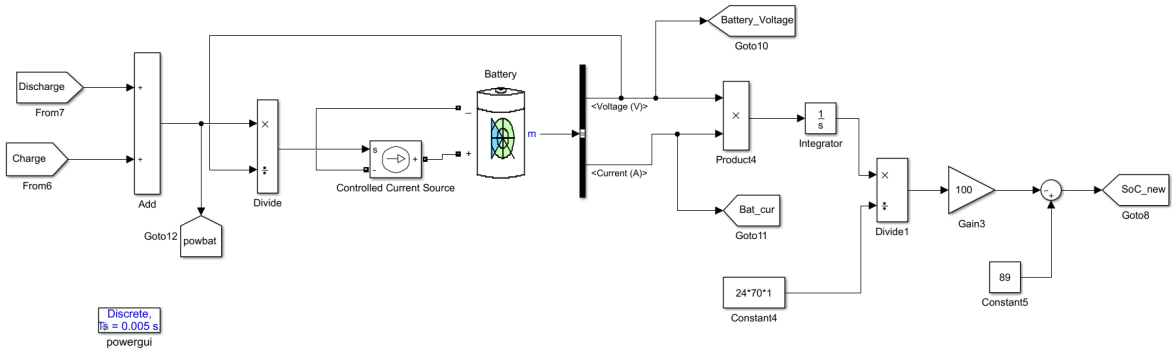

Figure A.2: Simulink block diagram representing the lead-acid battery model.

A.3. Simulink Model of the Water PEM Electrolyzer

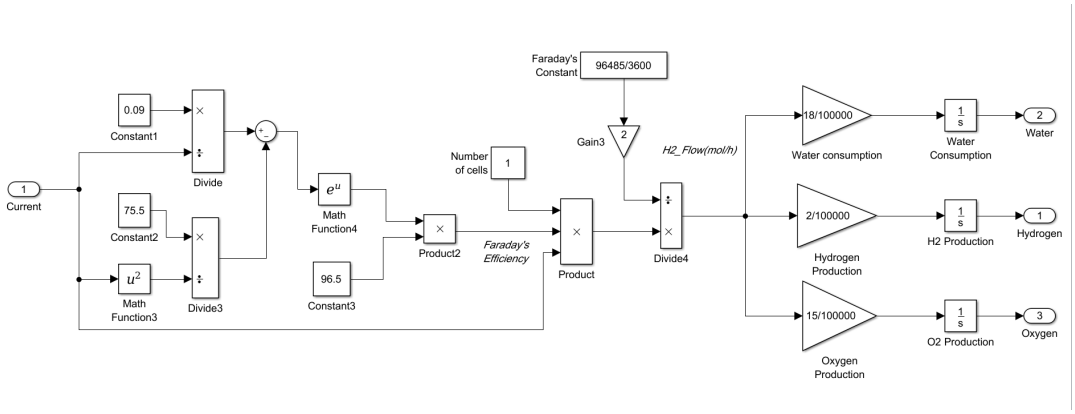

Figure A.3: Simulink block diagram representing the mass flow model of the water PEM electrolyzer.

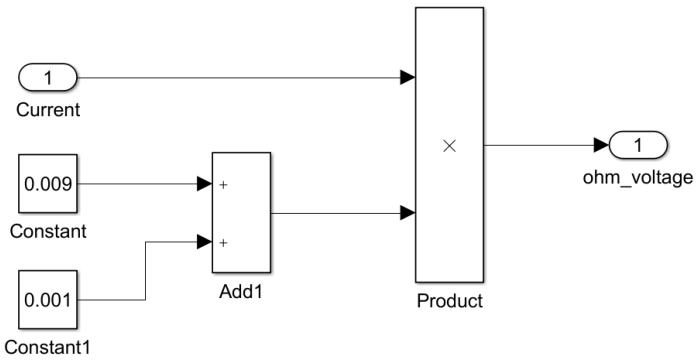

Figure A.4: Simulink block diagram representing the ohmic voltage model of the water PEM electrolyzer.

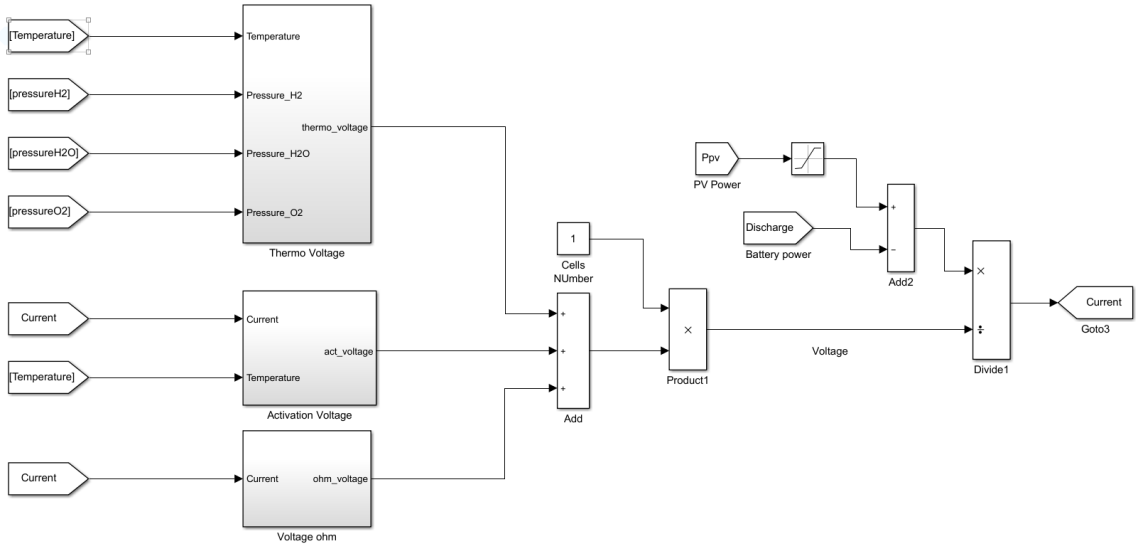

Figure A.5: Simulink block diagram representing the voltage model of the water PEM electrolyzer.

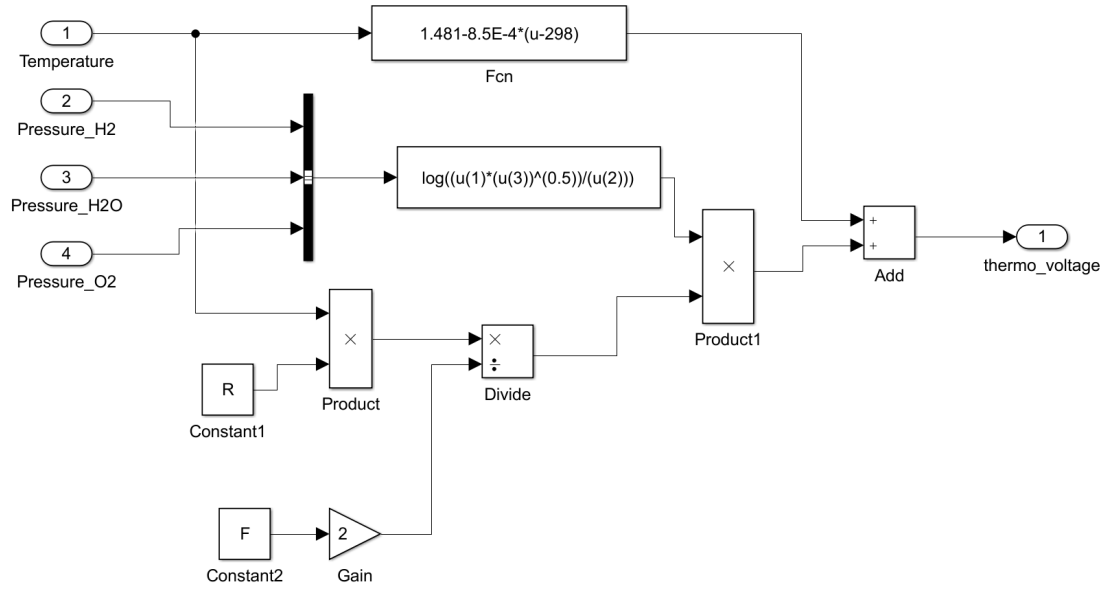

Figure A.6: Simulink block diagram representing the thermoneutral voltage model of the water PEM electrolyzer.

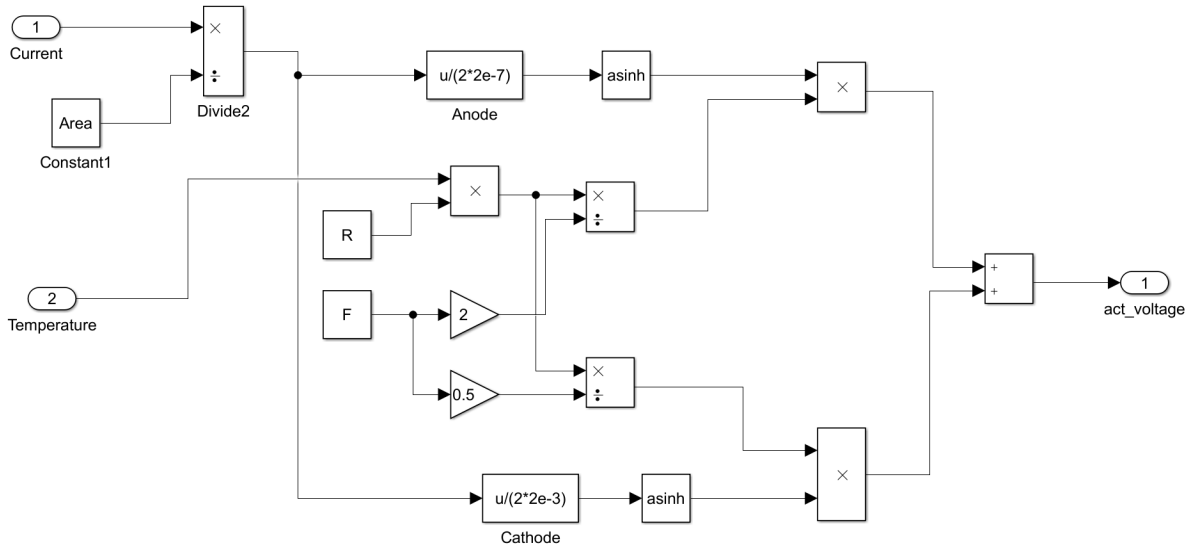

Figure A.7: Simulink block diagram representing the activation voltage model of the water PEM electrolyzer.

A.4. Simulink Model of the Gas Storage Tank

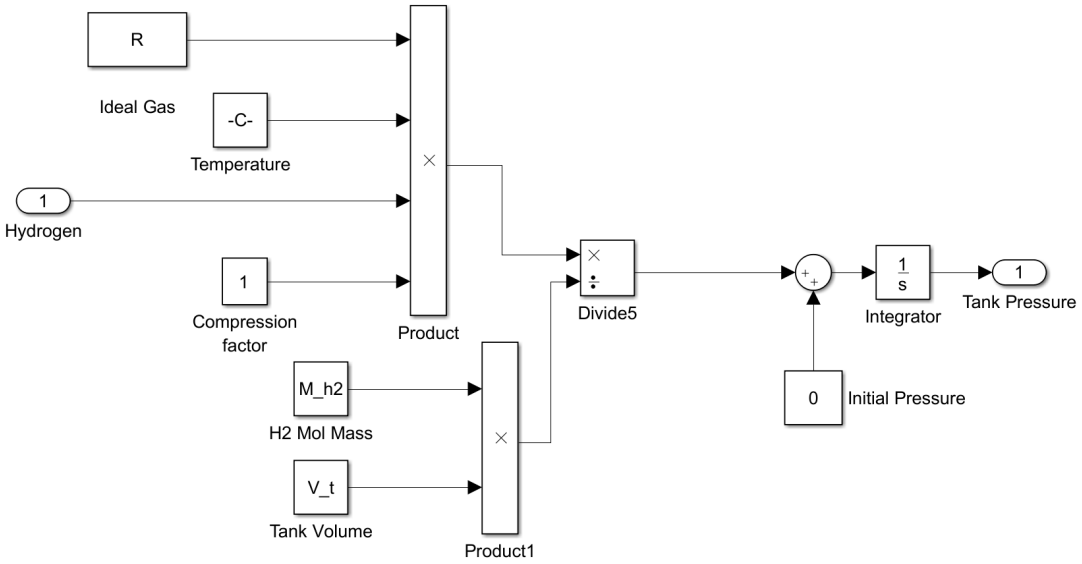

Figure A.8: Simulink block diagram representing the storage tank of hydrogen gas.

A.5. Simulink Model of the Power Control Strategy

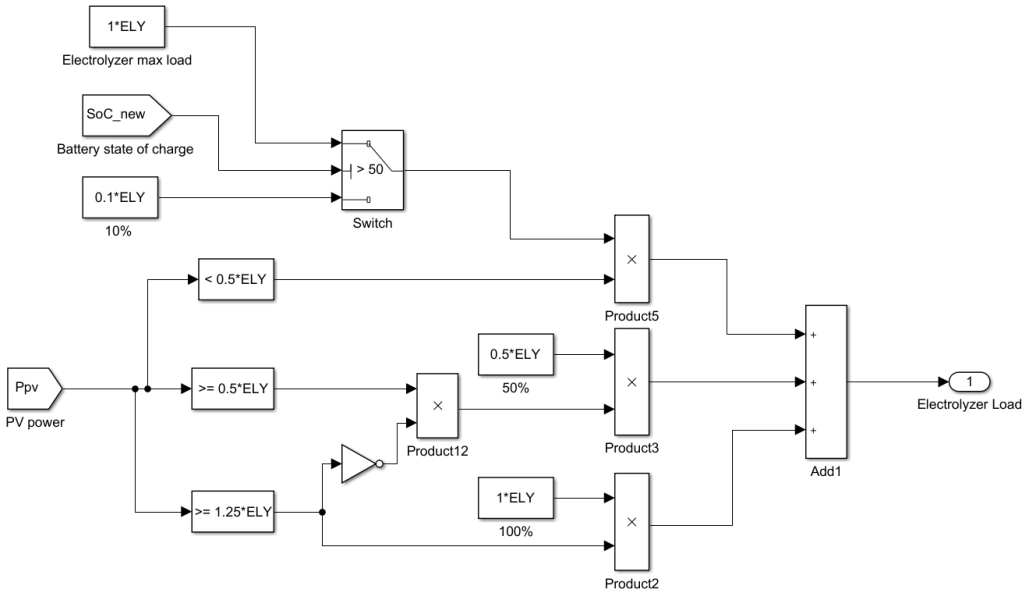

Figure A.9: Simulink block diagram representing the load values in function of the power delivered by the PV module.

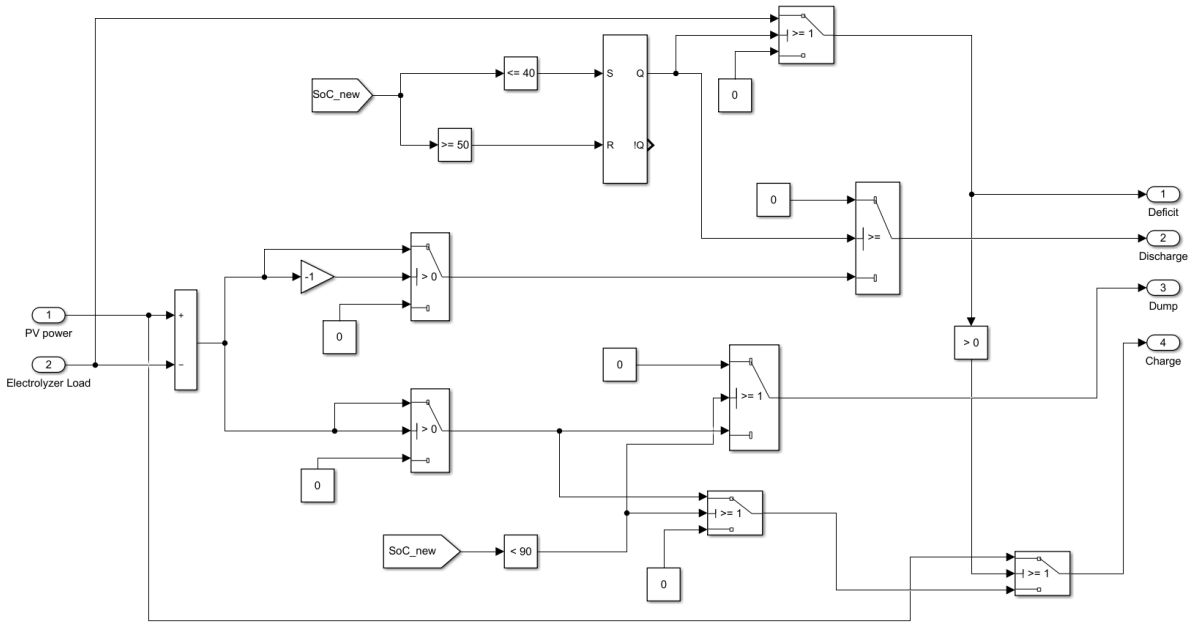

Figure A.10: Simulink block diagram representing the power control strategy.

B

Simulations Results of Different Component Sizes

B.1. Sizing Guidelines

The implemented model in Simulink allows to simulate the system for different component sizes and operational conditions. Several system configurations are analyzed using the six non-dimensional factors shown in table B.2, already introduced in Chapter 4. The factors relate the sizes and capacities of the main components of the system: the PV modules, the battery bank, and the electrolyzer. These factors provide a criterion for the design of a solar-to-hydrogen system. The selected component sizes are shown in Table B.1. Overall, one-hundred simulation were run for the irradiance conditions of Delft but different component sizes. The simulations used the system configuration III presented in Chapter 4. The results are presented in several charts that help the data interpretation. Moreover, a few design questions have been included as an example to explain the usefulness of the sizing factors.

Table B.1: Size components utilized for the performed simulations

PV modules (W)	**Battery bank (Ah)**	**Electrolyzer (W)**
600	70	120
1200	140	240
1800	210	480
2400	280	960
	350	1200

Table B.2: Non-dimensional factors

1.- $BEF = \frac{battery\ energy\ capacity\ [Wh]}{annual\ PV\ energy\ generated\ [Wh]}$	4.- $EDF = \frac{annual\ energy\ deficit\ [Wh]}{annual\ PV\ energy\ generated\ [Wh]}$
2.- $PVL = \frac{averange\ annual\ load\ [W]}{PV\ installed\ capacity\ [W_p]}$	5.- $SEF = \frac{annual\ energy\ dumped\ [Wh]}{annual\ PV\ energy\ generated\ [Wh]}$
3.- $LOF = \frac{averange\ annual\ load\ [W]}{maximum\ rated\ load\ [W]}$	6.- $ECF = SEF\text{-}EDF$

Figure B.1 shows the energy deficit factor (EDF) and the load factor (LOF). The data shows a hyperbolic shape with asymptotes in $EDF = 0$ and $LOF = 10\%$.

The last one is due to the fact that the control unit was defined at 10% of its peak load as a minimum possible value. The effect of increasing the battery size in a system with $LOF \geq 20\%$ becomes almost insignificant. A

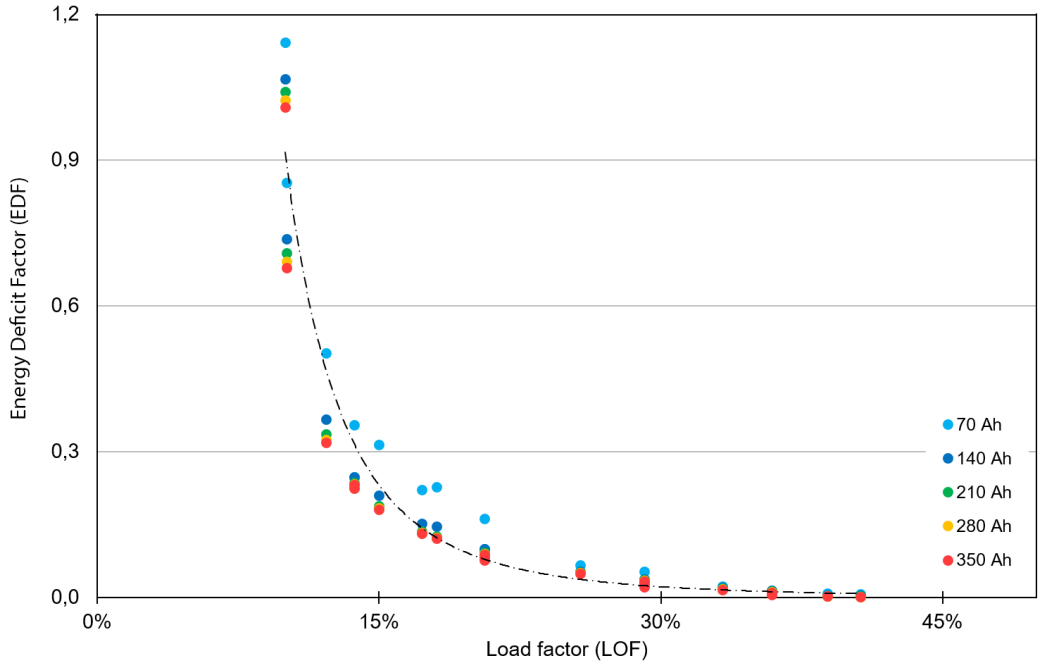

Figure B.1: Lack Energy Factor versus Load factor

high value of EDF is always negative for the system because the system is not able to run the electrolyzer with the generated power. Moreover, a high value of LOF is always good because it means the electrolyzer operates most of the time. An important feature of this plot is the point at which the energy deficit factor starts decreasing quickly as a function of the load factor. The fast reduction of EDF starts at 15% and ends at 30% Above 30% the reduction in the energy deficit factor becomes insignificant. In other words, a system with a LOF value higher than 30% demands a significant reduction of EDF. To reduce EDF, the system must either add more PV modules to generate more energy, reduce the electrolyzer load.

Figure B.3 shows the amount of non operative hours in the electrolyzer over in function of the PV to load factor and the battery size. The curve presents a half parabola shape with a vertical directrix $x = 0$. A value in the horizontal axis close to zero, represents a capacity factor of the electrolyzer about 100%. In other words a value of $PVL = 0.015$ means that the electrolyzer operates constantly for almost the entire year. In this point, the impact of including a battery in the system becomes minimal than for higher values of non operative hours. For instance, for PVL=0.20 a battery between 350 Ah and 70 Ah makes a difference of 1200 (5000-3800) operative hours. For smaller values of PVL the result is different. At PVL=0.20 the variation in battery size is relatively minimal. For high value of non-operative hours (top-right corner region), the increase in battery makes a difference in the value.

Figure B.2 presents a relationship between the energy deficit factor (EDF) and surplus energy facto (SEF). The figure also includes information about the size ratio between the electrolyzer load and PV module. This ratio is represented by the purple straight line in fig. B.2. A high ratio values is located over the top-left corner of the figure. In contrast a low ratio value is located at the lower-right corner area, almost showing as a dot. Figure B.2 shows the most suitable combination for balancing the surplus and deficit energy. For instance if there is a PV module of $800W$ and an electrolyzer of $960W$, then the ratio results into $960/800 = 1.2$. The energy deficit and surplus of the system can be regulated by varying the battery size (parallel line to 1). The figure B.2 tells that a battery of $70Ah$ it is expected to have a surplus energy factor of $SEF = 0.28$. Using a battery of $350Ah$, the surplus energy factor is reduced to 0.11.

Sizing Question:

- *For a PV system that generates a yearly energy surplus of 5300 kW in Delft, corresponding to two panels of 300 W each one. What should the battery and electrolyzer size be, if the goal is operating the electrolyzer*

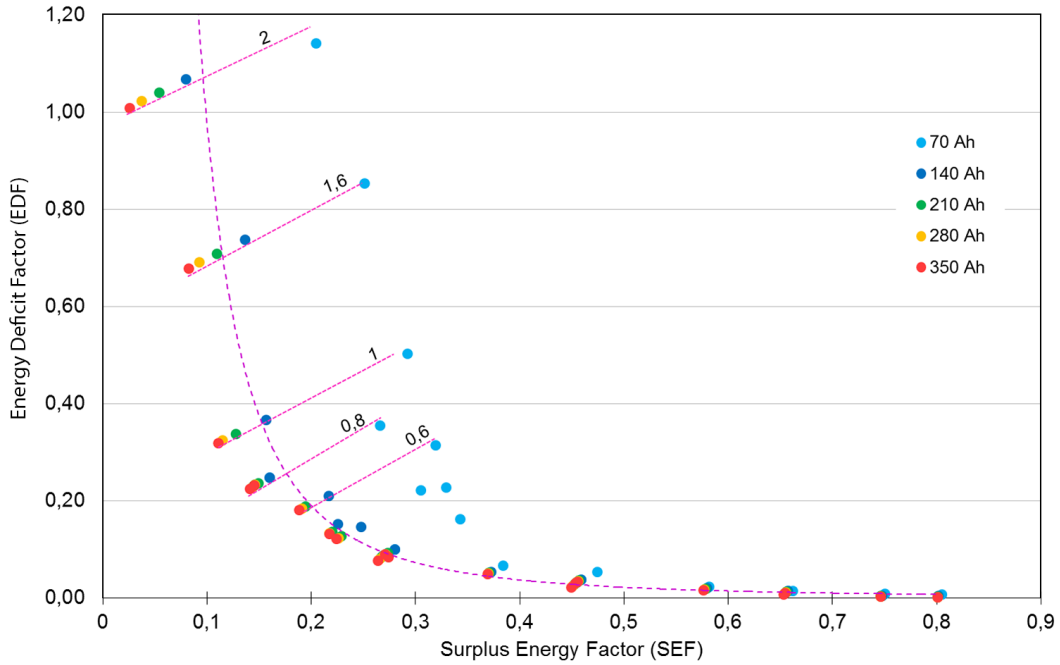

Figure B.2: Relationship between the energy deficit factor and surplus energy factor.

only during the highest irradiance months?

Operating the electrolyzer for half a year represents a non operative hours equal to $365 \times 24/2 = 4380$. A value of 4380 in Fig. B.3, gives a value of $PVL = 0.17$. Using the Eq.4.23, a value of the averange annual load is equal to $0.17 * 600W = 102W$. Knowing that the goal is a system operation of halve a year, then $LOF = 50\%$. Consequently the size of the electrolyzer should be equal to $102/2 = 51W$.

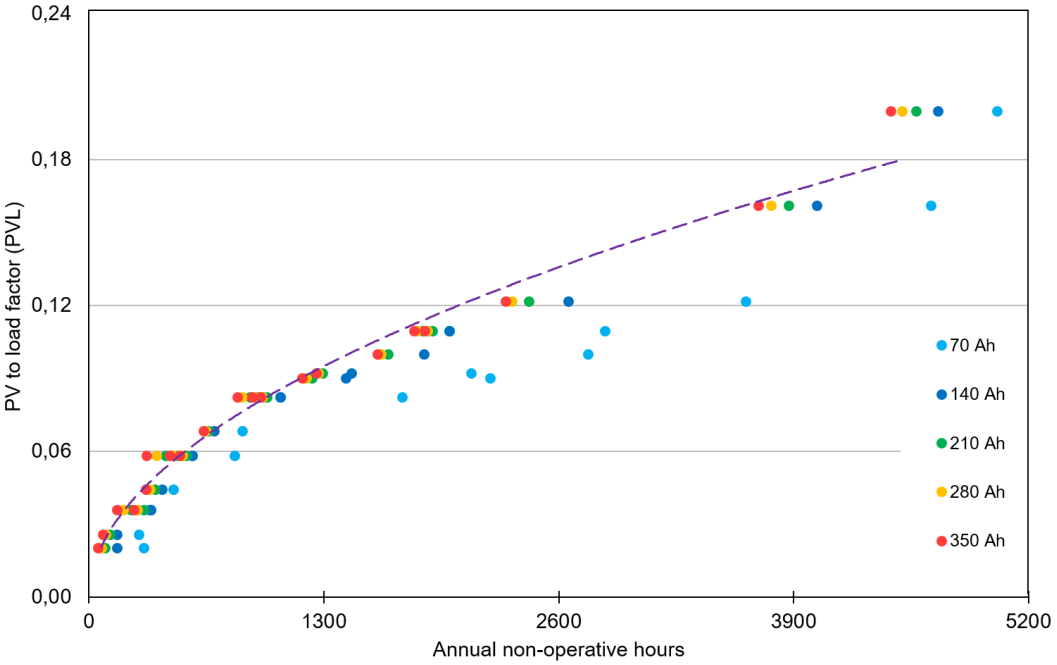

Figure B.3: Relationship between PV power to load factor and the annual non-operative hours.

For each combinations, the system had a certain amount of energy deficit usually during low irradiance periods. Similarly, a energy surplus during high irradiance periods. Those values are represented by SEF (Surplus) and EDF (Deficit) factors. When subtracting those two factors, the result represent the relative energy that the system is consuming. This value is called the Energy consumed factor (ECF), shown in Fig. B.3 Important to notice is the linear relationship with a negative slope between the ECF and the PVL. The yellow region represents all the values when the system has higher amount of energy in excess. The blue area represent all the negative values, when the system has energy deficit. A value of $PVL = 0.1$ represents a system operation of equal energy deficit and energy surplus. Knowing the value at which the consumption becomes negative or positive it is possible to select the right size of electrolyzer. This concept is explained more in detail in the following question.

Sizing Question:

- *What should the electrolyzer and battery size be for an hybrid system where the PV array has a 1000 Wp installed and the goal is to have a balance between the surplus and deficit of energy?*

A balance between surplus and deficit energy means having a value of $ECF = 0$. Hence in Fig. B.4 results a value of $PVL = 0.1$. Now, using the formula Eq(4.23) with a value of 1000 W, returns an averange load value of $1000 * 0.1 = 100W$. Then using the last value in figure B.5 results in a value of $SEF = 0.18$. Using Fig. B.2 its is possible to identify the possible values of the battery size. Given a $LEF = SEF = 0.2$ the battery size options are from 210 to 350 Ah. Hence a final size of the battery size could be 280 Ah. The size of the electrolyzer can be determined by using Fig. B.1. Given a value of $EDF = 0.18$ results a value of $LOF = 15\%$. Consequently using Eq.(4.26) results an electrolyzer size equal to 660 W.

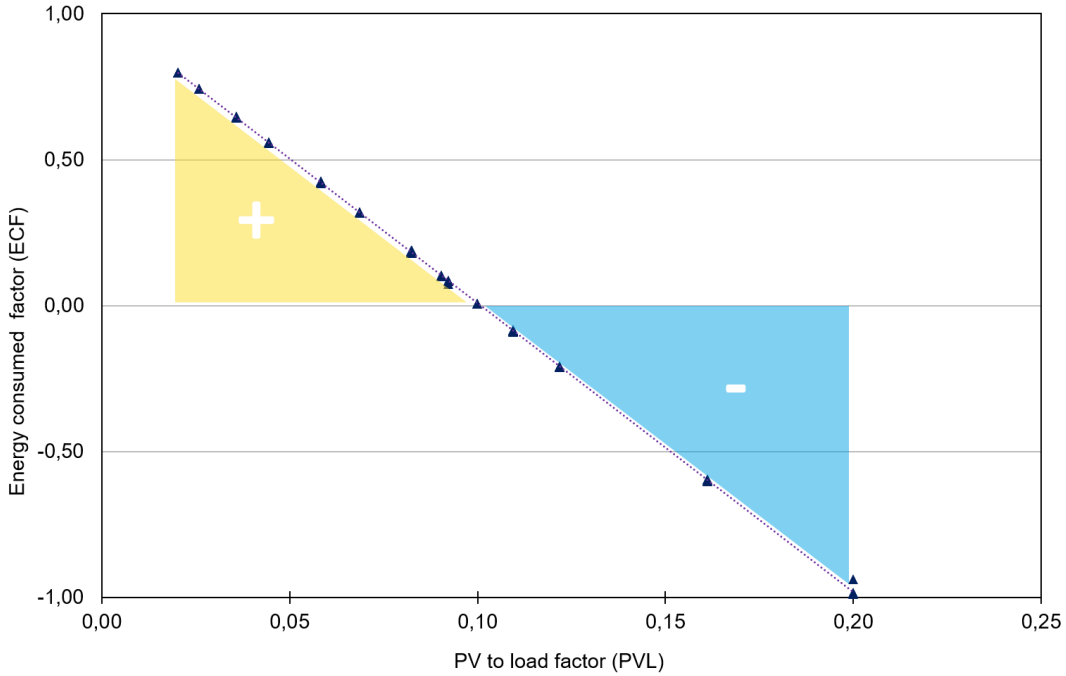

Figure B.4: Energy consumption factor (ECF) and PV power to load factor (PVL)

Sizing Question:

- *What should the Electrolyzer size be, if there is a PV module size of 1800 W_p, and the goal is to have the least possible energy deficit (EDF=0.1) but maximum load factor?*

First, using Fig. B.6 and the value of $EDF = 0.1$ it is possible to find ad values of $PVL = 0.09$. With this value and using the definition of PVL in 4.23, the average load value is equal to $0.09 \times 1800W = 162W$. Then in Fig.B.1 for a value of $EDF = 0.1$, correspond a values of $LOF = 17\%$. Finally, using the definition of LOF and the calculated average annual load, the value of the electrolizer size should be $162 \times 100/17 = 952W$

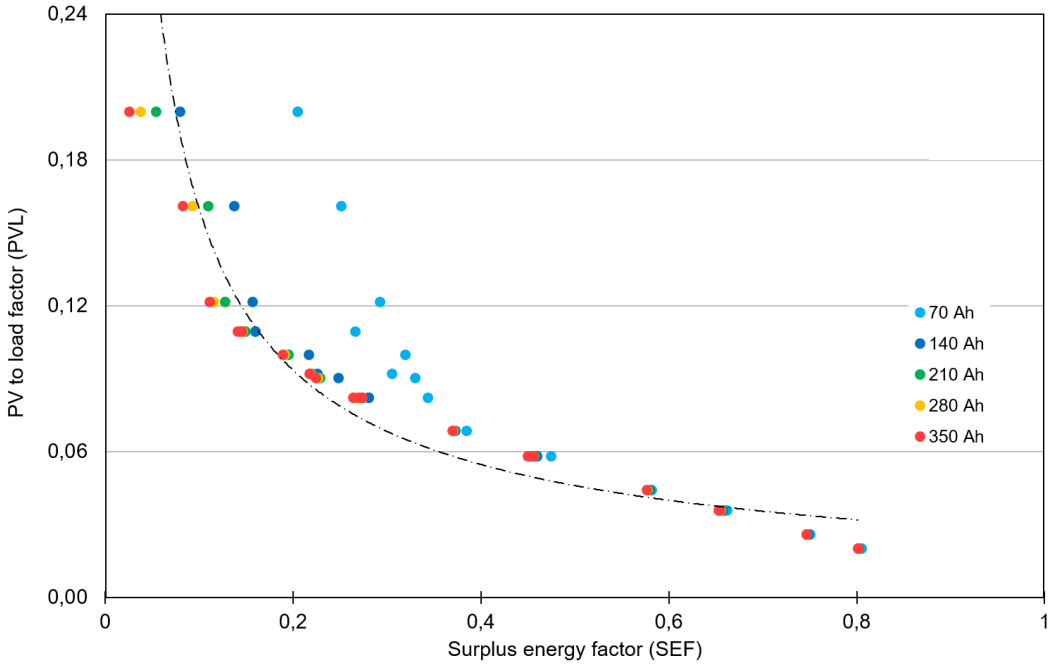

Figure B.5: PV power to load factor (PVL) versus surplus energy factor (SEF)

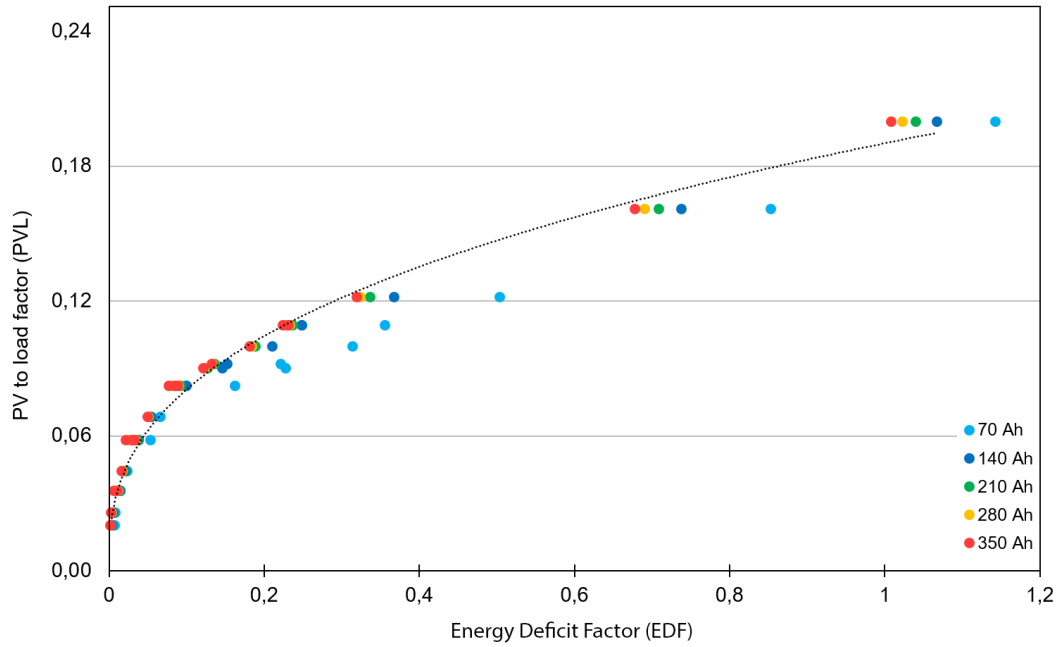

Figure B.6: PV power to load factor (PVL) versus energy deficit factor (EDF)

Additionally, Figures B.6 and B.5, present the relative values of how much energy the system is lacking or dumping. This relationship includes the sizes of the PV modules and the electrolyzer. Overall, in an solar to hydrogen system, having higher values of EDF or SEF is not wanted. Figures B.6 and B.5 presents the relationship of the size of the battery. For lower values of LEF the impact of a different battery size is almost insignificant. Similarly happens for high values of SEF.

Sizing Question:

- *What should the battery and electrolyzer size be for an solar to hydrogen system with 1200 W_p of installed PV, and the goal is having no more than 15% of energy surplus?*

First, having a energy surplus no more than 15% means a value of $SEF = 0.15/1$. Using this value in Fig. B.5, results is $PVL = 0.12$. Then, using $PVL = 0.12$ in Fig. B.6, the EDF value can be determined. Given a battery size of 210 Ah, results in a value of $LEF = 0.38$. Using definition of PVL 4.23 and the PV peak value, results in a an averange annual load equal to $0.12 * 1200W = 144W$. Consequently, using Fig. B.6 and $LEF = 0.38$, a value of $LOF = 13\%$ is determined. Finally, using the definition of LOF in Eq. 4.26, the electrolizer size should be equal to $1107W$

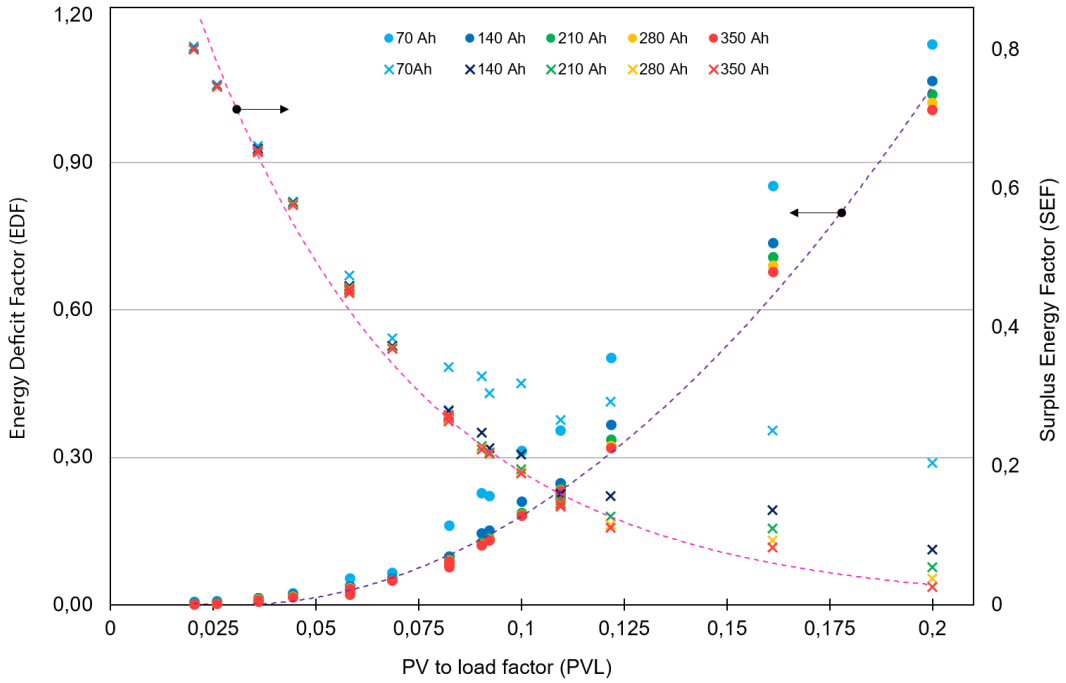

Figure B.7: Representation of the surplus energy factor (SEF), the energy deficit factor (EDF), and the PV and load size (PVL)

Table B.3: Raw data taken from the computational simulations for a system configuration with several size combinations of PV modules, batteries, and electrolyzer.

Load [W]	**PV** [W]	**Batt** [Wh]	**PV** [Wh/y]	**Load** [Wh/y]	**Avg. Load** [W]	**Deficit** [Wh/y]	**Surplus** [Wh/y]	**BEF**	**PVL**	**EDF**	**SEF**	**LOF**	**ECF**
120	600	1680	528200	306000	34,9	17990	240900	3,18	0,06	0,03	0,46	0,29	0,42
120	600	3360	528200	306000	34,9	16370	239900	6,36	0,06	0,03	0,45	0,29	0,42
120	600	5040	528200	306000	34,9	14730	238900	9,54	0,06	0,03	0,45	0,29	0,42
120	600	6720	528200	306000	34,9	13060	238000	12,72	0,06	0,02	0,45	0,29	0,43
120	600	8400	528200	306000	34,9	11120	237300	15,90	0,06	0,02	0,45	0,29	0,43
240	600	1680	528200	432900	49,4	47410	143400	3,18	0,08	0,09	0,27	0,21	0,18
240	600	3360	528200	432900	49,4	45400	142100	6,36	0,08	0,09	0,27	0,21	0,18
240	600	5040	528200	432900	49,4	44080	141300	9,54	0,08	0,08	0,27	0,21	0,18
240	600	6720	528200	432900	49,4	41870	140300	12,72	0,08	0,08	0,27	0,21	0,19
240	600	8400	528200	432900	49,4	40630	139500	15,90	0,08	0,08	0,26	0,21	0,19
480	600	1680	528200	575400	65,7	130900	84450	3,18	0,11	0,25	0,16	0,14	-0,09
480	600	3360	528200	575400	65,7	122900	77160	6,36	0,11	0,23	0,15	0,14	-0,09
480	600	5040	528200	575400	65,7	121300	76200	9,54	0,11	0,23	0,14	0,14	-0,09
480	600	6720	528200	575400	65,7	119500	75250	12,72	0,11	0,23	0,14	0,14	-0,08
480	600	8400	528200	575400	65,7	118200	74470	15,90	0,11	0,22	0,14	0,14	-0,08
960	600	1680	528200	846700	96,7	450500	132700	3,18	0,16	0,85	0,25	0,10	-0,60
960	600	3360	528200	846700	96,7	389300	72240	6,36	0,16	0,74	0,14	0,10	-0,60
960	600	5040	528200	846700	96,7	374100	57790	9,54	0,16	0,71	0,11	0,10	-0,60
960	600	6720	528200	846700	96,7	364700	48910	12,72	0,16	0,69	0,09	0,10	-0,60
960	600	8400	528200	846700	96,7	358000	43520	15,90	0,16	0,68	0,08	0,10	-0,60
1200	600	1680	528200	1051000	120,0	603040	108100	3,18	0,20	1,14	0,20	0,10	-0,94
1200	600	3360	528200	1051000	120,0	563600	42030	6,36	0,20	1,07	0,08	0,10	-0,99
1200	600	5040	528200	1051000	120,0	549300	28470	9,54	0,20	1,04	0,05	0,10	-0,99
1200	600	6720	528200	1051000	120,0	540000	19750	12,72	0,20	1,02	0,04	0,10	-0,98
1200	600	8400	528200	1051000	120,0	532500	13600	15,90	0,20	1,01	0,03	0,10	-0,98
120	1200	1680	1056000	377200	43,1	14700	694500	1,59	0,04	0,01	0,66	0,36	0,64
120	1200	3360	1056000	377200	43,1	11580	692000	3,18	0,04	0,01	0,66	0,36	0,64
120	1200	5040	1056000	377200	43,1	9973	691300	4,77	0,04	0,01	0,65	0,36	0,65
120	1200	6720	1056000	377200	43,1	8091	690200	6,36	0,04	0,01	0,65	0,36	0,65

Table B.3: Raw data taken from the computational simulations for a system configuration with several size combinations of PV modules, batteries, and electrolyzer.

Load	PV	Batt	PV	Load	Avg.	Deficit	Surplus	BEF	PVL	EDF	SEF	LOF	ECF
120	1200	8400	1056000	377200	43,1	6611	689500	7,95	0,04	0,01	0,65	0,36	0,65
													0,00
240	1200	1680	1056000	612000	69,9	39950	484900	1,59	0,06	0,04	0,46	0,29	0,42
240	1200	3360	1056000	612000	69,9	35989	481700	3,18	0,06	0,03	0,46	0,29	0,42
240	1200	5040	1056000	612000	69,9	34020	480500	4,77	0,06	0,03	0,46	0,29	0,42
240	1200	6720	1056000	612000	69,9	32730	479800	6,36	0,06	0,03	0,45	0,29	0,42
240	1200	8400	1056000	612000	69,9	31250	479000	7,95	0,06	0,03	0,45	0,29	0,42
480	1200	1680	1056000	865900	98,8	104700	295800	1,59	0,08	0,10	0,28	0,21	0,18
480	1200	3360	1056000	865900	98,8	94830	286800	3,18	0,08	0,09	0,27	0,21	0,18
480	1200	5040	1056000	865900	98,8	92460	285100	4,77	0,08	0,09	0,27	0,21	0,18
480	1200	6720	1056000	865900	98,8	90810	284200	6,36	0,08	0,09	0,27	0,21	0,18
480	1200	8400	1056000	865900	98,8	89110	289100	7,95	0,08	0,08	0,27	0,21	0,19
960	1200	1680	1056000	1151000	131,4	374900	281100	1,59	0,11	0,36	0,27	0,14	-0,09
960	1200	3360	1056000	1151000	131,4	261800	168900	3,18	0,11	0,25	0,16	0,14	-0,09
960	1200	5040	1056000	1151000	131,4	249600	157500	4,77	0,11	0,24	0,15	0,14	-0,09
960	1200	6720	1056000	1151000	131,4	245800	154300	6,36	0,11	0,23	0,15	0,14	-0,09
960	1200	8400	1056000	1151000	131,4	244200	153200	7,95	0,11	0,23	0,15	0,14	-0,09
1200	1200	1680	1056000	1280000	146,1	531300	308700	1,59	0,12	0,50	0,29	0,12	-0,21
1200	1200	3360	1056000	1280000	146,1	387500	165700	3,18	0,12	0,37	0,16	0,12	-0,21
1200	1200	5040	1056000	1280000	146,1	355500	134600	4,77	0,12	0,34	0,13	0,12	-0,21
1200	1200	6720	1056000	1280000	146,1	342000	121700	6,36	0,12	0,32	0,12	0,12	-0,21
1200	1200	8400	1056000	1280000	146,1	337000	117200	7,95	0,12	0,32	0,11	0,12	-0,21
120	1800	1680	1584606	408600	46,6	12840	1189000	1,06	0,03	0,01	0,75	0,39	0,74
120	1800	3360	1584606	408600	46,6	7261	1185000	2,12	0,03	0,00	0,75	0,39	0,74
120	1800	5040	1584606	408600	46,6	5376	1183000	3,18	0,03	0,00	0,75	0,39	0,74
120	1800	6720	1584606	408600	46,6	4359	1,18E+06	4,24	0,03	0,00	0,75	0,39	0,74
120	1800	8400	1584606	408600	46,6	3598	1,18E+06	5,30	0,03	0,00	0,75	0,39	0,74
240	1800	1680	1584606	699700	79,9	37330	922000	1,06	0,04	0,02	0,58	0,33	0,56
240	1800	3360	1584606	699700	79,9	32190	918200	2,12	0,04	0,02	0,58	0,33	0,56
240	1800	5040	1584606	699700	79,9	29180	916000	3,18	0,04	0,02	0,58	0,33	0,56

Table B.3: Raw data taken from the computational simulations for a system configuration with several size combinations of PV modules, batteries, and electrolyzer.

Load	**PV**	**Batt**	**PV**	**Load**	**Avg.**	**Deficit**	**Surplus**	**BEF**	**PVL**	**EDF**	**SEF**	**LOF**	**ECF**
240	1800	6720	1584606	699700	79,9	26830	914300	4,24	0,04	0,02	0,58	0,33	0,56
240	1800	8400	1584606	699700	79,9	25000	913500	5,30	0,04	0,02	0,58	0,33	0,56
					0,0								
480	1800	1680	1584606	1081000	123,4	104600	609000	1,06	0,07	0,07	0,38	0,26	0,32
480	1800	3360	1584606	1081000	123,4	85560	590700	2,12	0,07	0,05	0,37	0,26	0,32
480	1800	5040	1584606	1081000	123,4	81340	587300	3,18	0,07	0,05	0,37	0,26	0,32
480	1800	6720	1584606	1081000	123,4	79570	586200	4,24	0,07	0,05	0,37	0,26	0,32
480	1800	8400	1584606	1081000	123,4	77990	585400	5,30	0,07	0,05	0,37	0,26	0,32
					0,0								
960	1800	1680	1584606	1453000	165,9	350800	483000	1,06	0,09	0,22	0,30	0,17	0,08
960	1800	3360	1584606	1453000	165,9	241000	357200	2,12	0,09	0,15	0,23	0,17	0,07
960	1800	5040	1584606	1453000	165,9	214500	348400	3,18	0,09	0,14	0,22	0,17	0,08
960	1800	6720	1584606	1453000	165,9	210300	345000	4,24	0,09	0,13	0,22	0,17	0,09
960	1800	8400	1584606	1453000	165,9	208800	344300	5,30	0,09	0,13	0,22	0,17	0,09
1200	1800	1680	1584606	1576000	179,9	497100	506200	1,06	0,10	0,31	0,32	0,15	0,01
1200	1800	3360	1584606	1576000	179,9	333200	343000	2,12	0,10	0,21	0,22	0,15	0,01
1200	1800	5040	1584606	1576000	179,9	297900	308700	3,18	0,10	0,19	0,19	0,15	0,01
1200	1800	6720	1584606	1576000	179,9	290900	302400	4,24	0,10	0,18	0,19	0,15	0,01
1200	1800	8400	1584606	1576000	179,9	287000	299000	5,30	0,10	0,18	0,19	0,15	0,01
120	2400	1680	2112800	427100	48,8	14750	1701000	0,80	0,02	0,01	0,81	0,41	0,80
120	2400	3360	2112800	427100	48,8	7478	1694000	1,59	0,02	0,00	0,80	0,41	0,80
120	2400	5040	2112800	427100	48,8	4303	1692000	2,39	0,02	0,00	0,80	0,41	0,80
120	2400	6720	2112800	427100	48,8	3280	1692000	3,18	0,02	0,00	0,80	0,41	0,80
120	2400	8400	2112800	427100	48,8	2460	1692000	3,98	0,02	0,00	0,80	0,41	0,80
240	2400	1680	2112800	754500	86,1	28730	1398000	0,80	0,04	0,01	0,66	0,36	0,65
240	2400	3360	2112800	754500	86,1	29410	1389000	1,59	0,04	0,01	0,66	0,36	0,64
240	2400	5040	2112800	754500	86,1	25930	1386000	2,39	0,04	0,01	0,66	0,36	0,64
240	2400	6720	2112800	754500	86,1	23160	1384000	3,18	0,04	0,01	0,66	0,36	0,64
240	2400	8400	2112800	754500	86,1	21400	1383000	3,98	0,04	0,01	0,65	0,36	0,64
480	2400	1680	2112800	1224000	139,7	112600	1002000	0,80	0,06	0,05	0,47	0,29	0,42
480	2400	3360	2112800	1224000	139,7	79900	969800	1,59	0,06	0,04	0,46	0,29	0,42

Table B.3: Raw data taken from the computational simulations for a system configuration with several size combinations of PV modules, batteries, and electrolyzer.

Load	**PV**	**Batt**	**PV**	**Load**	**Avg.**	**Deficit**	**Surplus**	**BEF**	**PVL**	**EDF**	**SEF**	**LOF**	**ECF**
480	2400	5040	2112800	1224000	139,7	74930	965600	2,39	0,06	0,04	0,46	0,29	0,42
480	2400	6720	2112800	1224000	139,7	71950	963400	3,18	0,06	0,03	0,46	0,29	0,42
480	2400	8400	2112800	1224000	139,7	69750	962000	3,98	0,06	0,03	0,46	0,29	0,42
					0,0								
960	2400	1680	2112800	1732000	197,7	342900	724400	0,80	0,08	0,16	0,34	0,21	0,18
960	2400	3360	2112800	1732000	197,7	209400	591500	1,59	0,08	0,10	0,28	0,21	0,18
960	2400	5040	2112800	1732000	197,7	194900	577800	2,39	0,08	0,09	0,27	0,21	0,18
960	2400	6720	2112800	1732000	197,7	189700	573500	3,18	0,08	0,09	0,27	0,21	0,18
960	2400	8400	2112800	1732000	197,7	187600	572100	3,98	0,08	0,09	0,27	0,21	0,18
1200	2400	1680	2112800	1898000	216,7	481200	696100	0,80	0,09	0,23	0,33	0,18	0,10
1200	2400	3360	2112800	1898000	216,7	308000	523600	1,59	0,09	0,15	0,25	0,18	0,10
1200	2400	5040	2112800	1898000	216,7	267200	483600	2,39	0,09	0,13	0,23	0,18	0,10
1200	2400	6720	2112800	1898000	216,7	260400	477700	3,18	0,09	0,12	0,23	0,18	0,10
1200	2400	8400	2112800	1898000	216,7	255700	473700	3,98	0,09	0,12	0,22	0,18	0,10

Bibliography

[1] Power-to-gas: the solution that recovers surplus green power. URL https://www.engie.com/en/news/power-to-gas/.

[2] URL http://www.beatriceco.com/bti/porticus/bell/images/solar_battery2.gif.

[3] Standard solar spectra. URL http://www.pveducation.org/pvcdrom/appendices/standard-solar-spectra.

[4] Record annual increase of carbon dioxide observed at mauna loa for 2015, March 2016. URL http://www.noaa.gov/news/record-annual-increase-of-carbon-dioxide-observed-at-mauna-loa-for-2015.

[5] WMO Statement on the State of the Global Climate in 2016. Technical Report 1189, 2016.

[6] Denmark targets 100% renewable electricity by 2050, July 2016. URL http://www.climateactionprogramme.org/news/denmark_targets_100_renewable_electricity_by_2050.

[7] Japan eyes 40,000 fuel-cell cars, 160 hydrogen stations by 2020, March 2016. URL https://www.japantimes.co.jp/news/2016/03/16/business/japan-eyes-40000-fuel-cell-cars-160-hydrogen-stations-by-2020/.

[8] Japan building world's largest floating solar power plant, January 2016. URL https://spectrum.ieee.org/energywise/energy/renewables/japan-building-worlds-largest-floating-solar-power-plant.

[9] Hr gmbh co. kgaa inaugurates world's largest dynamic hydrogen electrolysis plant, November 2017. URL http://www.dgap.de/dgap/News/corporate/hr-gmbh-kgaa-inaugurates-worlds-largest-dynamic-hydrogen-electrolysis-plant/?newsID=1039525.

[10] World's largest dynamic hydrogen electrolysis plant inaugurated, November 2017. URL https://www.thechemicalengineer.com/news/world-s-largest-dynamic-hydrogen-electrolysis-plant-inaugurated/.

[11] Renewable power: sharply falling generation costs. 2017. URL https://www.irena.org/-/media/Files/IRENA/Agency/Publication/2017/Nov/IRENA_Sharply_falling_costs_2017.pdf?la=en&hash=124D0C6FF4AE247D8CFB4FF7F064F5F25432AC5B.

[12] Saudi arabia gets cheapest bids for solar power in auction, October 2017. URL https://www.bloomberg.com/news/articles/2017-10-03/saudi-arabia-gets-cheapest-ever-bids-for-solar-power-in-auction.

[13] The relentless rise of carbon dioxide, Jan 2018. URL https://climate.nasa.gov/climate_resources/24/.

[14] International Energy Agency. Time to shine : Solar power is fastest-growing source of new energy. pages 9–12, 2017.

[15] International Energy Agency. Renewables 2017. pages 1–16, 2017. URL https://www.iea.org/publications/renewables2017/.

[16] Mustafa A Al-refai. Matlab / Simulink Simulation of Solar Energy Storage System. 8(2):297–302, 2014.

[17] Eric Wesoff April, The International, Energy Agency, and Allow Gtm. IEA : Global Installed PV Capacity Leaps to 303 Gigawatts. pages 12–14, 2017.

[18] A Awasthi, Keith Scott, and S Basu. Dynamic modeling and simulation of a proton exchange membrane electrolyzer for hydrogen production. *International Journal of Hydrogen Energy*, 36(22):14779–14786, 2011. ISSN 0360-3199. doi: 10.1016/j.ijhydene.2011.03.045. URL http://dx.doi.org/10.1016/j.ijhydene.2011.03.045.

[19] Allen J Bard, Larry R Faulkner, et al. Fundamentals and applications. *Electrochemical Methods*, 2, 2001.

[20] Theodore E Brown, H Eugene H LeMay, Bruce E Bursten, and Catherine Murphy. *Chemistry the central science 13th Edition*. Prentice Hall, 2014.

[21] DVGW Research Centre. Storego. URL https://www.storeandgo.info/about-the-project/.

[22] Greig Chisholm and Leroy Cronin. Hydrogen from water electrolysis. *Storing Energy: with Special Reference to Renewable Energy Sources*, page 315, 2016.

[23] RE Clarke, S Giddey, FT Ciacchi, SPS Badwal, B Paul, and J Andrews. Direct coupling of an electrolyser to a solar pv system for generating hydrogen. *International Journal of Hydrogen Energy*, 34(6):2531–2542, 2009.

[24] Christophe Coutanceau, Stève Baranton, and Thomas Audichon. Chapter 3 - Hydrogen Production From Water Electrolysis. In Christophe Coutanceau, Stève Baranton, and Thomas Audichon, editors, *Hydrogen Electrochemical Production*, Hydrogen Energy and Fuel Cells Primers, pages 17–62. Academic Press, 2018. ISBN 978-0-12-811250-2. doi: https://doi.org/10.1016/B978-0-12-811250-2.00003-0. URL http://www.sciencedirect.com/science/article/pii/B9780128112502000030.

[25] Perry Williams December, A M Gmt, Billionaire Elon Musk, South Korea, Hyundai Electric, Energy Systems Co, Bloomberg New, Energy Finance, and Ali Asghar. Elon Musk ' s Battery Boast Will Be Short-Lived. pages 1–4, 2017.

[26] ESRL Global Monitoring Division. Trends in atmospheric carbon dioxide, January 2017. URL https://www.esrl.noaa.gov/gmd/ccgg/trends/index.html.

[27] Solar Energy. Photovoltaics report. (July), 2017.

[28] T Estermann, M Newborough, and M Sterner. Power-to-gas systems for absorbing excess solar power in electricity distribution networks. *International Journal of Hydrogen Energy*, 41(32):13950–13959, 2016.

[29] Hassan Fathabadi. Novel standalone hybrid solar / wind / fuel cell / battery power generation system. *Energy*, 140:454–465, 2017. ISSN 0360-5442. doi: 10.1016/j.energy.2017.08.098. URL http://dx.doi.org/10.1016/j.energy.2017.08.098.

[30] Gerda Gahleitner. Hydrogen from renewable electricity: An international review of power-to-gas pilot plants for stationary applications. *international Journal of hydrogen energy*, 38(5):2039–2061, 2013.

[31] Thomas L Gibson and Nelson A Kelly. Optimization of solar powered hydrogen production using photovoltaic electrolysis devices. *International journal of hydrogen energy*, 33(21):5931–5940, 2008.

[32] Lukas Grond, Paula Schulze, and Johan Holstein. Systems analyses power to gas: a technology review. *DNV KEMA Energy & Sustainability, Groningen*, 2013.

[33] ENGIE group. The grhyd demonstration project. URL https://www.engie.com/en/innovation-energy-transition/digital-control-energy-efficiency/power-to-gas/the-grhyd-demonstration-project/.

[34] The Guardian. Time to shine: Solar power is fastest-growing source of new energy. October 2017. URL https://www.theguardian.com/environment/2017/oct/04/solar-power-renewables-international-energy-agency.

[35] Hanjin. Price per watt history for conventional (c-si) solar cells since 1977, 2017. URL https://en.wikipedia.org/wiki/Timeline_of_solar_cells#/media/File:Price_history_of_silicon_PV_cells_since_1977.svg.

[36] Fatemeh Homayouni, Ramin Roshandel, and Ali Asghar Hamidi. Sizing and performance analysis of standalone hybrid photovoltaic/battery/hydrogen storage technology power generation systems based on the energy hub concept. *International Journal of Green Energy*, 14(2):121–134, 2017.

[37] Joern Hoppmann, Jonas Volland, Tobias S Schmidt, and Volker H Hoffmann. The economic viability of battery storage for residential solar photovoltaic systems–a review and a simulation model. *Renewable and Sustainable Energy Reviews*, 39:1101–1118, 2014.

[38] Fraunhofer Research Institute. Photovoltaics report. (July), 2017.

[39] Gso July and The Golden State. California confronts solar power glut with novel marketplace Negative wholesale power prices proliferate in. pages 1–7, 2017.

[40] Ersan Kabalci. Design and analysis of a hybrid renewable energy plant with solar and wind power. *Energy Conversion and Management*, 72:51–59, 2013.

[41] SV Karemore and SY Kamdi. Multi-objective design procedure for hybrid (wind–photovoltaic) system by ga. *International Journal Of Innovative Research In Electrical, Electronics, Instrumentation And Control Engineering*, 1(4):144–147, 2013.

[42] Seul-Ki Kim, Jin-Hong Jeon, Chang-Hee Cho, Eung-Sang Kim, and Jong-Bo Ahn. Modeling and simulation of a grid-connected pv generation system for electromagnetic transient analysis. *Solar Energy*, 83 (5):664–678, 2009.

[43] Jeremy Lagorse, Marcelo G Simoes, Abdellatif Miraoui, and Philippe Costerg. Energy cost analysis of a solar-hydrogen hybrid energy system for stand-alone applications. *International journal of hydrogen energy*, 33(12):2871–2879, 2008.

[44] R Luna-Rubio, M Trejo-Perea, D Vargas-Vázquez, and GJ Ríos-Moreno. Optimal sizing of renewable hybrids energy systems: A review of methodologies. *Solar Energy*, 86(4):1077–1088, 2012.

[45] Gilbert M Masters. *Renewable and efficient electric power systems*. John Wiley & Sons, 2013.

[46] Johannes N Mayer, P Simon, Noha Saad Hussein Philipps, Thomas Schlegl, and Charlotte Senkpiel. Current and future cost of photovoltaics. *Long-term Scenarios for Market Development, System Prices and LCOE of Utility-Scale PV Systems (Fraunhofer ISE, Study on behalf of Agora Energiewende, Freiburg, 2015)*, 2015.

[47] Ni Meng, KH Michael, and YC Dennis. Electrochemistry modeling of proton exchange membrane (pem) water electrolysis for hydrogen production. 2006.

[48] P. Millet. 9 - hydrogen production by polymer electrolyte membrane water electrolysis. In Velu Subramani, , Angelo Basile, , and T. Nejat Veziroğlu, editors, *Compendium of Hydrogen Energy*, Woodhead Publishing Series in Energy, pages 255 – 286. Woodhead Publishing, Oxford, 2015. ISBN 978-1-78242-361-4. doi: https://doi.org/10.1016/B978-1-78242-361-4.00009-1. URL `https://www.sciencedirect.com/science/article/pii/B9781782423614000091`.

[49] Pierre Millet and Sergey Grigoriev. Chapter 2 - water electrolysis technologies. In Luis M. Gandía, Gurutze Arzamendi, and Pedro M. Diéguez, editors, *Renewable Hydrogen Technologies*, pages 19 – 41. Elsevier, Amsterdam, 2013. ISBN 978-0-444-56352-1. doi: https://doi.org/10.1016/B978-0-444-56352-1.00002-7. URL `http://www.sciencedirect.com/science/article/pii/B9780444563521000027`.

[50] Gregory F Nemet. Beyond the learning curve: factors influencing cost reductions in photovoltaics. *Energy policy*, 34(17):3218–3232, 2006.

[51] Snapshot Of and Global Photovoltaic. Snapshot of global photovoltaic markets. pages 1–16, 2017.

[52] By Ivan Penn. California invested heavily in solar power . Now there ' s so much that other states are sometimes paid to take it. pages 1–20, 2017.

[53] Hydrogen Production, Electrochemical Reactions, Transport Process Analyses, Ion Conduction, Proton Conduction, Hydrogen Production, Water Electrolysis, Biomass Power, Generators Integrated, With Water, Electrolysis Systems, and Study Problems. *Hydrogen Production by Electrical Energy*. 2016. ISBN 9780128015636. doi: 10.1016/B978-0-12-801563-6.00003-0.

[54] I E A Pvps. Global installed PV capacity exceeds 300 GW , IEA PVPS The world ' s cumulative PV capacity had surpassed. pages 2016–2017, 2016.

[55] Krishnan Rajeshwar, Robert McConnell, and Stuart Licht. Solar hydrogen generation. *Toward a renewable energy future. Springer: New York*, 2008.

[56] C Riordan and R Hulstron. What is an air mass 1.5 spectrum?(solar cell performance calculations). In *Photovoltaic Specialists Conference, 1990., Conference Record of the Twenty First IEEE*, pages 1085–1088. IEEE, 1990.

[57] Arno HM Smets, Klaus Jäger, Olindo Isabella, René ACMM van Swaaij, and Miro Zeman. *Solar Energy: The physics and engineering of photovoltaic conversion, technologies and systems*. UIT Cambridge Limited, 2016.

[58] Hongmei Tian, Fernando Mancilla-david, Kevin Ellis, Peter Jenkins, and Eduard Muljadi. A Detailed Performance Model for Photovoltaic Systems Preprint. (July), 2012.

[59] Hongmei Tian, Fernando Mancilla-David, Kevin Ellis, E Muljadi, and P Jenkins. Detailed performance model for photovoltaic systems: Preprint. Technical report, National Renewable Energy Laboratory (NREL), Golden, CO., 2012.

[60] GN Tiwari and AK Tiwari. Handbook of solar energy: Theory, analysis and applications: 2016, 2016.

[61] Trina Solar. Trina Solar Announces Fourth Quarter and Full Year 2015 Results. pages 1–10, 2016. URL `http://www.trinasolar.com/en-uk/resources/newsroom/trina-solar-announces-fourth-quarter-and-full-year-2015-results`.

[62] Jeff Tsao, Basic Energy Science, Nate Lewis, and George Crabtree. Solar FAQs. pages 1–24, 2006.

[63] John Sauven Tuesday, Henrik Poulsen, Dong Energy, and Dong Energy. Wind power is now cheaper than nuclear – the energy revolution is happening | John Sauven | Opinion | The Guardian. pages 9–12, 2017.

[64] Kunta Yoshikawa, Wataru Yoshida, Toru Irie, Hayato Kawasaki, Katsunori Konishi, Hirotaka Ishibashi, Tsuyoshi Asatani, Daisuke Adachi, Masanori Kanematsu, Hisashi Uzu, and Kenji Yamamoto. Solar Energy Materials and Solar Cells Exceeding conversion e ffi ciency of 26 % by heterojunction interdigitated back contact solar cell with thin fi lm Si technology. *Solar Energy Materials and Solar Cells*, 173(June): 37–42, 2017. ISSN 0927-0248. doi: 10.1016/j.solmat.2017.06.024. URL `https://doi.org/10.1016/j.solmat.2017.06.024`.

[65] Yang Zhang, Anders Lundblad, Pietro Elia, and Jinyue Yan. Comparative Study of Battery Storage and Hydrogen Storage to Increase Photovoltaic Self-sufficiency in a Residential Building of Sweden. *Energy Procedia*, 103(April):268–273, 2016. doi: 10.1016/j.egypro.2016.11.284. URL `http://dx.doi.org/10.1016/j.egypro.2016.11.284`.